Biophysical and molecular mechanisms of mean and variance adaptation in the *Drosophila* ear

Dissertation
for the award of the degree
"Doctor rerum naturalium"
of the Georg-August-Universität Göttingen

within the doctoral program Sensory and Motor Neuroscience
of the Georg-August University School of Science (GAUSS)

submitted by
Julian R. Rottschäfer

from Detmold, Germany
Göttingen 2023

Thesis Committee

Dr. Jan Clemens (supervisor)
Neural Computation and Behavior, European Neuroscience Institute Göttingen

Prof. Dr. Martin Göpfer
Cellular Neurobiology, Georg-August-University Göttingen

Prof. Dr. Tim Gollisch
Sensory Processing in the Retina, University Medical Center Göttingen

Members of the Examination Board

Referee: Dr. Jan Clemens
Neural Computation and Behavior, European Neuroscience Institute Göttingen

2nd Referee: Prof. Dr. Martin Göpfert
Cellular Neurobiology, Georg-August-University Göttingen

Further members of the Examination Board

Prof. Dr. Tim Gollisch
Sensory Processing in the Retina, University Medical Center Göttingen

Prof. Dr. Luis A. Pardo
Oncophysiology, Max Planck Institute for Multidisciplinary Sciences, Göttingen

Prof. Dr. Ralf Heinrich
Cellular Neurobiology, Georg-August-University Göttingen

Prof. Dr. Carolin Wichmann
Center for Biostructural Imaging of Neurodegeneration, University Medical Center Göttingen

Date of oral examination: 25.04.2023

Abstract

Adaptation is an important mechanism found across sensory systems and species. This important ability of sensory systems expands our range of perception. Giving us the ability to perceive a quiet whisper as well as a loud heavy metal concert. For many receptors, adaptation is well described, but often their underlying mechanisms are still poorly understood. For example in the case for the auditory receptor of *Drosophila melanogaster*. Two forms of adaptation happen in the auditory sensory system of the fly. First, an adaptation to the slow changing mean of a stimulus, called offset or mean adaptation. Secondly, an adaptation to the faster changing intensity of the stimulus, commonly referred to as intensity or variance adaptation.

In this thesis we explored the mechanisms underlying the different forms of adaptation in the primary auditory receptor neurons (Johnston's organ neurons) of the fruit fly, by screening candidate mutant fly strains. The choice of candidates were based on their expression in the Johnston's organ neurons and a hypothetical way the molecule could induce adaptation. In total we screened 17 different mutant strains, including mutations of K^+ channels, motor proteins and small GTPases and characterized adaptation in these mutants. Current clamp recordings of compound action potentials from the Johnston's organ neurons were used to access the adaptation properties of the fruit fly and their change induced by certain mutations. We recorded reduced speed and strength of variance adaptation in six different mutants, including mutations of eag, rgk1 and dynein. The most prominent effects could be measured in the mutations of eag. While the Eag channel is known to be mediated by Ca^{2+} via Calmodulin, we did not observe any effect of mutations interfering with this Eag/Ca^{2+} interaction, suggesting that this process is insignificant for adaptation. Furthermore, while this K^+ channel mutant influenced variance adaptation, it did not influence mean adaptation properties.

We found evidence that the Eag channel is part of the molecular mechanism of variance adaptation, but not involved in mean adaptation. The mutations affecting variance adaptation in general did not affect mean adaptation. This corroborates the hypothesis that different mechanisms are involved in these two types of adaptation in the fly.

Declaration

Herewith I declare, that I prepared the doctoral dissertation "Biophysical and molecular mechanisms of mean and variance adaptation in the *Drosophila* ear" independently and with no other sources and aids than quoted.

Göttingen, February 2023

Julian R. Rottschäfer

Contents

1 Introduction **1**
1.1 Sensory adaptation . . . 1
1.2 Hearing in *Drosophila melanogaster* . . . 3
1.3 Adaptation in JON . . . 6
1.4 Candidate molecules . . . 7
1.5 The Eag channel and its interaction with calcium . . . 10
1.6 The different approaches for generating mutants . . . 12
1.7 Aim of this thesis . . . 13

2 Materials **14**
2.1 Software . . . 17
2.2 Adapted elements of figures . . . 17

3 Methods **18**
3.1 Electrophysiology . . . 18
3.1.1 Collection of flies for the experiments . . . 18
3.1.2 Genotypes . . . 18
3.1.3 Preparation of the flies . . . 20
3.1.4 Fixing the flies in the flyholder . . . 20
3.1.5 Preparing the electrophysiology rig and connecting the fly . . . 22
3.1.6 Pulling electrode tips . . . 24
3.1.7 Stimulus design . . . 24
3.1.8 Stimulus delivery . . . 30
3.1.9 Experiments for probing variance adaptation . . . 31
3.1.10 Mean adaptation probing experiments . . . 31
3.1.11 Piezoelectric actuation . . . 32
3.2 Data analysis . . . 32
3.2.1 Processing variance adaptation data . . . 32
3.2.2 Processing mean adaptation data . . . 33
3.2.3 Estimating the timescale of variance adaptation . . . 34
3.2.4 Estimating the strength of variance adaptation . . . 34

3.2.5 Estimating the curve shift of tuning curves in mean adaptation experiments . . . 37
3.2.6 Estimating the speed of mean adaptation . . . 37
3.2.7 Estimating the strength of mean adaptation . . . 38
3.2.8 Statistics . . . 40

4 Results **42**
4.1 The screening identified multiple candidate molecules affecting variance adaptation . . . 42
4.1.1 Potassium channels . . . 42
4.1.2 Rad, Gem/Kir family small G-proteins . . . 48
4.1.3 Motor proteins . . . 51
4.1.4 Miscellaneous . . . 54
4.2 Eag influenced both speed and strength in the screening making it the strongest candidate molecule . . . 57
4.3 Investigation of mean adaptation dynamics . . . 59
4.3.1 Mean adaptation did not show changes in screened mutant flies . . . 62
4.3.2 The mean and variance adaptation mechanisms employ distinct molecules 65
4.4 The effects of different Eag mutations confirm Eag as a part of the variance adaptation mechanisms . . . 65
4.5 Investigating the possible interaction of Eag and CaM during variance adaptation . . . 68

5 Discussion **73**
5.1 All three Eag mutants showed effects in both data sets . . . 73
5.2 Smaller variation in the hit data set revealed smaller effects . . . 73
5.3 Possible compensation within the mechanism of adaptation . . . 74
5.4 Tuning differences between fly strains . . . 75
5.5 The role of Eag in variance adaptation . . . 76
5.6 Eag mutations did not influence mean adaptation . . . 78
5.7 The Eag channel as a candidate of adaptation . . . 78
5.8 The methodological limitations of CAP recordings . . . 79
5.9 Alternative readouts . . . 80
5.10 Outlook . . . 81

6 Bibliography **82**

7 Acknowledgments **93**

8 Abbreviations **94**

9 List of Figures **96**

10 List of Tables **98**

11 Appendix **99**

1 Introduction

1.1 Sensory adaptation

Sensory adaptation, also called neural adaptation, can be observed in most sensory systems and many neurons of the peripheral and central nervous system (Benda, 2021; Wark et al., 2007; Whitmire et al., 2016). Commonly, this process is caused by prolonged or repeated exposure to a sensory stimulus (e.g. a visual or auditory stimulus) but can also be elicited by injected currents or light activated constructs (Benda, 2021). In response to such a persistent or repetitive stimulus an adapting neuron would first show an initial onset response, in form of a sharp onset peak, then the response magnitude would decrease over time, as shown in Figure 1.1 (Benda, 2021; Whitmire et al., 2016).

The input-output function of a neuron can be separated into two parts. First a temporal filter that describes the neurons frequency preference and secondly an intensity tuning curve, describing the relation between stimulus and response magnitude. This adjustment of the sensory system's sensitivity allows for its dynamic range to stay relevant within the current environment. For example the ear can register both whispers and loud music. This raises the question why not just increase the dynamic range of a sensor to encompass the whole stimulus range, instead of shifting a more limited dynamic range around? The answer to this is a trade-off between the steepness of the tuning curve and its dynamic range in neural coding. If the sensitivity in a neuron is too high, so its tuning curve would be very steep, the response would often saturate, leading to loss of information. If on the other hand the sensitivity was too low, so a very flat tuning curve, this would lead to a greater dynamic range, but less clear response difference between inputs and also some parts of the response range would be underutilized, because they correspond to the extremes of the input range (Laughlin, 1981; Benda, 2021). So there needs to be a compromise between steepness of the tuning curve and dynamic range, which is then shifted depending on the environment to be more sensitive to changes in the relevant context. This tuning depends on the environment also helps filtering out irrelevant information. Furthermore, it optimizes the speed of information transfer and ambiguity. This ambiguity is caused because the input can not be inferred from for example the spiking pattern of the output due to trade-offs in

the adaptive code. Since the meaning of such a spike pattern depends on context, which constantly changes in a dynamic environment and forces the trade-off between tracking the rapid changes and optimizing the code to the current context (Fairhall et al., 2001; Benda, 2021).

This adaptation process often works through an inhibitory or mediating mechanism adjusting the excitability of the system to the stimulus. One way to achieve this on a single neuron level is by inhibitory counteracting currents, evoked through voltage or calcium-gated ion channels (e.g. K^+-currents) (Ozuysal et al., 2012; Hildebrandt et al., 2009; Nagel et al., 2011). But adaptation can also occur on the receptor level. For example, in the eye the signal transduction cascade is regulated to adapt to different light conditions. This happens by adapting the recovery of rhodopsin in the eye, which is ultimately controlled by the calcium concentration in the receptor (Hardie, 2002; Kalloniatis et al., 1995). Another example is the mammalian ear where the transduction from the receiver is tuned by motor proteins. In the ear prestin influences the outer hair cells' sensitivity (Zheng et al., 2000; He, Lovas, et al., 2014). Such a mechanism can be revealed by an increased spiking threshold (Benda, 2021; Benda et al., 2010). When looking at the network level, this suggests a mechanism of excitatory connections counteracted by inhibitory inputs (Benda, 2021). There are different arithmetic form of adaptation, which are relevant in the JON. The first is called subtractive adaptation, here the tuning curve shifts to correct for the stimulus mean. The second is divisive adaptation, which scales the tuning curve to correct for the variance of the stimulus. After a neuron adapted to a stimulus it will respond with reduced spiking to subsequent exposure to this stimulus. For a new stimulus to elicit a large (non-adapted) response from this neuron, it needs to differ from the previous stimulus (the neuron has adapted to) in at least one feature (e.g. sound frequency). This indicates that adaptation does not take place close to the spike generator of the neuron, since the spike generator would adapt to all stimuli the same way. Making it impossible to elicit a non-adapted response by changing one feature of the stimulus. It is believed that stimulus specific adaptation is achieved by separate pathways that process and adapt to the different stimuli (Clemens et al., 2018; Benda, 2021).

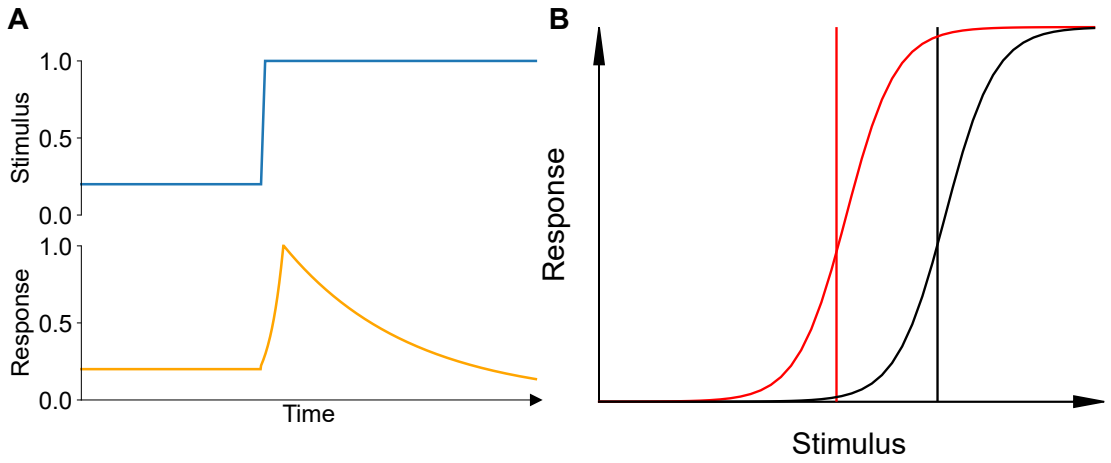

Figure 1.1: **Adaptation of a hypothetical neuron over time. A:** When the stimulus (blue) changes intensity the response of the stimulated neuron (orange) follows suit. If the stimulus persists at the elevated level the neuron response will not mirror it, but decay over time. **B:** The intensity tuning curve of an non-adapted neuron is shown in red. After exposure to a persisting higher intensity stimulus the tuning curve of the neuron is shifted to the right (shown in black), meaning now a stronger stimulus is required to illicit a response in the adapted neuron that is comparable to the neuron in a not adapted state. The vertical lines show the steepest part of the corresponding tuning curve, the neuron is most sensitive to changes around this point.

1.2 Hearing in *Drosophila melanogaster*

Like most animals the fruit fly, *Drosophila melanogaster*, has the ability to perceive its environment through auditory cues. While some members of the class Insecta developed tympanal ears, reminiscent of the human ear, others, like the fruit fly, rely on antennal appendages to perceive sound (Göpfert and Hennig, 2016; Hoy et al., 1996; Nadrowski, Effertz, et al., 2011). Similar to their tympanal counterparts the antennal ears can be found in pairs and are connected to chordotonal organs to work as auditory receptors (Göpfert and Hennig, 2016; Jörg T Albert et al., 2015; Boekhoff-Falk et al., 2014). In the fruit fly the antenna is divided into three segments (a1–a3), the arista, a feathery appendage which serves as sound receiver, is located at the funiculus (a3 segment) (see Figure 1.2). The arista vibrates in response to sound stimuli, translating them into a mechanical signal. The movement of the arista causes the a3 segment to move against the pedicle (a2 segment), this movement activates the stretch-receptor neurons of the fly's auditory organ. The fruit fly's auditory organ is a chordotonal organ is called the Johnston's organ (JO), which is located

in the a2 segment(Göpfert and Hennig, 2016; Jörg T Albert et al., 2015; Boekhoff-Falk et al., 2014; Ishikawa et al., 2016). The JO consists of around 500 stretch-receptor neurons in total, these are called the Johnston's organ neurons (JONs). The JONs are connected to the a3 segment via ciliated dendrites, which transduce the antennal movement into electrical signals (Jörg T Albert et al., 2015; Boekhoff-Falk et al., 2014; Todi et al., 2004; H. Kim et al., 2020). The population of JONs is divided into five subpopulations A–E. Subpopulations A and B make up about 200 of the JONs and mainly respond to sound-induced fast vibrations. Contrary to that, the subpopulations C and E of about 250 neurons respond to static, slow deflections of the antenna, like for example caused by wind or gravity. Except, that during very intense vibrations of the antenna (above 200 nm) these two subpopulations are also activated (Jörg T Albert et al., 2015; Effertz et al., 2011; Kamikouchi, Inagaki, et al., 2009; Ishikawa et al., 2016). Finally, the smallest subpopulation D only consists of about 50 neurons and responds to both fast vibrations and slow deflections. One theory for this hybrid behavior is that these JONs are involved in flight control, monitoring wind and wing-beat sounds (Jörg T Albert et al., 2015; Kamikouchi, Shimada, et al., 2006; Matsuo et al., 2014; Kamikouchi, Inagaki, et al., 2009; Yorozu et al., 2009; Matsuo et al., 2014). In addition to to responding to different classes of stimuli it is hypothesized that the JONs are also direction sensitive, different JONs are activated or inactivated depending on their position in the pedicle and the direction of the antenna movement. For example a posterior deflection of the antenna activates JON, that are connected to the posterior side of the a2 segment, but inactivates the ones on the anterior side. Subpopulation A and B neurons are suspected to connect medially to the antenna, since they are activated by both anterior and posterior antennal movement. C and D neurons on the other hand are connecting on the anterior side and are therefore activated by posterior movements, while the opposite is the case for the subpopulation E. Additionally there is also data suggesting that the bidirectionality observed is a property of individual JONs and not the subpopulation as a whole (Jörg T Albert et al., 2015; Matsuo et al., 2014; Yorozu et al., 2009; Kamikouchi, Inagaki, et al., 2009; Lehnert et al., 2013).

The transduction of a mechanical stimulus to an electrical signal is achieved by mechano-electrical transduction (MET) channels, transient receptor potential (TRP) channels were proposed as candidates for this role, in the JON (Jörg T. Albert et al., 2007; Jörg T Albert et al., 2015; Lehnert et al., 2013). Two prevalent models about this transduction exist. The first model (NompC model) states that the no mechanoreceptor potential C (NompC) channel mediates transduction and mechanical amplification in the A and B type JONs, while a different, less sensitive, channel mediates this independently in the C and E type JONs (Jörg T Albert et al., 2015; Lehnert et al., 2013; Göpfert, Jörg T. Albert, et al., 2006). Downstream of this the electrical signals are amplified by the Nanchung (Nan) and Inactive (Iav) channels, two types of TRPV channels which are necessary for signaling in

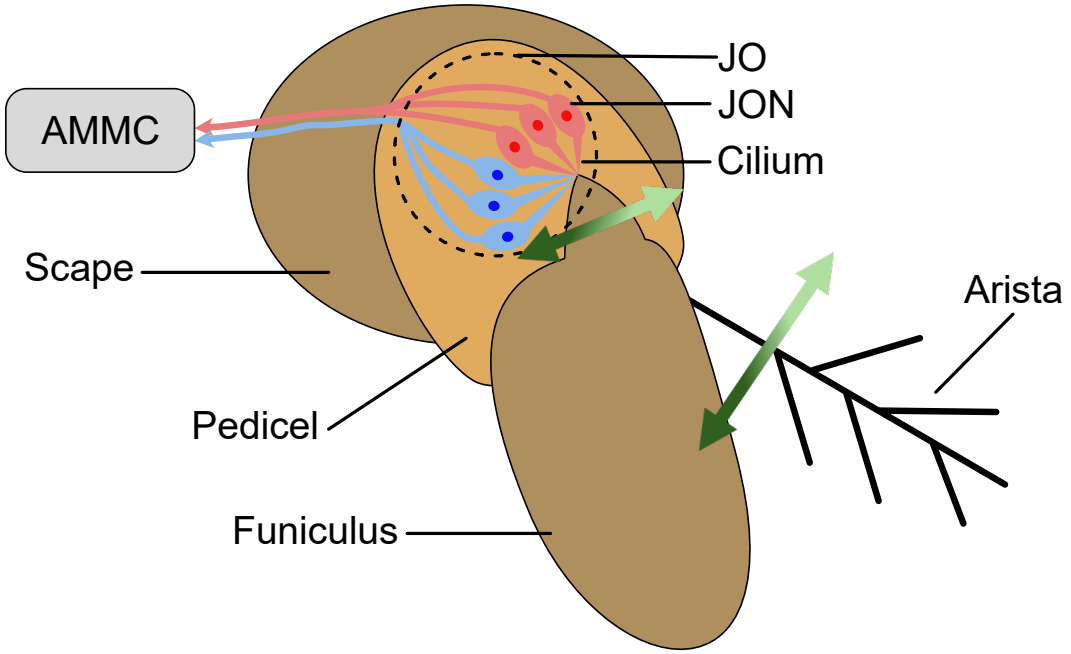

Figure 1.2: **Antenna of *Drosophila melanogaster* and its JO.** The JO and its connections are superimposed on the three antennal segments. Different colored JONs indicate different subpopulations. Double-sided green arrows indicate movement and its translation. AMMC = antennal mechanosensory motor center. JO = Johnston's organ. JON = Johnston's organ neuron.

the JON (Clemens et al., 2018; Jörg T Albert et al., 2015; Lehnert et al., 2013). The second model (Nan-Iav model) suggests that transduction in all JONs is achieved by the Nan and Iav channels and NompC only acts as a mechanical pre-amplifier in the A and B type JONs (Jörg T Albert et al., 2015; Lehnert et al., 2013). The axons of the JONs then project into two brain regions of the fly, the antennal mechanosensory motor center (AMMC) and the wedge (WED). The regions of the AMMC or WED the JONs terminate was reported to be tonotopically organized. In the AMMC mainly low frequency stimuli were represented, while extreme frequencies (high or low) are mainly represented in the WED. JONs responding to vibration seem to terminate preferably in the lateral AMMC and WED, while the ones responding to static deflections seem to mainly project to the medial subregions. There are also subregions, in both AMMC and WED, that mainly represent push or pull displacements. Courtship song was reported to recruit the most subregions in these two brain areas. While the AMMC responds mainly to vibration of the ipsilateral antenna, the WED was reported to integrate vibrations from both, the ipsi- and contralateral, antenna (Patella et al., 2018). The subregion of the AMMC were the JON subtypes A and B project

to (AMMC zone AB) is regarded as primary auditory center of the fly. From these AMMC zones there are connections downstream to the inferior ventrolateral protocerebrum (IVLP), which was suggested to function as a second-level auditory processing center, via the giant fiber neuron (GFN), AMMC-A1 and AMMC-B2 neurons. Also the respective hemispheres are connected by multiple commissural neurons, like for example the AMMC-B2 neurons connecting the AMMC zone B of both sides. (Kamikouchi, Shimada, et al., 2006; Lai et al., 2012; Kamikouchi, Inagaki, et al., 2009).

1.3 Adaptation in JON

In *Drosophila melanogaster* the auditory system adapts to two different aspects—the mean and the variance of the stimulus (Clemens et al., 2018). It was hypothesized that this is a two stage process in which the JON first adapts to the slowly changing mean of the stimulus, by low-pass filtering the stimulus. This produces an adaptation signal, which represents the slowly changing mean of the stimulus, and is then subtracted from the stimulus. This process is called "subtractive adaptation". Next, the stimulus is rectified via full-wave rectification. In the final step this rectified signal is again low-pass filtered and the stimulus is divided by this adaptation signal. Thus the response is scaled to the input. This process is called "divisive adaptation" (Benda, 2021; Clemens et al., 2018). The mean adaptation process was shown to be partly mechanical in nature and partly arise on the neuronal level, visible in the CAPs of the JONs. The mechanical component of mean adaptation arises from readjustment of the gating-spring tension of transducer channels in the flies antenna, as shown in prior publications of the Göpfert lab (Jörg T. Albert et al., 2007; Nadrowski, Jörg T. Albert, et al., 2008). It was shown that these are two distinct processes, as mean adaptation does not affect sound sensitivity. It was hypothesized that this separation occurs due to the order of computations not a difference in timescale. The mean adaptation occurs first, during the mechanotransduction, and then the rectification and variance adaptation follow after that. This is why variance adaptation influences mean adaptation unidirectionally (Clemens et al., 2018; Jörg T. Albert et al., 2007). A lot is known about hearing in insects and *Drosophila melanogaster*, also the existence of both, mean and variance adaptation, is well established in many systems. Nevertheless, the biophysical and molecular mechanisms of these are often still poorly understood. For example, it is unknown how the different forms of adaptation (mean and variance adaptation) and the mechanisms of these forms of adaptation (e.g. shift and scaling of the JON's tuning curve) are achieved on a molecular level. As well as how these two mechanisms are interacting with one another. Therefore, in this thesis we employed the great accessibility of *Drosophila melanogaster* as a genetic model to try to unravel components of these molecular mechanisms through a mu-

tant screening. Furthermore, we tried to put our findings into a greater molecular context to form a hypothesis about further interactions in these molecular mechanisms, as well as their influence on molecular and biophysical processes in the fly ear.

1.4 Candidate molecules

We considered different classes of candidate molecules for the screening: Ion channels, more precisely K^+ channels, small GTPases that interacted with Ca^{2+} channels, motor proteins and some miscellaneous molecules, which were involved in other receptors (e.g. Stops). Generally molecules would be included in the candidate list if they were expressed in the JO and if there was a hypothesis how a molecule of this class could work with in a molecular mechanism of adaptation. For example, the ability of ion channels to affect the sensitivity and kinetics of neurons (Ozuysal et al., 2012). Other obvious candidates would include for example NompC, Iav and Nan for their aforementioned vital role in the JON signal transduction (Göpfert, Jörg T. Albert, et al., 2006; Gong, 2004; Effertz et al., 2011). But there is a major difficulty investigating the effect of these molecules, for mutation of iav or nan abolishes the generator current in the JONs. Making it impossible to record CAPs. Furthermore, nompC mutants were shown to have no effect on variance adaptation, but to only affect the sound sensitivity of the fly (Lehnert et al., 2013; Clemens et al., 2018).

The first class of molecules we suspected to play a role in auditory adaptation of the fly were the K^+ channels. There are eight major families of known voltage-gated K^+ channels, which were often named based on phenotypic properties of the mutant flies after being discovered. Three of the most well known ones are Shaker (Sha), Slowpoke (Slo) and Ether a go-go (Eag) (Frolov et al., 2012). The Shaker channel was the first of these to be discovered, its name is based on the mutant fly's seizure-like leg shaking during ether anesthesia (Kaplan et al., 1969; Frolov et al., 2012). Its expression in neurons is restricted to nerve terminals and axons (Rogero et al., 1997; Frolov et al., 2012). The channel's K^+ current undergoes rapid activation and inactivation, making it an A-type current (Salkoff and Wyman, 1981; Frolov et al., 2012; Niven et al., 2003). The channel is well known for its role of neuron repolarization and its involvement in regulating sleep homeostasis of the fly (Frolov et al., 2012; Tanouye et al., 1985; Pimentel et al., 2016). The Slowpoke channel got its name from the reduced and uncoordinated movement the mutants display (Elkins et al., 1986; Frolov et al., 2012). The channel is defined by its Ca^{2+}- and Na^+-dependence and large channel conductance of over 250 pS (Atkinson et al., 1991; Tamsett et al., 2009; Salkoff, Butler, et al., 2006; Frolov et al., 2012). The channel is ubiquitously expressed and regulates membrane excitability (Becker et al., 1995; Frolov et al., 2012).

It also has multiple mammalian homologs (Pallanck et al., 1994; Salkoff, Butler, et al., 2006). Lastly, the Eag channel is a founding member of a large family of K^+ channels in *Drosophila melanogaster*, with multiple homologs in mammals (J. W. Warmke et al., 1994; Li et al., 2015). In *Drosophila melanogaster* the eag gene encodes the EAG subunit, the channel is a tetramere made up out of four of these subunits (see Figure 1.3) (J. Warmke et al., 1991; Brüggemann et al., 1993; Bronk et al., 2018; Lörinczi et al., 2016). The Eag channel is a voltage-gated rectifier channel, which plays an important role in repolarization and that way changing the excitability of the neurons in the fly. The mutant phenotype shows hyperexcitability in the larval neuromuscular junction (NMJ) and memory formation defects in adult animals, also its name stems from the shaking of the flies legs after being exposed to ether (Kaplan et al., 1969; Wu et al., 1983; Griffith et al., 1994; Frolov et al., 2012).

The second class of molecules within our list of candidate molecules were the small GTPases of the Rad, Gem/Kir family (Rgk), in this screen we included mutations of Rgk1 and Rgk3. GTPases are important players in many signal transduction pathways in cells (Colicelli, 2004). The Rgk molecules are known to interact with voltage-gated Ca^{2+} channels. After Rgk molecules bind Ca^{2+}/CaM and subsequent cytoplasmic localization, they are known to inhibit Ca^{2+} expression at the cell surface by interacting with its β-subunit (Béguin et al., 2001; Finlin et al., 2003; Puhl 3rd et al., 2014). This regulation of Ca^{2+} concentration could be related to regulation gain in a sensory system and inducing adaptation, which is why we were interested to see if the GTPases will show an effect in the screening. Furthermore, Rgk1 is also known to affect memory and anesthesia-resistance in *Drosophila* (Murakami et al., 2017).

The third class of molecules we considered likely candidates for the adaptation mechanism were motor proteins. Motor proteins are categorized into three superfamilies: Myosins, kinesins and dyneins. All of these families generate movement through ATP-hydrolysis (Sweeney and Holzbaur, 2018). One of their main differences are the structures they attach to and move on. Myosin attaches to actin filaments, while kinsin and dynein attach to microtubules (Vale et al., 1985; Rayment et al., 1993; Z. Wang et al., 1995; Sweeney and Holzbaur, 2018). Myosin is best known for its role in muscle contraction. Structurally myosin can be divided in four domains. The motor domain contains the catalytic site for the ATP-hydrolysis. This connects to a lever arm of variable length, to amplify the movements of the motor domain. The arm connects to a coil of two-headed myosins, which can act as site for protein folding. The last of these domains is the targeting domain, which binds the motor protein to their cellular target (Rayment et al., 1993; De La Cruz et al., 1999; Odronitz et al., 2007; Sweeney and Holzbaur, 2018; Sweeney and Hammers, 2018). Kinesin was the first motor protein discovered that moves cargo along microtubules (Vale et

al., 1985; Sweeney and Holzbaur, 2018). While all members of the kinesin family have great similarity in the sequence of their motor domains not all function as cellular motors, but regulate microtuble dynamics. Kinesin shares a lot of similarities with myosin, especially regarding the structure of its motor domain. Kinesin motor proteins are often dimeric. Their motor domain is followed by an array of protein- and cargo-binding domains (Jon Kull et al., 1996; Clancy et al., 2011; Kull et al., 2012; Sweeney and Holzbaur, 2018). Dyneins are large motor proteins, that can move along microtubles and take part in a multitude of roles like vesicle and organelle movement or spindle assembly during cell division (Gibbons et al., 1965; Sweeney and Holzbaur, 2018). The structure of dynein can also be divided into four domains. First is the tail domain, containing the motor region. This connects via the linker domain to the AAA (ATPases associated with cellular activities) domains, AAA1 being the main location of ATP-binding and hydrolysis. Lastly, on the very tip of the stalk the microtuble-binding domain is located (King, 2000; Carter et al., 2011; Schmidt et al., 2015; Sweeney and Holzbaur, 2018). beyond these three motor proteins there is a fourth, discovered in the outer hair cells (Zheng et al., 2000; He, Lovas, et al., 2014). Prestin differs from the other cellular motors since its movement is not based on ATP-hydrolysis, but is directly linked to voltage, making it a faster than any other motor protein. It consists out of 12 transmembrane domains and has at least two functional domains, the voltage sensor and the actuator. Prestin is best know for its role in the hair cell of the ear, where it helps achieving the impressive sensitivity and range of the mammalian ear (Dallos and Evans, 1995; He and Dallos, 2000; Dallos and Fakler, 2002; He, Lovas, et al., 2014).

The last group of tested molecules (which were not part of a shared class of molecules) were some miscellaneous molecules we included in the screening. The first molecule in this group was water witch (Wtrw), a TRP channel involved in sound perception and response to humidity in *Drosophila* (Liu et al., 2007; Senthilan et al., 2012). Being a TRP channel with a known effect on hearing makes the channel an interesting additional target to include in the screening, since TRP channels are also known to play an important role in signal transduction within the JON (Göpfert, Jörg T. Albert, et al., 2006). The next miscellaneous molecule was Stops (slow termination of phototransduction). Stops encodes for a SOCS (suppressor of cytokine signaling) box protein, which is involved in deactivation of rhodpsin mediated signaling and perception of sound in the fruitfly (T. Wang et al., 2008; Senthilan et al., 2012). This known regulatory effect in the visual system and Stops known role in hearing of the fly made it a potential candidate molecule as part of the mechanism of adaptation. The last molecule included in the screening was nAChα5, which encodes for a subunit of the nicotinic acetylcholine receptor, a pentameric neurotransmitter-gated ion channel. The nicotinic acetylcholine receptor are important neurotransmitter receptors expressed throughout the nervous system of insects (Sattelle et al., 2005; Jones et al., 2007; Lansdell et al., 2012). Because of its widespread expression and ligand-gated ion channel

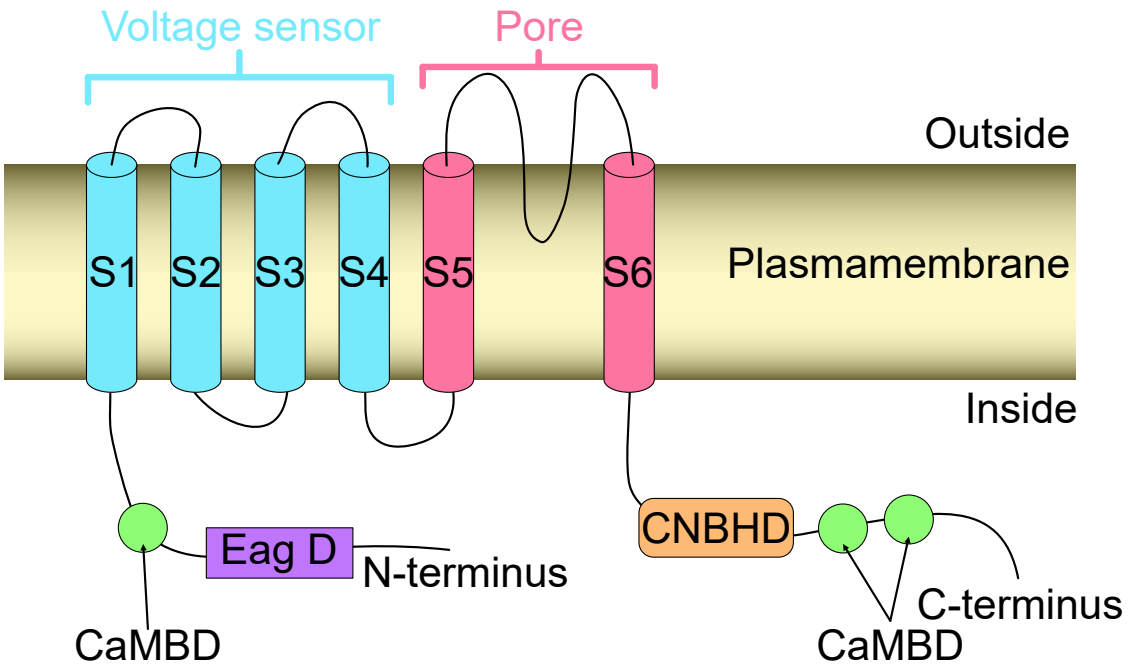

Figure 1.3: **Structure of Eag EAG subunit.** The channel is a tetramere made up out of four EAG subunits. The domains S1–S4 of the subunits form the voltage sensor of the channel, while S5 and S6 form the pore. CaMBD = Calmodulin binding domains (green circles). Eag D = ether a go-go domain. CNBHD = cyclic nucleotide-binding homology domain.

activity nAChα5 was an early candidate based on a possible ligand controlled excitability modulation in the neurons. Unfortunately nAChα5 does not seem to be expressed in the JON, making it a unlikely candidate for the adaptation mechanism (Albuquerque et al., 2009; Senthilan et al., 2012). Nevertheless, the molecule was kept in the screening to test if it really would not affect adaptation and for the sake of completeness.

1.5 The Eag channel and its interaction with calcium

In this section we talk about the structure of the Eag channel and its interactions involving Ca^{2+}. We looked into these interactions since Ca^{2+} often plays a role in adaptation processes, like for example in photoreceptors (Krizaj, 2002). Eag was known to interact with Ca^{2+}, which was another indication that Eag might be a strong candidate for partaking in the mechanism of adaptation (Bronk et al., 2018). The EAG subunit itself has six transmembrane domains, and strongly conserved NH_2- and COOH-terminal sites. The domains S1–S4 make up the voltage sensor, while S5 and S6 form the channel's pore (see Figure 1.3).

During deactivation of the channel the eag domain binds to the cyclic nucleotide-binding homology domain (CNBHD) and closes the channel (see Figure 1.4)(J. W. Warmke et al., 1994; Gianulis et al., 2013; Frolov et al., 2012; Whicher et al., 2016). Furthermore, the channel is inactivated in the presence of high Ca^{2+} concentrations, for example at plasma membrane Ca^{2+} channel microdomains. The Eag channel in flies is a lot less sensitive to Ca^{2+} than its mammalian counterparts (Bronk et al., 2018). The observed inhibition of the Eag channels in presence of Ca^{2+} is caused by binding of activated Calmodulin (CaM) to the CaM binding domains (CaMBD) at the C- and N-terminal of the channel. When activated Ca^{2+}/CaM complexes bind at the CaMBD of both termini, simultaneously the channel is closed (Lörinczi et al., 2016; Bronk et al., 2018). Furthermore, the Ca^{2+}/calmodulin-dependent protein kinase II (CaMKII) binds to the Eag channel after being activated by CaM, allowing autophosphorylation (Sun et al., 2004). When binding to the channel the kinase phosphorylates threonine 787 of Eag. This was reported to lead to substantial increase in channel current (Zheng Wang et al., 2002). Mutation of the CaMKII causes the same mutant phenotype as mutation of the Eag channel—hyperexcitability in the NMJ of larva and memory formation defects in the adult fly. CaMKII is thought to maintain or enhance Eag activity in *Drosophila*, since inhibition of the kinase caused visible reduction of the Eag current amplitude (Zheng Wang et al., 2002; Griffith et al., 1994). If Eag is revealed to play a role in adaptation in the JO of *Drosophila melanogaster* this Ca^{2+} related interactions might provide information about further parts of the mechanism. Since it would be possible for this mechanism to be modulated by for example Ca^{2+} concentration.

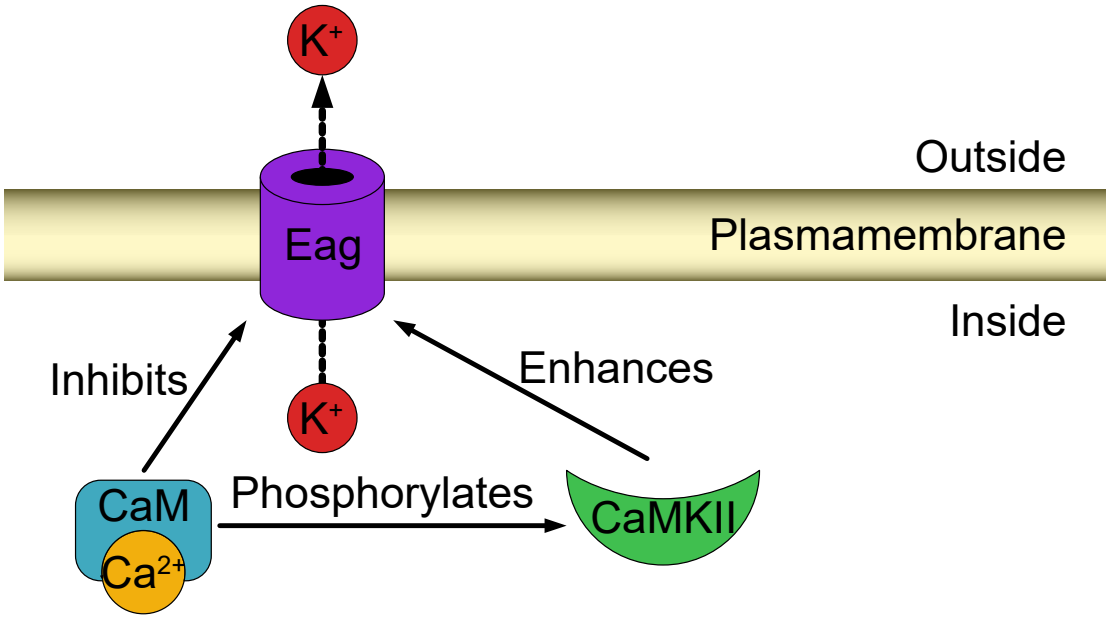

Figure 1.4: **The Eag channel's Ca^{2+} mediated interaction with CaM and CaMKII.** Eag is inhibited by Ca^{2+}/CaM complexes. These complexes also phosphorylate CaMKII, making it able to bind to and enhance Eag. An active binding of Ca^{2+}/CaM to CaMKII is not required for the kinase to bind to the channel, only for its activation. Eag = ether a go-go channel. CaM = Calmodulin. CaMKII = Ca^{2+}/calmodulin-dependent kinase II.

1.6 The different approaches for generating mutants

There are many different methods of mutagenesis and the flies we tested were created using many different examples of this. The Eag^{sc29} for example was created trough classic X-ray-induced deletion (Drysdale et al., 1991). Over the year more sophisticated methods were developed. Like for example the use of the *Minos*-mediated integration cassette (MiMIC), this transposon insertion has the advantage of being very versatile, it contains a gene-trap cassette and a $yellow^+$ marker and the intervening sequence could be replaced using recombinase-mediated cassette exchange if desired. This way it would also be possible to revert back to the wild type (Venken et al., 2011). Other examples of transposons, which are often designed with a more specialized purpose, are *Minos* and *piggyBac* (PBac). *Minos* while imprecise, can insert stable and efficiently in many organisms with little insertion bias compared to PBac (Pavlopoulos et al., 2007; Metaxakis et al., 2005; Venken et al., 2011). PBac is for example precise when doing excisions (Witsell et al., 2009). Another very common transposon was the *P*element (PE), which while quite efficient is imprecise

during excisions and has much stronger insertion bias then PBac (Bellen et al., 2011; Venken et al., 2011). Finally there was also the CRISPR-mediated integration cassette (CRIMIC) approach. Like the name implies this technique uses CRISPR-mediated homologous recombination to integrate a swappable integration cassette between two coding exons. This can produce a strong loss of function of the targeted gene. This can be used to determine gene expression patterns, study the effect of loss of function of genes and can also used for rescue experiments (Kanca et al., 2022; Lee et al., 2018). Compared to classical mutagenesis these more modern transposon insertions have the advantage that they can be used for a variety of applications and can reliably cause loss of function of a targeted gene.

1.7 Aim of this thesis

In this thesis we aimed to identify molecular players in the adaptation of the JONs. We screened mutant fly stocks to assess whether they play a role in adaptation mechanisms, by comparing the adaptation in mutants to the adaptation in wild type controls. The mutants chosen for the screening were narrowed down by setting two conditions for candidate molecules. First, they should belong to a class of molecules, which would fit the function of achieving adaptation, based on literature, e.g. ion-channel, motor proteins, etc. Second, they would need to be expressed in the JONs, which was determined through a transscriptome kindly provided by the Göpfert lab. We investigated the influence of mutations on both, the variance and the mean adaptation mechanism, to assess whether or not these might share some molecular components despite being to separate mechanisms.

We found that mutations of the Eag channel reduced speed and strength of variance adaptation. Subsequently, we investigated the effect of a possible Ca^{2+} mediated inhibition of the channel, by testing strains bearing a mutated CaM binding domain of Eag. Expecting an increase in adaptation due to interfering with the Ca^{2+}/CaM complex induced inhibition of the Eag channel. Contrary to our expectations we did not observe any effect. Furthermore, none of the screened mutants did affect mean adaptation.

2 Materials

Table 2.1: General laboratory materials and equipment

Brush	Synthetic hairbrush size 1, Baier & Schneider GmbH & Co. KG, Heilbronn Germany
Dental wax	Surgident Periphery Wax Sticks, Heraeus Kulzer GmbH, Hanau Germany
Fly vials (big)	Product No. 41171, ⌀46 mm, 168 ml, K-TK e.K., Retzstadt Germany
Fly vials (small)	Product No. 789008, ⌀25 mm, Kisker Biotech GmbH & Co. KG, Steinfurt Germany
Fly Pushing Brush	Flystuff 59-204 Superconductive Static Discharge Fly Brush, Genesee Scientific Corporation, San Diego California USA
Forceps	Dumoxel No. 3 & 5, Manufactures d'Outilis Dumont SA, Montignez Switzerland
Freezer	Liebherr Premium, Lieberherr-International S.A., Bulle Switzerland
Hypodermic needle	Sterican® 0.60 × 60 mm hypodermic needle, B. Braun SE, Melsungen Germany
Incubator	Memmert HPP 750, Memmert GmbH & Co. KG, Schwabach Germany
Light source	Schott KL 1500 LCD, Schott AG, Mainz Germany
Micropipette	100 µl Eppendorf Research® mechanical pipette, Eppendorf SE, Hamburg Germany
Micropipette tips	200 & 1000 µl Eppendorf epT.I.P.S.®, Eppendorf SE, Hamburg Germany

Petri dish	CytoOne® 40 × 11 mm dish, Starlab International GmbH, Hamburg Germany
Refrigerator	Liebherr Premium, Lieberherr-International S.A., Bulle Switzerland
Reaction tube	0.5 ml reaction tube , Sarstedt AG & Co. KG, Nümbrecht Germany
Soldering iron	Precision soldering iron "CT-LS Micro", ChiliTech GmbH, Lehre-Essenrode Germany
Stereo microscope	Olympus SZ61, Olympus Corporation, Tokyo Japan
UV-adhesive	BONDIC Starter Plus, VIKO UG, Kranzberg Germany

Table 2.2: Solutions

Extracellular saline	108 mM NaCl, 5 mM KCl, 2 mM $CaCl_2$, 8.2 mM $MgCl_2$, 4 mM $NaHCO_3$, 1 mM NaH_2PO_4, 5 mM Trehalose, 10 mM Sucrose, 5 mM HEPES. When bubbled with carbogen the pH value should equilibriate near 7.25.

The chemicals used in the extracellular saline (see Table 2.2) were bought from Carl Roth GmbH + Co. KG, Karlsruhe Germany.

Table 2.3: Fly food (for 5 liters)

Agar threads (soak overnight)	51 g dissolved in 2.5 l demineralised H_2O
Soy flour + brewer's yeast	50 g + 90 g dissolved in 0.5 l demineralised H_2O
Corn flour	400 g dissolved dissolved in 1 l demineralised H_2O
Beet syrup	110 g dissolved dissolved in 0.5 l demineralised H_2O

Malzin	400 g dissolved dissolved in 0.5 l demineralised H_2O
Propionic acid	31.5 ml
Nipagin	7.5 g slowly dissolved in Ethanol

Table 2.4: Components of the electrophysiology rig

Amplifier	npi ELC-03XS, npi electronic GmbH, Tamm Germany
Camera	Hamamatsu XC-ST70CE, Hamamatsu Photonics K.K., Shizuoka Japan
Camera Controller	Hamamatsu C2741–62, Hamamatsu Photonics K.K., Shizuoka Japan
DAQ card	NI PCIe-6323, National Instruments, Austin Texas USA.
Light-source	Olympus TH4-200, Olympus Corporation, Tokyo Japan
Loudspeaker	HP Cone Swans F6, Swan Acoustic Technology Co., Ltd., Guangzhou China
Micromanipulator controller	MPC-200, Sutter Instrument, Novato California USA
Micromanipulator (electronic)	MP-225, Sutter Instrument, Novato California USA
Micromanipulator (mechanical)	Märzhäuser Wetzlar MM33, Märzhäuser Wetzlar GmbH & Co. KG, Wetzlar Germany
Microscope	Olympus BX51WI, Olympus Corporation, Tokyo Japan
Oscilloscope	Tektronix TBS 1052B-EDU, Tektronix Inc., Beaverton USA
Piezo actuator	PI P-841.60, Physik Instrumente GmbH & Co. KG, Karlsruhe Germany

Piezo Servo Controller	PI E-625, Physik Instrumente GmbH & Co. KG, Karlsruhe Germany
Pre-amplifier	Douk Audio G4, Douk Audio & Nobsound, Guangdong, China

2.1 Software

- Affinity Designer
- LaTeX in Overleaf (TeX Live 2020)
- Microsoft Excel
- Python 3.9.7 (Anaconda 4.11.0 distribution)

2.2 Adapted elements of figures

Parts of fly clipart from the de Bivort lab (de Bivort, 2022) were used in some figures of the methods section (Figures 3.2 and 3.4).

3 Methods

3.1 Electrophysiology

3.1.1 Collection of flies for the experiments

The flies were group housed and virgin females were collected for the recordings. The experiments were performed within 2-5 days after eclosion. The flies were reared on a 12 h light-dark cycle, at 25 °C and 60 % humidity. The experiments were conducted 2–10 hours after the light in the incubator was switched on. In the case of mutant strains, only flies that were homozygous for the mutant allele were used for the recordings.

3.1.2 Genotypes

Table 3.1: Genotypes of the fly stocks used

Abbreviation	**Genotype**	**BDSC No.**[1]
CaMBD (8.8.1)	w^-; CaMBD Mut8.8.1	Bronk et al., 2018
CaMBD (17.4.1)	w^-; CaMBD Mut17.4.1	Bronk et al., 2018
CaMKII (MiMIC)	y^1; Miy[+mDint2]=MICCaMKII^{MI03976}	60770
CaMKII (PE)	y^1 w^{1118}; Py[+mDint2] w[+mC]=EPgy2CaMKII^{EY14097}	22325
Control Mut 8.7.1	w^-, control 8.7.1	Bronk et al., 2018

[1]Bloomington Drosophila Stock Center number or if not available other reference

Control Mut 17.4.1	w^-, control 17.4.1	Bronk et al., 2018
CG9313	w^{1118}; Mi{GFP[E.3xP3]=ET1}CG9313^{MB06913}	25631
Dhc93ab	w^{1118}; Mi{GFP[E.3xP3]=ET1}Dhc93AB^{MB05444}	25298
dnai2	w^{1118}; Mi{ET1}CG6053^{MB06262}	Göpfert lab stock 421
dnah3	w^{1118}; Mi{GFP[E.3xP3]=ET1} Dnah3^{MB05004}/TM6C, Sb^1	24844
eag^{sc29}	ln(1)sc[29], sc[29]w[a]eag[sc29]	1442
eag-crimic	y[1] w[*]; TI{GFP[3xP3.cLa]=CRIMIC.TG4.1}eag [CR01421-TG4.1]	86374
eag delta-full	w-; eag delta-full #3	Bronk et al., 2018
nAChRalpha5	y^1 w^*; Mi{y[+mDint2]=MIC}nAChRalpha5^{MI05549}	41424
NM91	wild type control	—
Prestin	y^1 w^*; Mi{y[+mDint2]=MIC}Prestin^{MI03269}	36414
rgk1	w^{1118}; PBac{w[+mC]=WH}Rgk1^{f04245}	18749
rgk1 (Minos)	w^{1118} ; Mi{GFP[E.3xP3]=ET1}Rgk1^{MB02498}	23448
rgk3	y^1w^*; Mi{y[+mDint2]=MIC}Rgk3^{M102734}	35129
$shaker^5$	sha^5	Lichtinghagen et al., 1990
sha^{133}	sha^{133}	Lichtinghagen et al., 1990
slo (PBac)	w^{1118}; PBac{w[+mC]=WH}slo^{f05915}	18916
slo (Mimic)	y^1 w^*; +/+; Mi{y[+mDint2]=MIC}slo^{MI06325}/TM3, Sb1, Ser1	43884
stops	y^1 w^*; $stops^1$	24893
TH control	w^-, control 8.7.1/w^-, control 17.4.1	Bronk et al., 2018

wtrw	w^-; +; $wtrw^1$	Göpfert lab stock 400

3.1.3 Preparation of the flies

Flies were fixed in a custom holder for the electrophysiology experiments. First, the fly was anesthetized using CO_2. Then, its wings and legs were carefully removed at their base, using two pointed forceps (Dumoxel No.3). The Dumoxel No. 3 was ground down to a finer tip before it was used to remove the wings. We removed the legs by holding on to their base with an even finer forceps (Dumoxel No. 5) and pulling them off with one of the bigger forceps (Dumoxel No. 3). It was important to remove these as cleanly as possible, without leaving behind stumps, as the fly could still move them, which could cause loss of the signal during recording. Furthermore, it was important not to damage the fly to the point of it leaking hemolymph, as this could lead to the fly dying early or the hemolymph sticking to its aristae. If the leg stumps were leaking hemolymph these would be sealed with paraffin wax while fixating the fly in the fly holder (see subsection 3.1.4).

3.1.4 Fixing the flies in the flyholder

The flyholder consisted of a 1000 µl micropipette tip, which was cut ca. 2 mm from the tip and ca. 2 cm from the base. We fixed a setscrew into the base opening and placed some dental wax on the underside to set the holder down securely. We chose the length of the holder in a way that the fly would be in the field of view of the microscope if we placed the holder into the rig. Next, we removed half of the tip from the front end, for a length of about 3–4 mm, and filled that space with paraffin wax. Using the pointed forceps, we drilled a hole, big enough to fit a female fly's abdomen, inside the paraffin wax. Lastly, we molded the paraffin wax inside the tip, using a soldering iron, in a way that a small mound formed towards the base-side of the tip.

After we prepared the flyholder as shown in Figure 3.1, the fly was prepared according to the method described in subsection 3.1.3. First, we placed the fly into the paraffin hole of the holder, with the fly's ventral side facing the base end of the holder. We positioned the fly's abdomen completely and firmly inside the hole. Next, we affixed the abdomen to the wax of the holder by using a small soldering iron to melt the paraffin at the sides of the fly's abdomen, connecting the wax to the fly. Then we used the finer forceps (Dumoxel Nr. 5) to grab the fly's proboscis, pulling and stretching the fly forward carefully, and finally fixing the proboscis to the holder by melting wax with the soldering iron. This moved the fly into

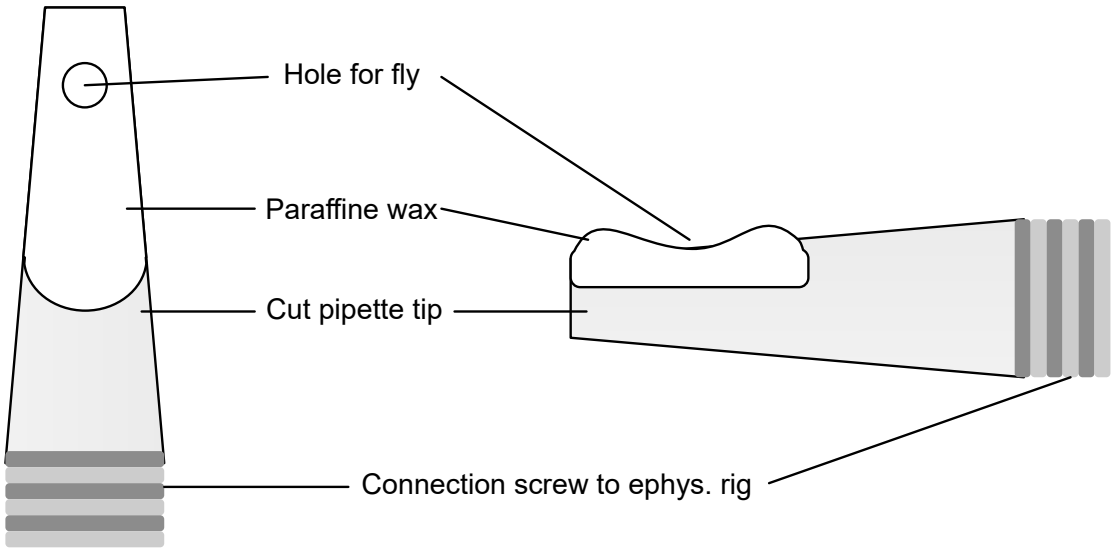

Figure 3.1: **Fly holder we used in the experiments.** The fly holder was constructed using a 1000 µl micropipette tip, paraffin wax and a setscrew. **Left:** top-down view; **right:** side view.

the correct position and reduced movement of the fly during the recording. The fly's neck would be in a lightly overstretched position after this. Next, we fixed the thorax of the fly by melting the paraffin wax underneath it, using the soldering iron, and connecting it to the thorax. Lastly, to immobilize the connection between the head and the thorax, we applied a drop of UV-adhesive on the neck of the fly (using an injection needle) and hardened it using UV light. At the end of this preparation the fly was fixed in the holder like illustrated in Figure 3.2.

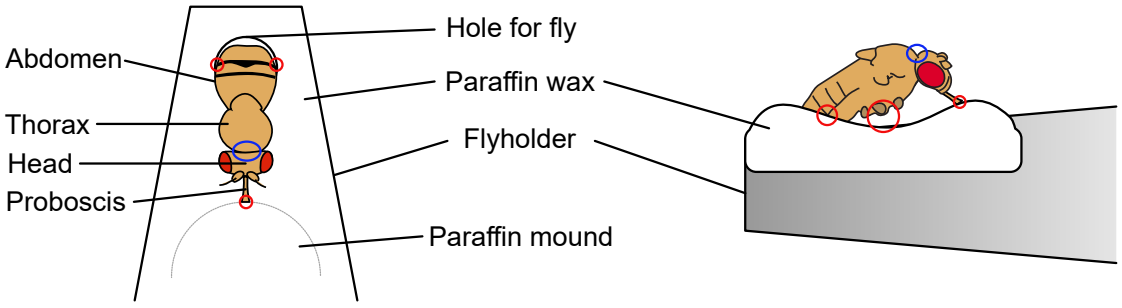

Figure 3.2: **Schematic of fly fixation inside the fly holder. Left:** top-down view; **right:** side view. Red circles indicate the use of the soldering iron to fix the fly with paraffin wax. Blue circles indicate the usage of UV-adhesive to fix the position of the fly's head.

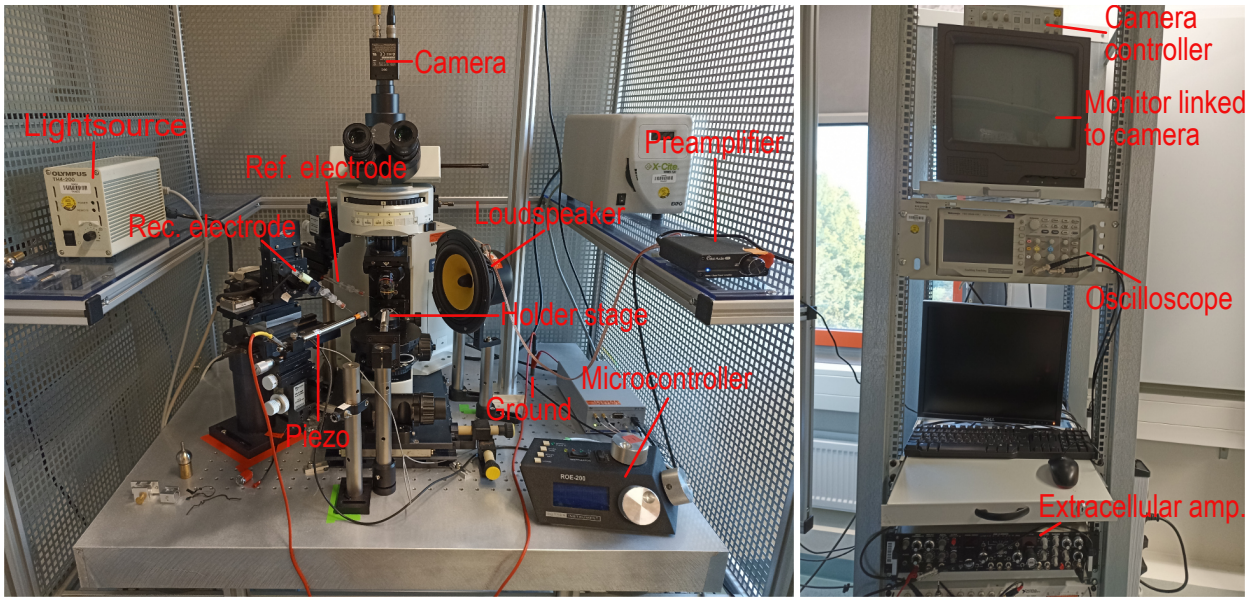

Figure 3.3: **Photo of the electrophysiology setup. Left:** Experimental setup; **right:** Monitoring setup, amplifier and PC for experiment control.

3.1.5 Preparing the electrophysiology rig and connecting the fly

The rig was set up for current clamp extracellular recordings (see Figure 3.3). The settings of the amplifier were as stated in the table below Table 3.2. The preamplifier of the speaker was set to ca. 75 % power. The electrodes were mounted on micromanipulators. Details concerning the components of the rig can be found in the material list (Table 2.4).

The flyholder was fixed in the rig using the screw, attached of the holder. The glass tips for the electrode were filled with saline (see Table 2.2) and placed over the silver wire electrodes. After placing the glass tips the amplifier was switched on so it could warm up during the time it took to prepare and fix the fly. Then, we placed the reference electrode in the eye of the fly, at an angle of around 45° from the fly and almost 90° from the base of the rig. Next, we placed the recording electrode in the base of the antenna, at an angle of around 20° from the centerline of the fly and 30° from the base of the rig. The electrode was pushed forward to penetrate the membrane where the fly's antenna meets the cuticle of its head (see Figure 3.4). If the placement was done correctly a change of the signal could be observed on the oscilloscope. Instead of the humming of the rig, it then showed a finer structured signal from the proximity to the fly's JONs. Furthermore, we confirmed the placement by playing a short test playlist, consisting of the same repeating pulse, and looking for a corresponding response using the oscilloscope.

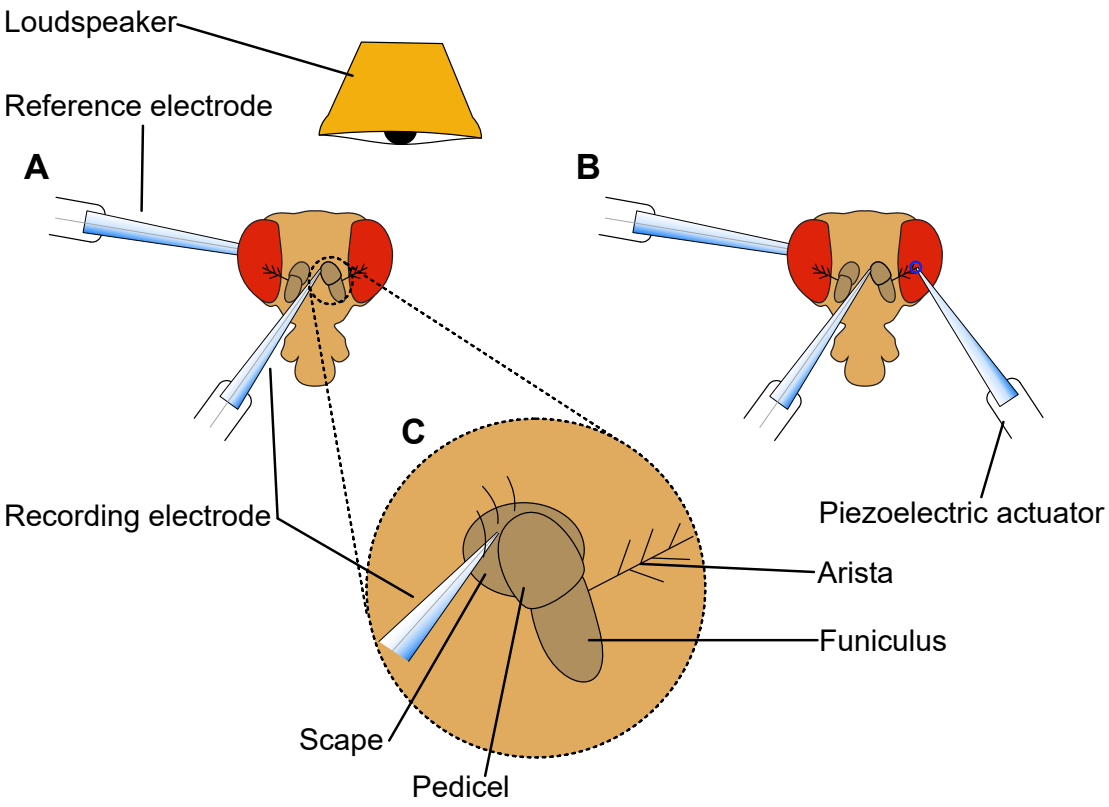

Figure 3.4: **Schematic of the electrode and stimulus source placement during the experiments.** **A:** Electrode placement during experiments using the loudspeaker. **B:** Placement electrodes and the piezo during experiments using it as stimulus source. The glass tip of the piezo was glued to the arista tip, as indicated by the blue circle. **C:** More detailed view of where the recording electrode was placed at the antenna base.

Potential output filter (lowpass)	5000 Hz
Potential output filter (highpass)	1 Hz
Potential output gain	1000
Current output sensitivity	10 V/nA
Current output filter (lowpass)	3000 Hz

Table 3.2: Settings of the extracellular amplifier

3.1.6 Pulling electrode tips

We pulled the electrode tips from thin walled 4 " glass capillaries (Fil 1.5 mm) using a model P-97 horizontal puller from Sutter. While the exact shape of the tips was shown to not influence our recordings to a recognizable degree, we took to using a broader tip for the reference electrode and finer, sharper tips for the recording electrodes, which could easier penetrate the membrane where the antenna entered the head cuticle. First the necessary temperature to melt the glass capillaries was determined by running a ramp test. The actual heat values used would change if the filament of the puller was changed, since the ramp value would differ. Usually we pulled the tips of the reference electrode at a heat setting 5 units lower than the ramp value and at a velocity setting of 40. The heat setting for the tips of the recording electrode was usually set to the ramp value or 5 units above it. Also the velocity setting was put 20–30 units higher than the one used for the reference electrode tips. Furthermore, for the mean adaptation experiments a glass tip was attached to the piezo actuator. This tip was pulled using the same settings as the recording electrodes, but its tip was covered with a thin layer of paraffin wax for better placement of the UV-adhesive. For the actual numbers used in our experiments refer to Table 3.3.

Ramp value:	605			
Electrode	Heat	Pull	Velocity	Time
Reference	600	-	40	250
Recording	610	-	70	250
Piezo	610	-	70	250

Table 3.3: Sutter horizontal puller settings

3.1.7 Stimulus design

Different stimuli were used in the experiments to probe specific aspects of the JON response. They will be further referred to in the thesis as seen in this subsection. The intensities of the stimuli were chosen based on the intensity tuning of *Drosophila melanogaster*, so that they were neither too soft nor too loud to be picked up by the flies. All stimuli types, probing adaptation, were constructed using the same principle. In the beginning adaptation was induced, on different levels (variance or mean adaptation). Next, followed a probe phase where stimulus feature (sound or static deflection) was changed. During the probe phase the changes in sensitivity induced by the adaptation, to the same or the other stimulus feature, was measured. So, depending on the stimulus, an adaptation phase containing a variance adaptation feature (sound) could be followed by a probe phase either containing another

variance adaptation feature (sound) or a mean adaptation feature (static deflection), or vice versa. Probe stimuli on many different levels were used to get complete tuning curves for each adaptation level. The various differences in intensity resulting from the different adaptation and probe phases were referred to as "steps". In the case of stimuli having one step introducing variance or mean adaptation and then probing with the other stimulus (mean/variance adaptation interaction and variance/mean interaction stimuli), was used to observe the interaction of the two mechanisms of adaptation with one another.

Noise intensity tuning. 12 stimuli of band-limited Gaussian white noise with varying fine structures (to avoid artifacts) and different fixed intensities ($\frac{1}{128}$, $\frac{1}{64}$, $\frac{1}{32}$, $\frac{1}{16}$, 0.125, 0.25, 0.5, 1, 2, 4, 8, 16 mm/s), each lasting 5 s (see Figure 3.5). These stimuli were used to estimate the intensity tuning to white noise stimuli of the flies.

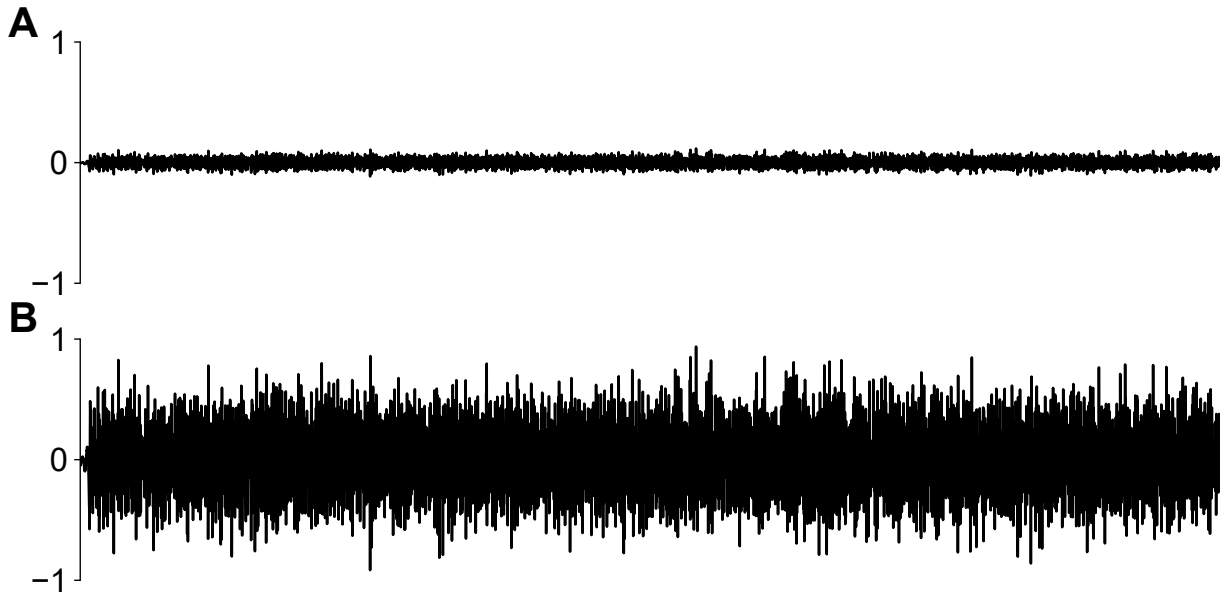

Figure 3.5: **Example of the noise stimuli used to determine intensity tuning. A:** Lower intensity noise stimulus. **B:** Noise stimulus of the same structure and length, but with a higher amplitude.

Sinusoid intensity tuning. 12 pure tone stimuli (sinusoids) each with a fixed frequency of 250 Hz, a phase of 0 rad and a duration of 500 ms, but each at a different intensity ($\frac{1}{128}$, $\frac{1}{64}$, $\frac{1}{32}$, $\frac{1}{16}$, 0.125, 0.25, 0.5, 1, 2, 4, 8, 16 mm/s) (see Figure 3.6). These stimuli were used to look into the intensity tuning to pure tone stimuli in the flies.

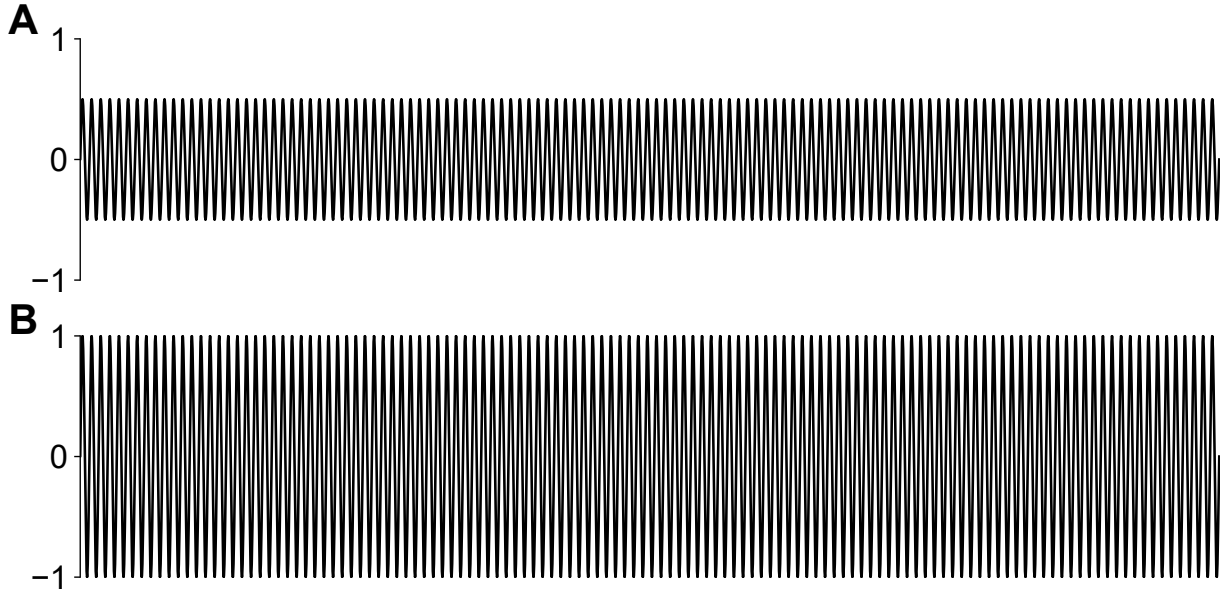

Figure 3.6: **Example of pure tone stimuli used to determine intensity tuning. A:** Lower intensity pure tone stimulus. **B:** Pure tone stimulus of the same frequency, but with a higher amplitude.

Sinusoid frequency tuning. 6 sinusoids each with a fixed intensity of 4 mm/s, a phase of 0 rad and a duration of 500 ms, but each with a different frequency (100, 200, 300, 400, 500, 600 Hz) (see Figure 3.7). These stimuli were used to look into the frequency tuning to pure tone stimuli in the flies.

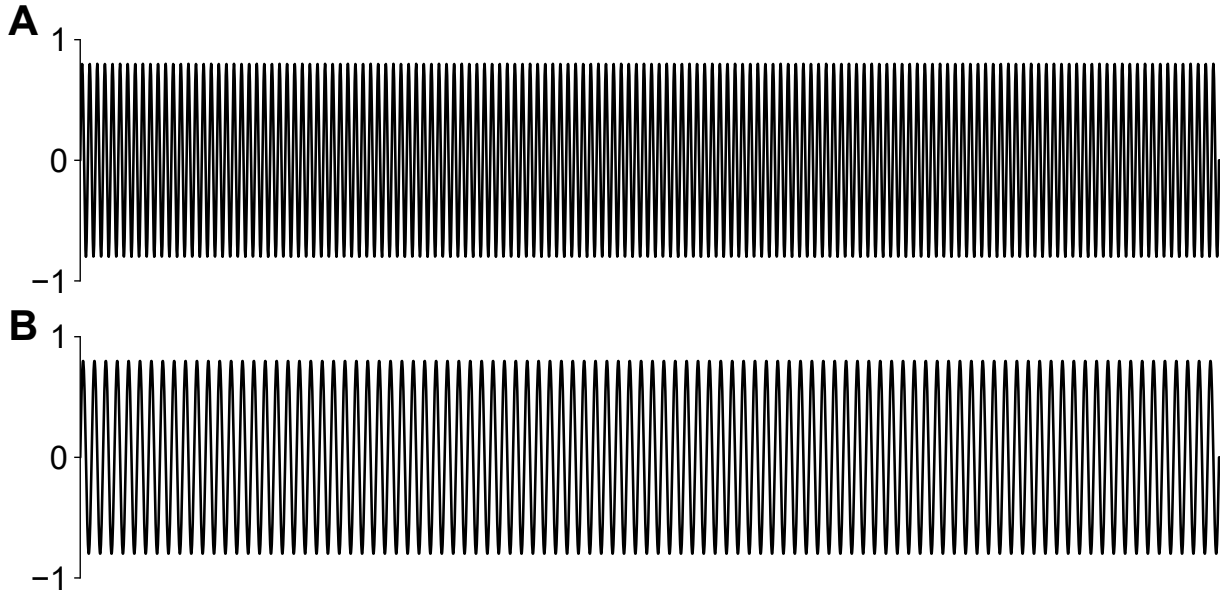

Figure 3.7: **Example of pure tone stimuli used to determine frequency tuning. A:** Pure tone stimulus with a higher frequency. **B:** Pure tone stimulus with the same amplitude, but a lower frequency.

Variance adaptation stimulus. 400 stimuli of band-limited (80–1000 Hz) Gaussian white noise with different fine structures, each 57 s long. The difference in the fine structures was intended to prevent possible artifacts from a reoccurring fine structure. The stimuli changed their intensity between 0–16 mm/s in different sized steps (0.5, 1.0, 1.5, 2.0, 3.0, 3.5 mm/s), steps from a higher to a lower intensity are represented as negative numbers (see Figure 3.8). These stimuli were used to probe variance adaptation dynamics.

Figure 3.8: **Example of the stimuli used for probing variance adaptation. A:** One iteration of the noise stimuli used to probe variance adaptation. **B:** Another iteration of the stimulus with a different fine structure to prevent artifacts.

Mean adaptation stimulus. The stimuli induced by the piezo described from here on have no fine structure, but are static deflections of the antenna. First, one of seven adaptation steps was applied for 20 ms via a piezo actuator (displacing the arista for -1, -0.5, -0.25, 0, 0.25, 0.5 or 1 µm, negative values stand for backwards movement of the piezo, positive values stand for forward ones). Then, one of 15 probe steps was applied for 20 ms (0, $\frac{1}{8}$, 0.177, $\frac{1}{4}$, 0.354, 0.5, 0.707, 1 µm, the same steps also existed as negative values) (see Figure 3.9). All combinations of adaptation step intensity and probe step intensity existed as stimuli variant. The total length of the stimuli was 120 ms and after the probe step the displacement changed to 0 µm for the rest of the stimulus duration. These stimuli were used to probe the dynamics of mean adaptation.

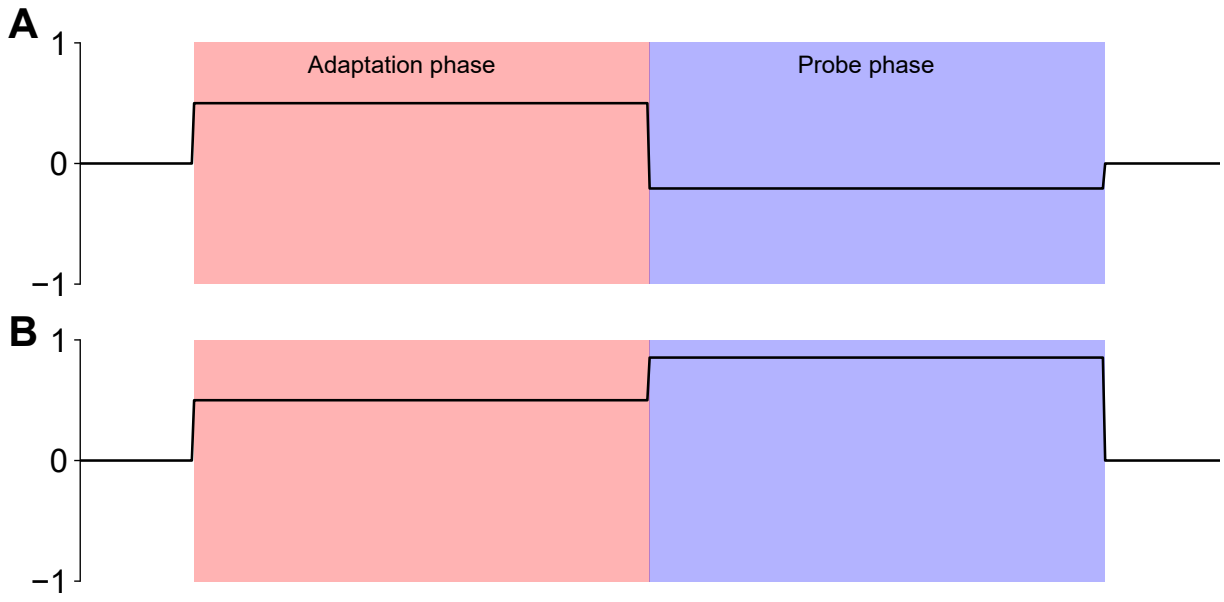

Figure 3.9: **Example of stimuli used to probe mean adaptation dynamics. A:** One version of the static deflection stimulus, used to probe mean adaptation. **B:** Another version of the static deflection stimulus, with the same adaptation step, but a different probe step. The period the adaptation step was presented (Adaptation phase) is indicated in red, the period the probe step was added (Probe phase) is indicated in blue.

Mean/variance adaptation interaction stimulus. First, one of eight adaptation steps (0, $\frac{1}{8}$, 0.177, $\frac{1}{4}$, 0.354, 0.5, 0.707, 1 µm, the same steps also existed as negative values) was applied for 50 ms via a piezo actuator. Then, a sinusoid probe step with a frequency of 300 Hz and a phase of 0 rad was applied for 50 ms, the probe step had one of five displacement magnitudes ($\frac{1}{16}$, $\frac{1}{8}$, $\frac{1}{4}$, 0.5 or 1 µm) (see Figure 3.10). All combinations of adaptation step intensity and probe step intensity existed as stimuli variant. These stimuli were used to look into the influence of mean adaptation on variance adaptation.

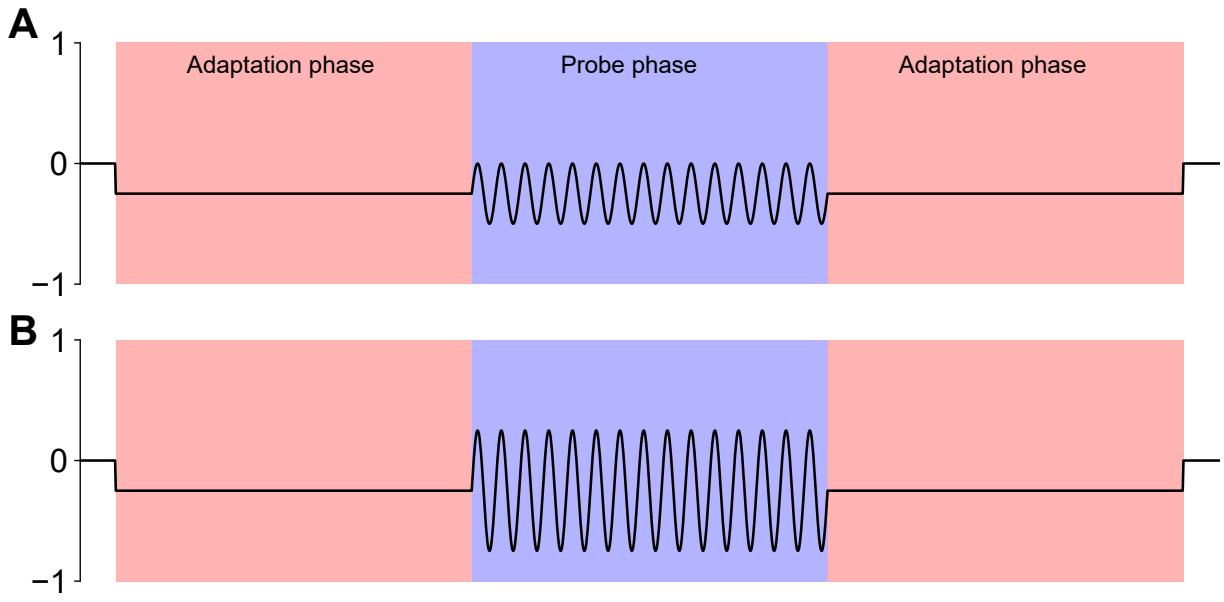

Figure 3.10: **Example of stimuli used to determine influence of variance adaptation on mean adaptation dynamics. A:** Example of the stimuli used to probe the interaction of mean and variance adaptation. The adaptation step was induced by a static deflection, while the probe step was induced through a sinusoid stimulus with a fixed frequency. **B:** Another version of the stimulus, with the same adaptation step, but a higher amplitude probe step. The period the adaptation step was presented (Adaptation phase) is indicated in red, the period the probe step was added (Probe phase) is indicated in blue.

Variance/mean adaptation interaction stimulus. First, a sinusoid adaptation step with a frequency of 300 Hz and a phase of 0 rad was applied via piezo for 50 ms, it had one of five displacement magnitudes (displacement: $\frac{1}{16}$, $\frac{1}{8}$, $\frac{1}{4}$, 0.5 or 1 µm). Then, one of eight step stimuli (displacement: 0, $\frac{1}{8}$, 0.177, $\frac{1}{4}$, 0.354, 0.5, 0.707, 1 µm, the same steps also existed as negative values) was applied as probe step for 50 ms (see Figure 3.11). All combinations of adaptation step intensity and probe step intensity existed as stimuli variant. These stimuli were used to look into the influence of variance adaptation on mean adaptation.

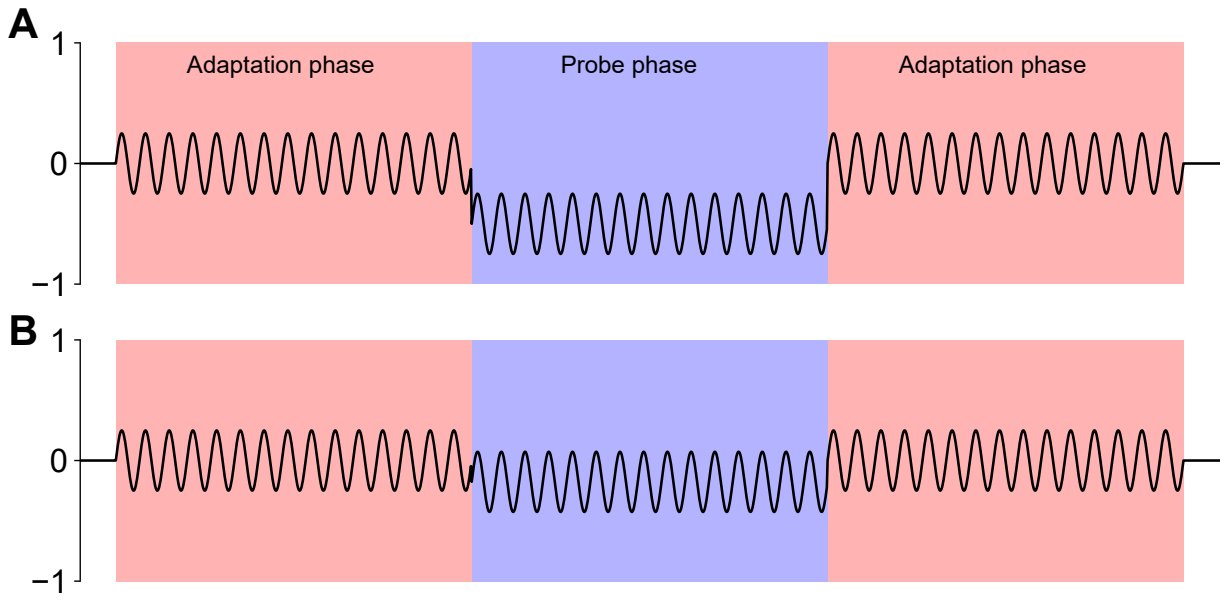

Figure 3.11: **Example of stimuli used to determine influence of mean adaptation on variance adaptation dynamics. E**xample of the stimuli used to probe the interaction of variance and mean adaptation. The adaptation step was induced using a sinusoid stimulus with a fixed frequency. while the probe step was induced by a static deflection. **B:** A different version of the stimulus, with the same adaptation step, but a smaller deflection during the probe phase. The period the adaptation step was presented (Adaptation phase) is indicated in red, the period the probe step was added (Probe phase) is indicated in blue.

3.1.8 Stimulus delivery

The angle of the loudspeaker to the arista had a big impact on the correct delivery of the stimulus, therefore it was important to align the arista and the loudspeaker as parallel as possible when placing and adjusting the fly in the rig. The loudness of the stimuli was calibrated prior to the experiments, so the magnitude of a stimulus was as intended when it would reach the fly. To achieve this we placed a pressure gradient microphone in the position of the fly and recorded the different kinds of stimuli we planned on using, recorded their actual magnitude and compared them to the intended values. The microphone was calibrated using a laser vibrometer (by Dr. Phillip Hehlert from the Göpfert lab). Based on the measurements with the microphone we calculated attenuation values to correct the loudness of the speaker for the pure-tone stimuli. The system was tuned for the white noise stimuli by adjusting the power of the preamplifier until the stimuli had the right amplitude. The sound was delivered using: A DAQ card (PCIe-6323), a mono channel amplifier (Douk Audio G4) and a loudspeaker (HP Cone Swans F6, 8 Ω impedance, 88 dB). To probe mean adaptation the stimuli were delivered using a piezo actuator instead of the loudspeaker. A

glass tip was attached to the piezo and connected to the arista we recorded from by placing a small drop of UV-adhesive at the tip and contacting the tip of the arista. The adhesive was then cured with UV light. It was important that the piezo tip was perpendicular to the arista, so that the deflection could be applied properly.

3.1.9 Experiments for probing variance adaptation

The fly and the rig were prepared as described above and the electrodes were placed into the fly. After the setup was ready all unnecessary electronics (e.g. lights, camera, etc.) were shut off to prevent noise. We started the protocol, left the room and carefully closed the door. The stimulus protocol for variance adaptation experiments ran for about one hour. Before and after each stimulus we played 1 s of silence. The rig again recorded the JONs response with a sampling rate of 10 kHz. The playlist used in this protocol contained all 400 variations of the variance adaptation stimulus. Furthermore, the playlist included ten iterations of all 12 variations of the noise intensity tuning stimulus. Lastly, the playlist also included the 12 variations of the sinusoid frequency tuning stimulus and of the six variations of the sinusoid intensity tuning stimulus. Both were also repeated 10 times. For a detailed description of all stimuli see subsection 3.1.7.

3.1.10 Mean adaptation probing experiments

For experiments probing mean adaptation the fly and rig were prepared as described above. Furthermore, we connected a glass tip to the piezo actuator placed in the rig. The glass tip was fixed to the fly's antenna using a small drop of UV-adhesive.
The movements of this piezo actuator were used to apply stimuli, instead of the loudspeaker. The playlist had 80 ms of no deflection before and after each stimulus. The playlist included 100 iterations of every variation of the mean adaptation stimulus. Furthermore, the playlist contained 100 iterations of all variations of the mean/variance adaptation interaction and variance/mean adaptation interaction stimuli. For a detailed description of all stimuli see subsection 3.1.7.

3.1.11 Piezoelectric actuation

A model P-841.60 preloaded piezo actuator and a model E-625 piezo servo controller from Physik Instrumente were used for the piezoelectric actuation in the mean adaptation experiments. To stay within the operational range of the piezo driver during the step deflections of the mean adaptation probing stimuli (see subsection 3.1.7), these were low-pass filtered using a 1 ms Gaussian window.

3.2 Data analysis

3.2.1 Processing variance adaptation data

First we extracted response transients from the 400 white noise stimuli (see subsection 3.1.9). We calculated the envelope for every data set by calculating its root mean squared envelope (RMS) and then corrected for the offset from the baseline created by this process. For the calculation of the RMS a Gaussian filter (F) was defined with a length of 40 ms and a standard deviation of 0.8 ms. Then the RMS was calculated using the following equation were x is the envelope and convolution was denoted by an asterisk: $\sqrt{x(t)^2 * (F(t)/\Sigma F(t))}$. Next, we had to extract the response transients for the different stimulus intensities out of the complete envelope of the response. Therefore, we separated the envelope of the stimulus and response into 140 ms chunks, by cutting them 20 ms before a step in intensity, which persisted for 100 ms, and then again 20 ms later. Furthermore, the 1 s of silence before and after the complete stimuli were cut out. Envelope chunks with very low or high stimulus intensities were excluded. This was done due to the fly's auditory system going into saturation during stimuli with too great intensities or being sub-threshold for a response in the case of too small intensity. The mean of the full chunk across the different versions (fine structures) of the variance adaptation stimulus was calculated for further analysis. This was done individually for each step size. Furthermore, due to the possibility of the recording quality changing over time for a number of reasons (e.g. electrode drift, declining fly health or outside vibrations) we checked the response envelope for stability of the recording. We did this by comparing the difference between the mean of the response envelope to the 400 consecutive white-noise stimuli. This provided us with a measure of the stability of the performance over time, since the mean should not vary greatly. First, we separated the response envelope by step size and calculated the individual means for every instance of the variance adaptation stimulus. This created a list for every step size with 400 entries from the earliest instance of the stimulus to the last in the playlist. We used either the first or the last 22 envelope means of each step size as reference, depending on which one had the

smaller standard deviation. The standard deviation of the envelope means was checked for each step size in increments of 50 envelope means. If more then half of the envelope means for a step size had a standard deviation more then 2.24 times the standard deviation of the reference these envelope means and all following ones were discarded. This threshold was chosen based on best practice recommendations concerning outliers (Aguinis et al., 2013). We also calculated the signal-to-noise ratio (SNR), a measure of the strength of the recorded signal relative to the background noise, to determine the quality of the recording. We estimated the noise by calculating the mean of the envelope between 100–900 ms (during the silence in the beginning of the stimulus) for each of the noise intensity tuning stimuli with an intensity of 16 mm/s. The signal was estimated by calculating the mean of the response envelope between 1000–4000 ms for the same stimuli. A SNR was calculated for each stimulus using the following formula: SNR = $|signal|/|noise|$. Finally we calculated the median of all the different SNRs to get one measure for the whole recording.

Furthermore, we estimated the frequency and intensity tuning of the flies. To estimate frequency tuning we calculated the mean of the response envelope between 1000–1500 ms for all the sinusoid frequency tuning stimuli of the different frequencies. The noise intensity tuning was estimated by extracting the maximum value of the response envelope for all the noise intensity tuning stimuli variants. Next, we calculated the mean of the maximum value over the repetitions of said stimuli.

3.2.2 Processing mean adaptation data

We constructed the response envelope, corrected the offset and chunked the response envelope for the response data from the mean adaptation stimuli, the mean/variance adaptation interaction type stimuli and the variance/mean adaptation interaction stimuli (see subsection 3.1.10) like we did for the data from the variance adaptation experiments (see subsection 3.2.1), while taking the difference in stimulus length and silence pre and post stimulus into account. Furthermore, we calculated the intensity tuning curves for further analysis. The curves with an adaptation step of -1.0 and 1.0 µm were omitted because they shifted visibly compared to the rest of the data. We deemed this to be a artifact, most likely caused by the great range of motion (problems with the coupling between the piezo and the antenna), since if it was an effect of change in mean adaption dynamics of the fly we would have observed a shift for all adaptation steps. Furthermore, this behavior was observed not just in mutants but also wild type flies.

3.2.3 Estimating the timescale of variance adaptation

To estimate the timescale of adaptation we fit an exponential curve to the trial-averaged traces of the different step sizes (see subsection 3.2.1) using the non-linear least squares method. The function $r(x) = gain * \exp(tau * x)$ was fit to the falling or rising phases of the negative or positive transients (see Figure 3.12B). The variable x was defined as the time between smallest CAP amplitude and the highest CAP amplitude in 20 ms. Lower/upper bounds and initial values, used as starting point for the fitting algorithm, (p_0) for $gain$ and tau were defined: $gain = -10$ to 10, $p_0 = 1$; $tau = -0.25$ to -0.025, $p_0 = -0.1$. The tau extracted from these fits was used to calculate the timescale of variance adaptation using the formula: $timescale = -1/tau$ (see Figure 3.12C). The smaller the resulting timescale was the faster was the adaptation (see Figure 3.14A). After inspection of the data we observed that the data for the step sizes –3.5, –1.5 and -0.5 mm/s tended to have bad fits. Since the difference of the onset depression and the steady state in the CAP for the negative step sizes were not as strong the difference between the onset peak and the steady state for the positive step sizes, these steps might have been more affected by noise, hence the bad fit. Therefore, we decided to omit these three steps sizes from further analysis.

3.2.4 Estimating the strength of variance adaptation

The strength of adaptation was estimated by comparing the slopes of the onset (s_{on}) and steady-state (s_{ss}) intensity tuning curves (see Figure 3.13). These slopes were estimated by calculating the average change of onset/steady state over the different steps: $s_{on} = \text{mean}(\Delta\text{onset}/\Delta\text{steps})$ and $s_{ss} = \text{mean}(\Delta\text{steady state}/\Delta\text{steps})$. $1 - s_{on}/s_{ss}$ approached 0 for no adaptation and 1 for complete adaptation respectively (see Figure 3.14B). This way of measuring the strength of adaptation made it independent of response magnitude.

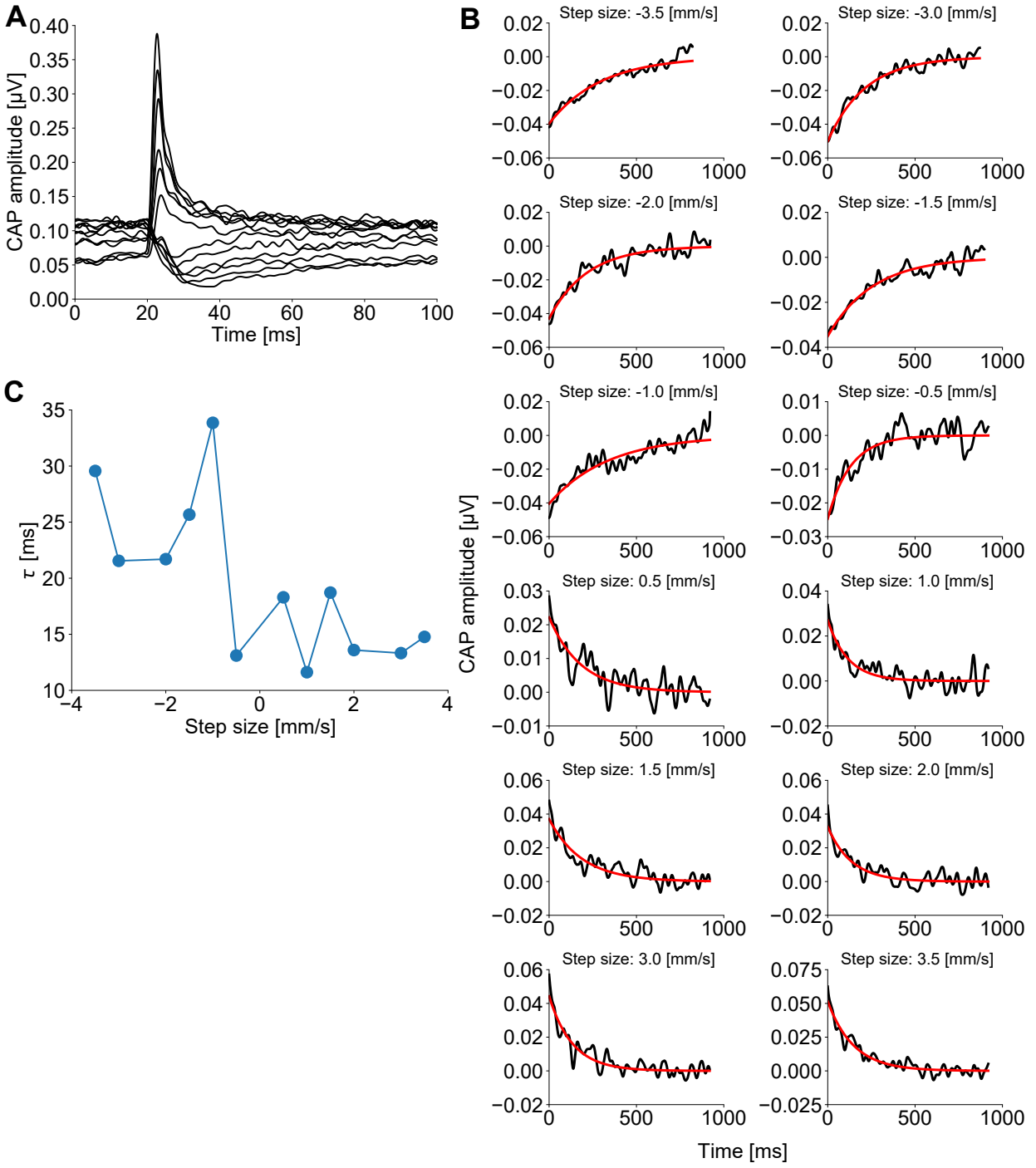

Figure 3.12: **Extracting the speed of variance adaptation from the envelope of the CAP response. A:** Example CAP envelopes of one fly, to which exponential curves would be fitted. **B:** Zoomed in look of the envelopes (black). The fitted curves (red) would be starting at either the minimal value (for negative transients) or at 28 ms of the envelope (for positive transients). The timescale of the fitted curves was then extracted. **C:** The τ was calculated from the timescale for each step size ($\tau = -1/\text{timescale}$).

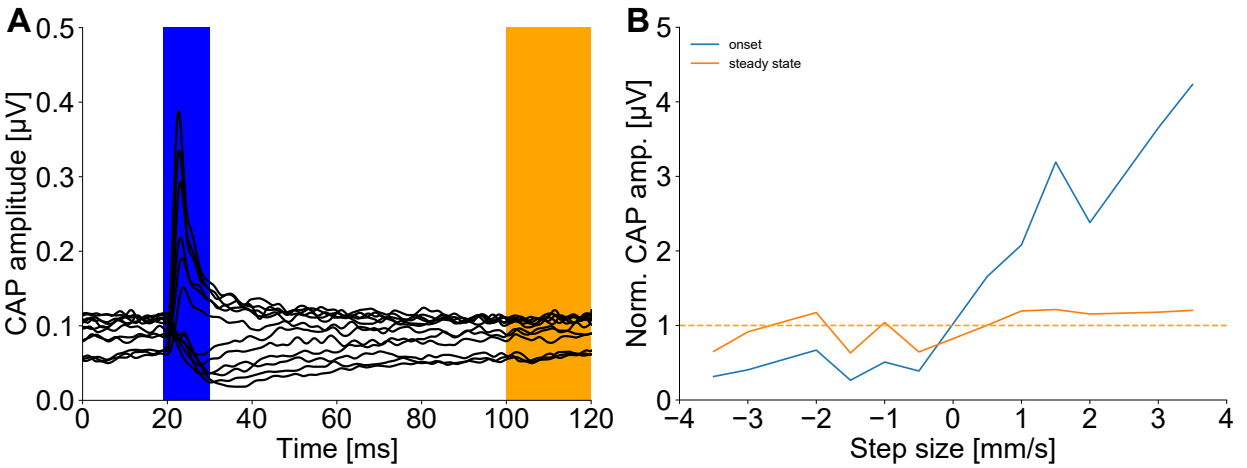

Figure 3.13: **Calculating the strength of variance adaptation from the CAP envelopes. A:** Example CAP of one fly. The onset values were taken from the lowest/highest value within the time window indicated in blue. The steady state values were the mean of the values within the time window indicated in orange. **B:** Intensity tuning curves of the onset (blue) and steady state (orange) for the different step sizes, the values were normalized so that the steady state averaged 1, which is indicated by the dotted orange line. Adaptation strength was based on the slopes of these curves (strength of adaptation $= 1 - s_{on}/s_{ss}$).

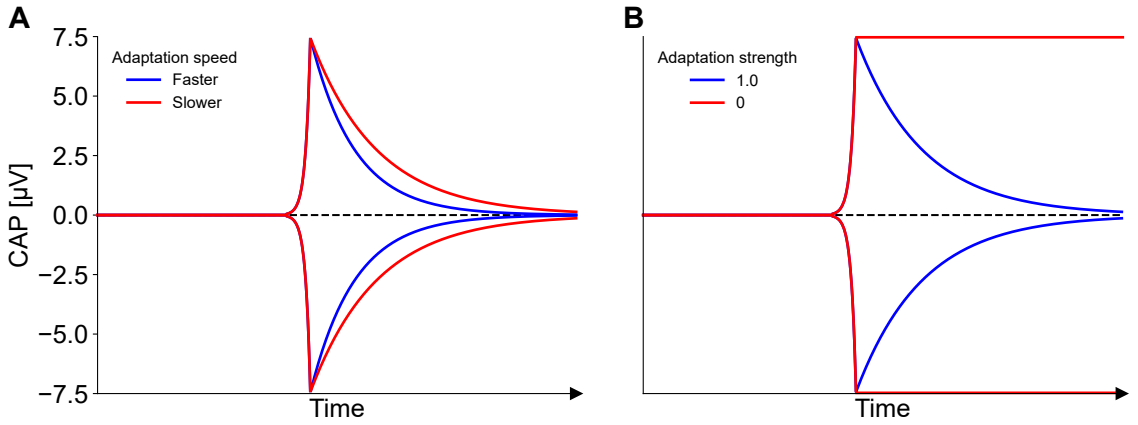

Figure 3.14: **Example of different variance adaptation dynamics. A:** The speed of adaptation was estimated looking at the steepness of the response envelope curves. If the curve was steeper (indicated in blue) the adaptation was faster than in less steep curves (indicated in red). **B:** Strength of adaptation was estimated by comparing the response during the steady state vs the response during the peak of the response envelope. A strength of adaptation of 1 (shown in blue) would mean complete adaptation, so the curve returning to steady state levels after the peak. A strength of 0 (shown in red) on the other hand means no adaptation at all, so the curve would just continue at peak levels. So strength of adaptation would fall between a value of 0–1, depending on the completeness of adaptation.

3.2.5 Estimating the curve shift of tuning curves in mean adaptation experiments

In order to estimate the curve shift in the mean adaptation data (for every adaptation step) we calculated the mean of the CAP amplitude of the tuning curves, for probe steps of the same magnitude (negative and positive) (see Figure 3.15). They were basically folded over, which transforms the tuning curves seen in Figure 3.15B, in the sigmoidal shaped curves seen in Figure 3.15C. We then fit the sigmoidal function $r(x) = (r_0 + r_{max})/(1+\exp(-\alpha(-x/\beta)))$ to these traces, where $r(x)$ is the CAP amplitude, r_0 and r_{max} denote the minimum and maximum CAP amplitude respectively. α denotes the slope and β denotes the shift of the curve. The amplitude of the fitted curve was limited by bounds set dependent on the trace it was fitted to, which were used as initial conditions for the fit. The lower bound was defined as the smallest absolute value of the trace and the upper bound was defined as the biggest value, these bounds limited the parameters during the fit. We also set the initial condition of the slope of the fits by first fitting to the tuning curve with an adaptation step of 0 µm and extracting the slope. Initial guesses and lower and upper bounds for the fit to the tuning curves were: r_0 =0 to r_-, $p0 = r_-$; $r_{max} = 0.8 * r_+$ to *upperbound*, $p0 =$ *upperbound*; $a = 0.8 * slope$ to ∞, $p0 = slope$; $b = -\infty$ to ∞, $p0 = 1$. r_- denotes the smallest value of the tuning curve, while r_+ denotes the biggest one. The tuning curve shift was extracted from the β parameter of these fits.

The curve shift (β) we extracted from those fits describes how much the midpoints of the tuning curves shifted with the different adaptation steps. So this parameter could also be called the midpoint The slope of the midpoint plotted against the adaptation steps was used to estimate the magnitude of this change. In a case of no mean adaptation the slope of the tuning curves would become less steep according to the size of the adaptation step (see Figure 4.9), which would lead to an increased magnitude of the shift (see Figure 3.15D). Finally, the slope of this shift for the different adaptation steps (as depicted in Figure 3.15D) would also change accordingly.

3.2.6 Estimating the speed of mean adaptation

The speed of mean adaptation was estimated by measuring the highest value of the CAP envelopes, between 20–30 ms after the beginning of the adaptation step and calculating the time for the response to decay to 37 % of its maximum value (see Figure 3.15A). When the peak of the curve was very small this could yield a tau of 0 mm/s, which was consequently omitted.

3.2.7 Estimating the strength of mean adaptation

The strength of mean adaptation was calculated by comparing the average slopes of the tuning curves of the peak (absolute maximum value during 5–10 ms of the trace) and steady state (absolute mean of values during 100–120 ms of the trace) of all CAP envelopes with a probe step size of 0 (see Figure 3.15A). Following the same formula as used for calculating the strength of variance adaptation (see subsection 3.2.4).

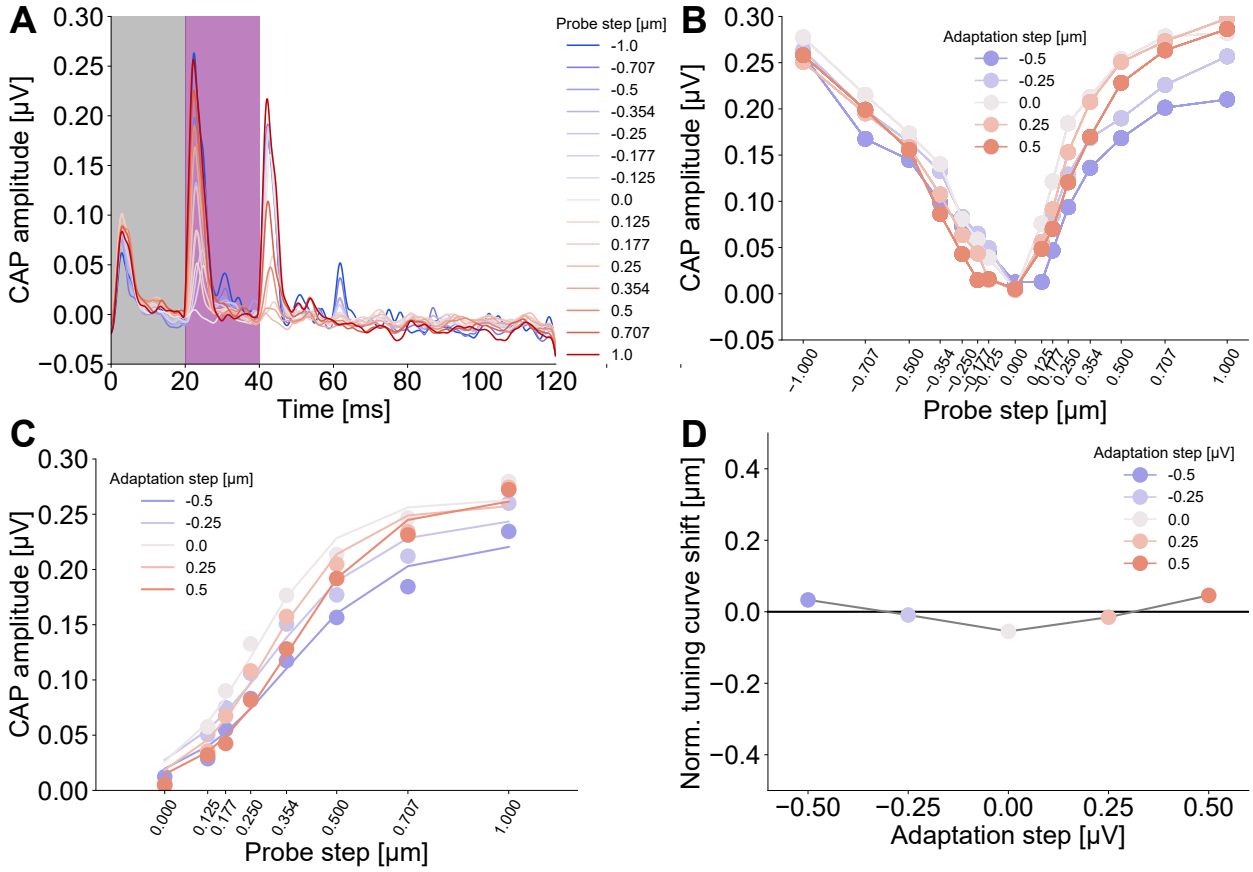

Figure 3.15: **Extraction of the measures of mean adaptation from the data. A:** CAP envelopes of the response traces measured in the mean adaptation experiments. The grey area indicates the phase when the adaptation step was introduced and the purple area denotes the time window of the probe step. The depicted traces are responses to different probe steps (color coded, see legend) for an adaptation step of 20 ms. The probe step denotes the change relative to the adaptation step, not the absolute deflection of the antenna. **B:** Intensity tuning curves calculated from the peak response during the probe step (purple period in A). The colors indicate the size of the adaptation step used during the trace it was constructed from. The curves should look overall similar during normal adaptation. **C:** We plotted the tuning curves against the absolute value of the probe step. We then fitted the a sigmoidal curve to the data (lines) and extracted the shift of these from one another. **D:** The shift of the intensity tuning curves. When adaptation is impaired the shift should increase towards the edges, with increasing adaptation step size. We calculated the slope of this tuning curve shift. This slope should be near 0 during no shift and getting bigger the bigger the shift is getting. The data was normalized subtracting the mean of the data. The black line indicates a curve shift of 0 µm.

3.2.8 Statistics

We employed a linear mixed effects model, which can be used to deal with nonindependent or hierarchical data. This model incorporates fixed and random effects and deals with hierarchical data through individual regression of the different "groups" in the data. In the model the fixed effects generally are variables that are expected to have an effect on the dependent variable. Random effects on the other hand are themselves random variables like for example grouping factors. We made use of this model to deal with parts of our data being nonindependent e.g. the data of different step sizes for the same fly. For data where the different step sizes were pooled (e.g. the strength of variance adaptation data) we used an ordinary least squares model. Following model structures were used for the different kinds of data. The StatsModels package employed used Patsy to handle passing the formulas to the model. Therefore the the model is described using the passed pseudo code formula.

Screening speed of variance adaptation. Due to the hierarchical nature of the data separated by step sizes, we had to account for this when testing for significance. Therefore, a linear mixed effect model was employed with tau as the dependent variable and the genotypes as the independent variable, the WT was used as reference. The data was grouped for the individual flies. Step size was the random effect in this model with eight levels. The fixed effect were the 18 different genotypes. The tau data was ranked for use of the model since it required the residuals in the end to be normally distributed. Formula: 'Tau 1+C(Genotype, Treatment(reference="NM91"))'.

Screening strength of variance adaptation. An ordinary least squares regression model was applied with strength of adaptation as the dependent and the genotypes as independent variable. The fixed effect had one level. The strength of adaptation screening data was ranked. The appropriate control was used as reference (e.g. NM91) Formula: 'adaptation strength' + ' 1 + C(Genotype, Treatment(reference="NM91"))'.

Screening maximum response amplitude in variance adaptation data. An ordinary least squares regression model was also applied with the maximum amplitude of the response envelope as the dependent and the genotypes as independent variable. The fixed effect had one level. The appropriate control was used as reference (e.g. NM91) Formula: 'amplitude' + ' 1 + C(Genotype, Treatment(reference="NM91"))'.

The hit data set. We tested the speed and strength of variance adaptation in the second data set, referred to as "hit data set" using a Mann–Whitney U test, with a Bonferroni correction for multiple comparison correction. The maximum response amplitude was tested for significant differences in the same manner.

Slope of tuning curve shift of mean adaptation data. A linear mixed effect model was used with the slope of the curve shift as the dependent variable and the genotypes as independent variable. The fixed effect had one level. Formula: 'slope' + ' 1 + C(Genotype, Treatment(reference="NM91")) + C(Adaptation step)'.

Speed of mean adaptation. A linear mixed effect model was used with the τ as the dependent variable and the adaptation step as random effect. The fixed effect had one level and random effect had seven. Formula: 'τ' + ' 1 + C(Genotype, Treatment(reference="NM91"))'.

Strength of mean adaptation. An ordinary least squares regression model was applied with the strength of mean adaptation as the dependent and the genotypes as independent variable. The fixed effect had one level. Formula: 'adaptation strength' + ' 1 + C(Genotype, Treatment(reference="NM91"))'.

The residuals of the models were tested for normality using a Lilliefors test. Since the residuals were normally distributed the model was adequate to test for significance. The Benjamini-Hochberg-procedure was used for multiple comparison correction.

4 Results

4.1 The screening identified multiple candidate molecules affecting variance adaptation

First, we set out to find molecules involved in the processes of variance adaptation of *Drosophila melanogaster* by screening an assortment of mutant flies. The mutations were chosen based on our predictions concerning candidate molecules (see section 1.4) and compared to either a NM91 wild type fly or, if available, a control better matching to the mutants genetic background. One aspect of variance adaptation we looked at was its speed, by comparing τ for the different strains. We averaged the τ over the different step sizes described in the methods section. In the NM91 wild type we recorded a mean τ of $17.42\,\text{ms} \pm 2.5$. The other aspect was the strength of variance adaptation, calculated from the averaged traces of the different step sizes (see Figure 4.1A). The mean strength of adaptation we could observe in NM91 wild type flies was 0.87 ± 0.08. The strength of adaptation data of the wild type showed a sizable spread, this again could possibly obscure some of the effects of the mutants, especially if the effect size was on the smaller side. The descriptions of the different genotypes' τ and strength values, in the following sections, refers to the mean plus/minus its standard deviation. τ is illustrated as the mean over the τ measured for the different step sizes. τ, strength of adaptation values and percentages were rounded to two decimal places and p-values were rounded to four decimal places. The speed and strength of variance adaptation data shown was quantified as one point per fly, for an example about how these effects would look in the raw data refer to Figure 4.2. Complete tables of the p-values can be found in the appendix.

4.1.1 Potassium channels

We first looked into three major voltage-gated K^+ channel families in *Drosophila melanogaster*, Shaker, Slowpoke and Eag (Frolov et al., 2012). K^+ ion channels induce the repolarization of neurons and are able to change their excitability, by changing the potential inside. This

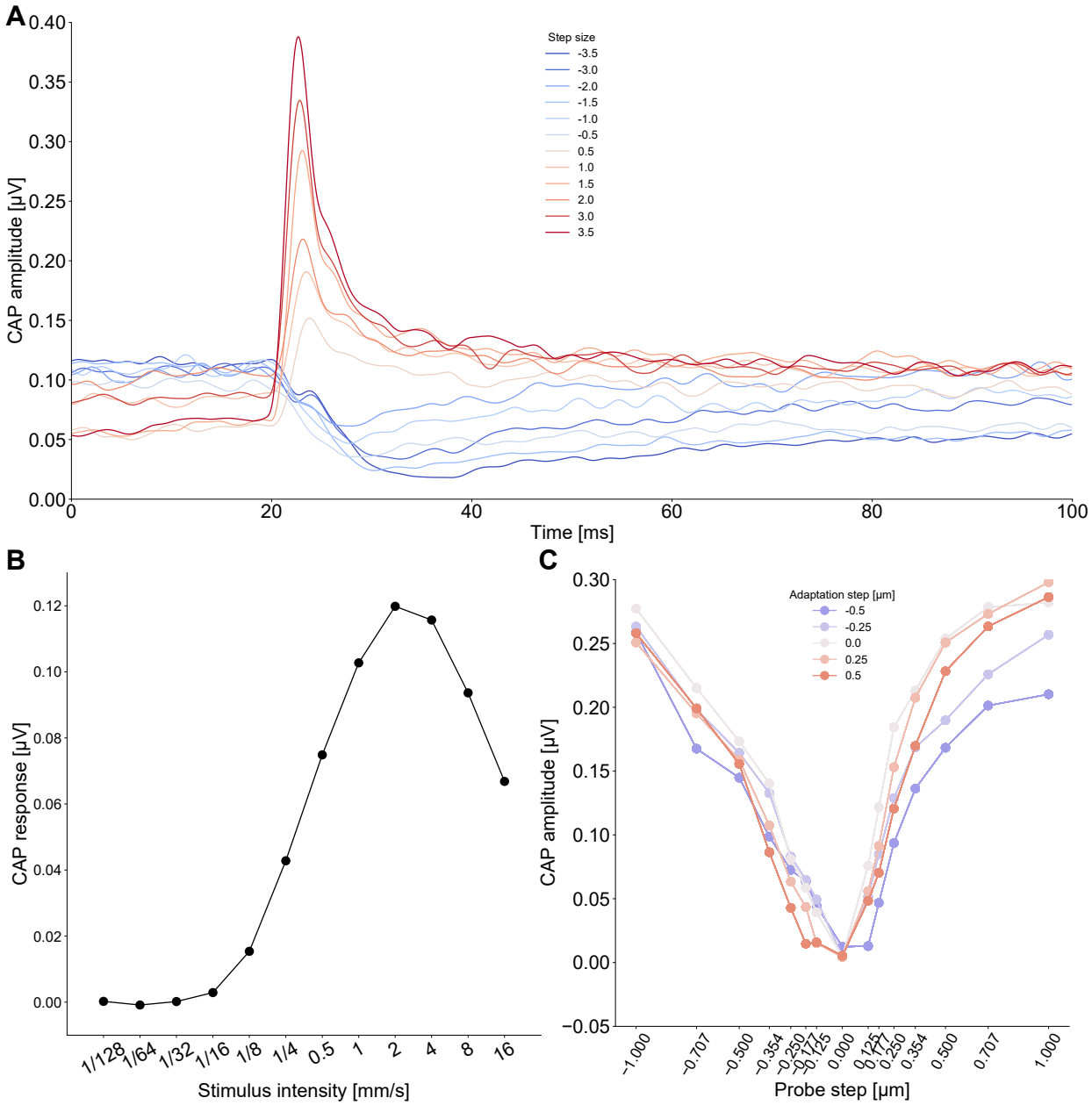

Figure 4.1: **Example of wild type CAP responses and tuning curves. A:** Example CAP traces of a NM91 wild type fly, from which the variance adaptation properties were extracted. The colors denote different step sizes (see legend). **B:** Example of NM91 wild type intensity tuning curve to noise stimuli. **C:** Example of NM91 wild type intensity tuning curve to static deflections, during different background intensities (see legend).

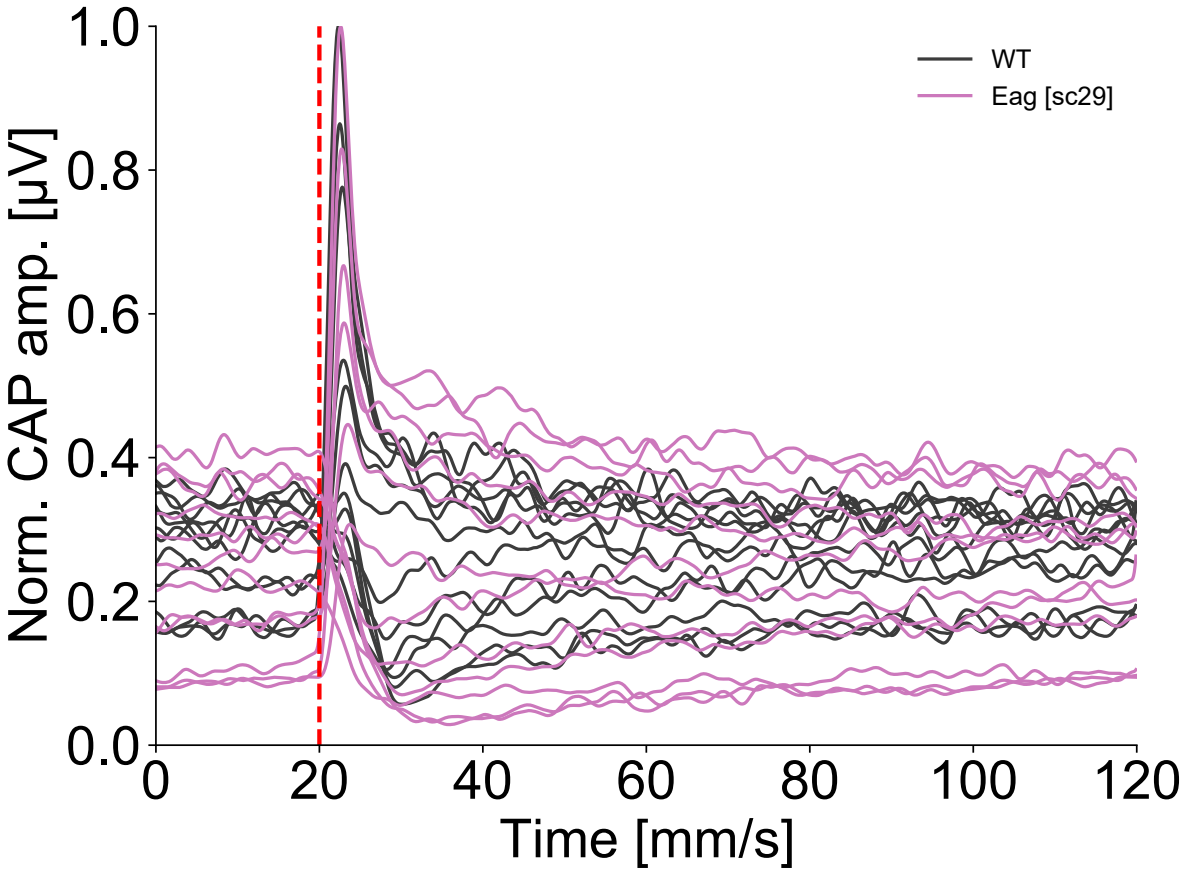

Figure 4.2: **Example for effect of impaired variance adaptation on CAP envelope traces.** The envelope traces of one NM91 wild type fly (black) and an Eag^{sc29} mutant fly (purple) to illustrate how a change in variance adaptation can affect the shape of the traces. Compared to the WT example the traces of the mutant example generally have a more gentle slope and fan out more during the steady state, which affects the speed and strength of variance adaptation respectively. The red dotted line indicates the time point of the change in stimulus intensity. The data was normalized by maximum scaling approach.

control of re- and hyperpolarization is a possible source of variance adaptation, also maybe in conjunction with Na^+ channel dynamics (Nagel et al., 2011; Ozuysal et al., 2012). Since expression in the JON would be a prerequisite this was controlled using a transscriptome from the Göpfert lab.

Tuning and CAP gain

The maximum CAP response was measured by taking the maximum response value measured for the biggest step size (3.5) in the corresponding CAP traces of the flies (see Figure 4.1A). The different strains all displayed different maximum CAP amplitudes, but nothing outside the range observed in the wild type (see Figure 4.3A). The PBac Slowpoke mutant showed the overall smallest response, but also the least variability, while the MiMIC variant had one of the highest overall responses. On the other hand this mutant also had a pretty substantial variability. The other K^+ channel mutants had a moderate response and standard deviation.

The intensity tuning curves of the screened K^+ channel mutants were very similar in their overall shape and the stimulus intensity which was sub-threshold (until 1/16 mm/s) and the point at which they went into saturation (4 mm/s) (see Figure 4.3B).

The shapes of the frequency tuning curves were also overall quite similar between the fly strains of this part of the screen (see Figure 4.3C). Most of the strains peaked at a frequency of 200 Hz. There were two exceptions, the $Shaker^5$ mutant already peaked at a frequency of 100 Hz and the Eag delta-full mutant peaked one step later at 300 Hz. Overall the fly strains seemed to go into saturation at a frequency of 500 Hz. The response of Slowpoke (MiMIC), Eag^{sc29} and $Shaker^5$ seemed to still reduce a little bit during a frequency of 600 Hz, suggesting they go into saturation later. In the case of $Shaker^5$ this would mean it had a bigger range compared to the other strains. Finally, in the Slowpoke (PBac) mutant its response increased again slightly during the highest frequency. This seemed to be an artifact probably induced by higher variability during this stimulus since it is unlikely that an even higher frequency would elicit a stronger response after the curve is clearly approaching or already in saturation. Comparing the intensity and frequency tuning curve it is very clear that the frequency response data seemed to have a much higher variability than the intensity tuning curves. This might be showing a difference in response to stimuli with pure-tone and whitenoise structure.

Looking at these response properties we learned that there are some minor differences between the fly strains concerning their maximum response amplitude and frequency tuning. The biggest difference was the possibly increased range of frequency response of $Shaker^5$.

An effect of Slowpoke and Shaker on the frequency tuning was suggested before (Zhang, 2022).

Speed of variance adaptation

In the next part of the screening process we compared the speed of adaptation, τ, of different K^+ channel mutants with the NM91 wild type control (see Figure 4.3D). The Slowpoke mutants, neither the PBac ($\tau = 17.16\,\text{ms} \pm 0.83$, p=0.7669) or the MiMIC variant ($\tau = 18.89\,\text{ms} \pm 2.03$, p=0.3565), showed a difference in speed compared to the wild type. Slowpoke (PBac) was only 0.26 ms (1.49 %) faster and Slowpoke (MiMIC) was 1.47 ms (8.44 %) slower. Neither did the two Shaker mutations—Shaker^5 ($\tau = 17.22\,\text{ms} \pm 1.28$, p=0.8814) and Shaker^{133} ($\tau = 19.60\,\text{ms} \pm 3.38$, p=0.0913). Shaker^5 was 0.2 ms (1.15 %) faster then the wild type and Shaker^{133} was 2.18 ms (12.51 %) slower. We observed a weakly significant slowing down in the eag^{sc29} ($\tau = 21.31\,\text{ms} \pm 1.92$, p=0.0216) and the CRIMIC insertion mutant ($\tau = 20.56\,\text{ms} \pm 5.38$, p=0.0311). The speed of adaptation slowing down by 3.89 ms (22.33 %) in the eag^{sc29} and by 3.14 ms (18.03 %) in the CRIMIC mutants compared to the NM91 wild type. The last of the three Eag mutations used—the Eag delta-full mutant—did not show any significant effect ($\tau = 18.94\,\text{ms} \pm 3.6$, p=0.074), but showed a trend similar to the other two mutants, slowing down by 1.52 ms (18.73 %). The Eag CRIMIC and Eag delta-full mutants also displayed a comparatively high variability of τ, which might have obscured some effects. The fact that not all Eag mutants have a measurable effect on speed might corroborate this.

Strength of variance adaptation

In the second part of the screening process we compared the strength of adaptation of the mutants to the wild type (see Figure 4.3E). We again first took a look at the K^+ channels. The PBac variant of the Slowpoke mutation had a average strength of adaptation of 0.82 ± 0.01. The mean strength of Slowpoke with a MiMIC insertion was 0.8 ± 0.05. While it showed a slight weakening in the strength of adaptation, 0.05 (5.75 %) in Slowpoke (PBac) and 0.07 (8.05 %) in Slowpoke (MiMIC), the effect was not significant for neither of the Slowpoke mutant strains. The PBac mutant had a p-value of 0.3819 and the MiMIC variant had a p-value of 0.2493. The Shaker^5 had a mean strength of adaptation of 0.88 ± 0.08, so even 0.01 (1.15 %) higher than for the wild type, but the effect was not significant (p=0.6925). The second mutant, Shaker^{133}, had a mean strength of 0.81 ± 0.07, 0.06 (6.89 % weaker then in the wild type, which was also not a statistically significant difference (p=0.3654). Next, in the screening were the Eag mutant strains. The Eag^{sc29} showed a reduced strength of

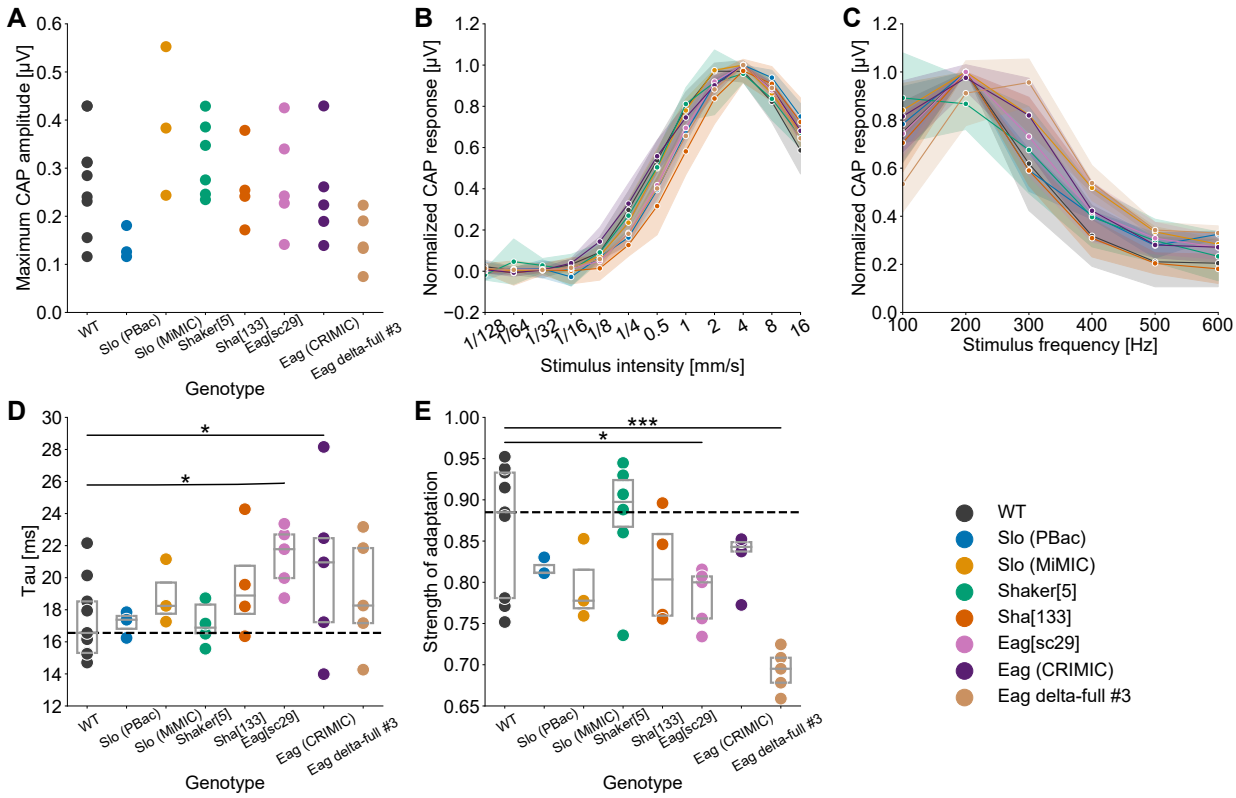

Figure 4.3: **Properties of the screened potassium channel mutants. A:** Maximal amplitude of the CAP for the different genotypes. The maximum amplitude of the K^+ channel mutants was within the range of the wild type. The WT control displayed in these plots is NM91. **B:** The average intensity tuning curve for the different genotypes is shown, with the shading representing the standard deviation. There was no difference in the shape of the intensity tuning curve between the screened fly strains. The data was normalized by maximum scaling approach. **C:** The average frequency tuning curve for the different genotypes is shown, with the shading representing the standard deviation. $Shaker^5$ responded to a wider range of frequencies, its response also peaking at lower frequency than the other strains. The Eag delta-full mutant on the other hand peaked at higher frequencies than the other fly strains. The data was normalized by maximum scaling approach. **D:** The median speed of adaptation of the individual flies is represented by the points, the box plot represents the individual genotypes. The dotted black line indicates the median tau of the control. Eag^{sc29} showed a slower adaptation (p=0.0216). **E:** The median strength of adaptation of the individual flies is represented by the points, the box plot represents the individual genotypes. The dotted black line indicates the median strength of the control. We observed a significant reduction of strength of adaptation in Eag^{sc29} (p=0.0368) and Eag delta-full (p=0.0004). n of flies: WT=9, Slo=3, Slo (MiMIC)=3, $Shaker^5$=6, $Shaker^{133}$=4, Eag^{sc29}=5, Eag (CRIMIC)=5, Eag delta-full=5. *=p<0.05, ***=p<0.001.

adaptation with a mean of 0.78 ± 0.04, a reduction of 0.09 (10.34 %). This difference was, other than in shaker, weakly significant (p=0.0368). The Eag CRIMIC mutation had an even stronger adaptation with a mean of 0.83 ± 0.03, a difference of only 0.04 (4.6 %). Therefore, this mutation had no significant effect (p=0.4277). While both of these Eag mutations had significant effects on the speed of adaptation these effects could not be observed in the strength of adaptation of both and only weakly in the Eag^{sc29} strain. The Eag delta-full mutant on the other hand showed a strongly significant reduced strength of adaptation (p=0.0004), with a mean strength of 0.69 ± 0.03, which was 0.18 (20.69 %) weaker than the wild type. The effect of Eag^{sc29} and Eag (CRIMIC) on only one of the aspects of variance adaptation might hint to a redundancy of the Eag channels. Maybe one isoform of Eag would be sufficient for complete adaptation, but acts on a different timescale. Nevertheless, this could also be influenced by the rather sizable variability of the NM91 data. Especially the three flies on the clustering to the lower ends of the data might skew the data in a way the effects of some mutants are obscured. Also Eag delta-full is quite variable in its τ data and almost significant, so here the variability might obscure at least a weak effect.

4.1.2 Rad, Gem/Kir family small G-proteins

The next class of molecules we included in our screening were two members of the Rad, Gem/Kir family (Rgk)—Rgk1 and Rgk3—small G-proteins (GTPases), with a Ca^{2+} channel regulator activity (Puhl 3rd et al., 2014; Béguin et al., 2001; Finlin et al., 2003). Ca^{2+} often plays an important role in adaptation, as a second messenger, in other sensory systems. We suspected that this might also be the case in the JONs (Eatock, 2000). Therefore, we included Rgk1 and Rgk3 in our screening to potentially unravel said mechanism. Rgk was also shown to be expressed in JONs in the transscriptome provided by Martin Göpfert's lab.

Tuning and CAP gain

First we looked at the maximum response of the Rgk mutants, but we did not observe a substantial difference between the mutants and the wild type (see Figure 4.4A and Table 11.4).

The intensity tuning curves of the Rgk mutants were also very similar, in all genotypes the response started to increase from 1/32 mm/s until saturation, but the curve of Rgk1 rose slower and therefore appeared shifted to the right (see Figure 4.4B). The response of Rgk1 (Minos) and Rgk3 saturated at 2 mm/s, while Rgk1 saturated at 4 mm/s like the wild type.

This suggests a higher sensitivity of Rgk1 (Minos) and Rgk3, but might also be caused by the variability of data, since the two Rgk1 mutants should show similar response profiles.

Looking at the frequency tuning curve of the Rgk mutants the Rgk3 mutant showed an overall higher response, which would support that this mutant might be more sensitive than the others (see Figure 4.4C). The other genotypes showed very similar tuning curves again. The response of all genotypes peaked at 200 Hz and saturated at 500 Hz. But Rgk3 showed an increase after its response fell to the lowest point at 600 Hz like previously observed in slowpoke. Here the frequency tuning curves showed a higher variability in the data than the intensity tuning curve again.

Speed of variance adaptation

Neither the Rgk1 PBac mutant ($\tau = 16.67\,\text{ms} \pm 2.26$, p=0.9776) nor the Minos insertion mutant ($\tau = 17.03\,\text{ms} \pm 3.75$, p=0.5541) showed a speed of adaptation different from NM91 on a significant level (see Figure 4.4D). Compared to the wild type Rgk1 (PBac) was 0.75 ms (4.31 %) and Rgk1 (Minos) was 0.39 ms (2.24 %) faster. The Rgk3 mutation also resulted in no significant change in speed ($\tau = 17.91\,\text{ms} \pm 1.89$, p=0.5541), which was 0.49 ms (2.81 %) slower than the wild type.

Strength of variance adaptation

The Rgk1 (PBac) showed a significant reduction in strength of adaptation (p=0.0104), the mean strength of this mutant was 0.76 ± 0.06, so its average strength of adaptation was 0.11 (12.64 %) weaker than the control (see Figure 4.4E). This mutation was also not showing an effect on speed of adaptation, but also has a great variability in the strength of adaptation data, which might explain this result. The Rgk1 (Minos) mutation affected neither strength nor speed of adaptation, its mean of strength was 0.84 ± 0.04 (p=0.525), so 0.03 (3.44 %) weaker compared to the control. The Rgk3 data displayed one data point of distinctly lower strength of adaptation than the rest of the data, its mean strength was 0.82 ± 0.1 (p=0.5252), which was 0.05 (5.75 %) weaker than the wild type.

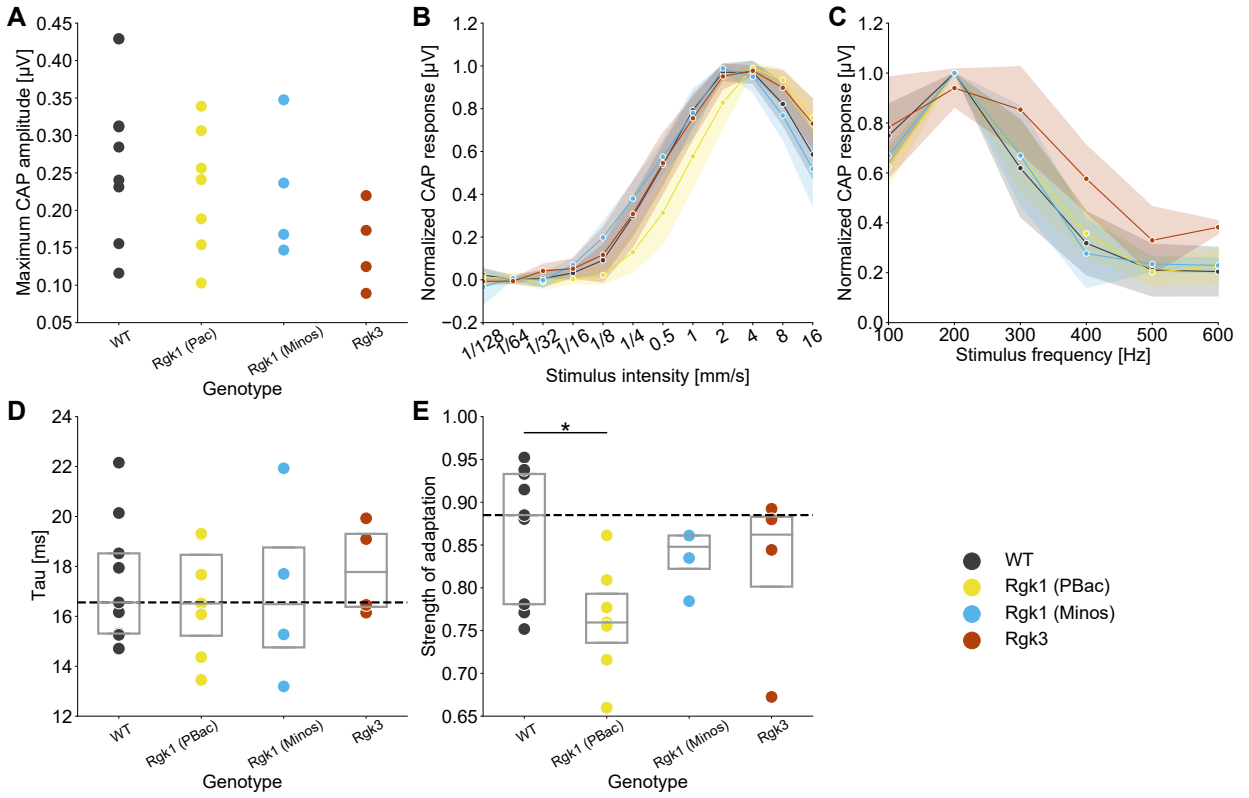

Figure 4.4: **Properties of the screened Rgk mutants. A:** Maximal amplitude of the CAP for the different genotypes. There was no substantial difference between the maximum response of the different mutants and the wild type. Rgk3 displayed the overall lowest response. The wild type depicted in these plots is NM91. **B:** The average intensity tuning curve for the different genotypes is shown, with the shading representing the standard deviation. The shape of the tuning curve was very similar for all genotypes, except for the Rgk1 (Minos) and Rgk3 mutants going into saturation earlier. The data was normalized by maximum scaling approach. **C:** The average frequency tuning curve for the different genotypes is shown, with the shading representing the standard deviation. Rgk3 showed a slightly higher response compared to the other genotypes, which did not differ substantially one from another. The data was normalized by maximum scaling approach. **D:** The median speed of adaptation of the individual flies is represented by the points, the box plot represents the individual genotypes. The dotted black line indicated the median tau of the control. None of the Rgk mutants influenced the speed of adaptation on a significant level. **E:** The median strength of adaptation of the individual flies is represented by the points, the box plot represents the individual genotypes. The dotted black line indicated the median strength of the control. Only one mutation, Rgk1 (PBac), reduced the strength of adaptation significantly ($p=0.0104$). n of flies: WT=9, Rgk1 (PBac)=7, Rgk1 (Minos)=4, Rgk3=4. *=$p<0.05$.

4.1.3 Motor proteins

The next part of the screening investigated motor protein related mutations. We included motor proteins into the screen, since it was likely that there is a mechanical component to adaptation in *Drosophila melanogaster*, for example on the level of mechanotransduction. Prestin is a well known example, inducing electromotility of the outer hair cells and cochlear amplification (Jia et al., 2005; Kennedy et al., 2005; Zheng et al., 2000). Expression or function within the JO was shown in previous studies (Senthilan et al., 2012) or through the transcriptome from Martin Göpfert's lab.

Tuning and CAP gain

With regards to their maximum CAP response the mutant strains did not differ majorly from the NM91 wild type (see Figure 4.5A and Table 11.4). The data shows a weak trend of the heavy chain mutants—Dnah3 (dynein, axonemal, heavy chain 3) and Dhc93AB (dynein heavy chain at 93AB)—having a higher amplitude than the intermediate chain mutant Dnai2 (dynein, axonemal, intermediate chain 2).

The intensity tuning curves of this set of genes looked very similar again, with the exception of Dnai2 (see Figure 4.5B). The response of all genotypes started increasing at around 1/16 mm/s and peaked at around 4 mm/s. The exception being the Dnai2 mutant, which started to increase its response already at the 1/32 mm/s stimulus and also peaked earlier at the 2 mm/s stimulus. Furthermore, Dnai2 displayed a comparably very sharp fall off for higher stimuli, but at the same time the standard deviation of this data increased greatly. So it is probably an artifact due to great variation in the Dnai2 intensity tuning data for the stronger stimuli.

Finally, the shape of the frequency tuning curves for the motor protein mutants was also very similar (see Figure 4.5C). The genotypes usually peaked at a frequency of 200 Hz and saturated around 500 Hz. The sole exception was again Dnai2, which already seemed to go into saturation at the 400 Hz stimulus, but then increased its response for the next stimuli. Also in the frequency adaptation data the standard deviation of this mutant increased strongly for the higher frequency stimuli.

Speed of variance adaptation

The two dynein heavy chain related mutants—Dnah3 and Dhc93AB—showed a slowed speed of adaptation on a weakly significant level (see Figure 4.5D). Dnah3 ($\tau = 20.40\,\text{ms} \pm 3.07$,

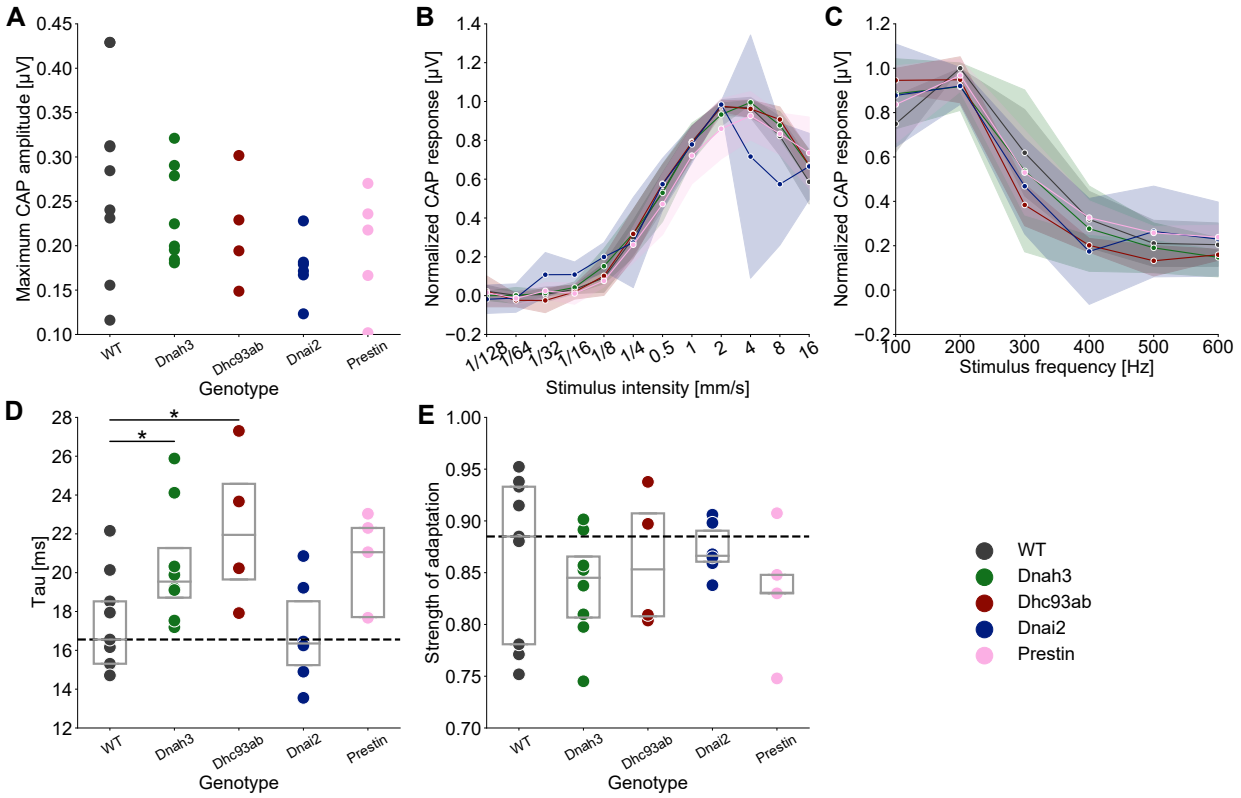

Figure 4.5: **Properties of the screened motor protein mutants. A:** Maximal amplitude of the CAP for the different genotypes. We could not observe a difference between the mutant genotypes and the wild type control. Dnah3 and Dhc93AB had slightly higher amplitudes then Dnai2. The wild type depicted in these plots is NM91. **B:** The average intensity tuning curve for the different genotypes is shown, with the shading representing the standard deviation. Dnai2 seems to be slightly more sensitive then the other genotypes, but also its standard deviation increased greatly for stimuli stronger then 2 mm/s. The data was normalized by maximum scaling approach. **C:** The average frequency tuning curve for the different genotypes is shown, with the shading representing the standard deviation. Dnai2 went seemingly into saturation earlier then the other genotypes, but increased its response again for the two highest frequency stimuli. The data was normalized by maximum scaling approach. **D:** The median speed of adaptation of the individual flies is represented by the points, the box plot represents the individual genotypes. The dotted black line indicated the median tau of the control. The dynein heavy chain mutations —Dnah3 and Dhc93AB—showed a reduced speed of adaptation ($p=0.0354$ and $p=0.0311$). **E:** The median strength of adaptation of the individual flies is represented by the points, the box plot represents the individual genotypes. The dotted black line indicated the median strength of the control. None of the mutant genotypes affected the strength of adaptation in a significant manner. n of flies: WT=9, Dnai3=8, Dhc93AB=4, Dnai2=6, Prestin=5. *=$p<0.05$.

p=0.0356) was slightly faster than Dhc93AB (τ = 22.28 ms ± 4.1, p=0.0299). Compared to the wild type control Dnah3 was 2.98 ms (17.11 %) slower and Dhc93AB even 4.86 ms (27.9 %) slower. The mutation of the dynein intermediate chain Dnai2 on the other hand showed no effect on the speed of adaptation (τ = 16.87 ms ± 2.72, p=0.5541), it was on average 0.55 ms (3.16 %) faster then the wild type. Finally, the mutation of prestin, not just a motor protein, but also a molecule known for its role in adaptation in the mammalian ear, caused a weakly statistically significant change in speed of adaptation (τ = 20.36 ms ± 2.53, p=0.0565) (Jia et al., 2005; Kennedy et al., 2005; Franchini et al., 2006; He, Lovas, et al., 2014). The mutation of prestin caused a 2.94 ms (16.88 %) slower variance adaptation. The τ data from the class of motor proteins again shows a rather big variability when compared to for example the Wtrw or Slowpoke τ data. This might again hide some smaller effects in some of the mutants. The effects measured in Dnah3 and prestin suggest that motor proteins in fact could influence adaptation in the JO.

Strength of variance adaptation

The dynein mutant Dnah3, opposing to its reduction in speed of adaptation, did not show a reduced strength of adaptation (p=0.43), with a mean strength of 0.84 ± 0.05, so a 0.03 (3.45 %) reduction compared to the strength of the control (see Figure 4.5E). The intermediate chain mutant Dnai2 had a mean strength of 0.87 ± 0.03, so it also didn't show a significant effect on strength of adaptation (p=0.6925). The Dnai mutant showed an average strength of adaptation on the same level as the wild type. Similar to the other dynein heavy chain mutant the Dhc93AB mutant had shown an effect on speed, but with a mean strength of 0.86±0.07 it did not affect the strength of adaptation in a statistically significant manner (p=0.8159). The difference to the wild type was only 0.01 (1.15 %). The last mutation belonging to the class of motor proteins was the mutation of prestin. In this mutant strain we measured a mean of 0.83 ± 0.06, which did also not prove significant (p=0.43), its strength was 0.04 (4.6 %) weaker than the control. It was surprising that we measured no effects on strength of adaptation, since we had some significant changes on the speed of adaptation. This could be a result of the effect being rather small and being masked by the great variability in the control. But also compared to the τ data, all the strength on between the mutants was really similar, whereas the τ of the significant slower genotypes was visibly increased compared to the others.

4.1.4 Miscellaneous

The last part of the screening included miscellaneous mutations, which were interesting candidates for their own reasons. First the Wtrw mutant, a TRP channel mutation, was shown to affect hearing in a similar way as nompC null mutations and to be expressed in the JO(Senthilan et al., 2012). Next, is the mutation of Stops, a SOCS box protein, mediating adaptation in the fruitfly's photoreceptors and expressed in the JONs (T. Wang et al., 2008; Kile et al., 2002; Senthilan et al., 2012). Lastly, nAChα5, a mutation of the a subunit of the nicotinic acetylcholine receptor, which is part of a widely expressed ligand-gated ion channel modulating excitability in neurons was also included in the screen (Albuquerque et al., 2009).

Tuning and CAP gain

The maximum CAP amplitudes of Wtrw and nAChα5 were very similar to the NM91 wild type, only the Stops mutant showed rather small CAP amplitudes compared to the wild type (see Figure 4.6A). The difference of amplitude of the stops mutants was weakly significant (p=0.0254) (see Table 11.4).

The intensity tuning curve of all four genotypes were almost identical, as all showed an increased response from the 1/16 mm/s stimulus and went into saturation after the 4 mm/s stimulus (see Figure 4.6B).

With respect to the frequency tuning curves they had a higher variation, much like seen in the data before (see Figure 4.6C). Stops seemed to already show its peak response at the 100 Hz stimulus, but the difference in response is so minimal that this as well might be to the standard deviation of the data. The other genotype clearly show a peak response for the 200 Hz stimulus. All genotypes do not decrease their response further after the 500 Hz stimulus.

Speed of variance adaptation

The Wtrw mutant, a mutation of a TRP channel, did not influence the speed of adaptation significantly ($\tau = 19.08\,\text{ms} \pm 1.55$, p=0.5726). Its speed of adaptation was 2.38 ms (13.66 %) slower than the wild type (see Figure 4.6D). The stops gene mutation was very interesting to look at, since it usually influences adaptation in the eye and was also shown to affect JO function (Senthilan et al., 2012). Nevertheless, involvement of Stops is unlikely since the mutation did not significantly affect speed of adaption ($\tau = 16.65\,\text{ms} \pm 3.59$, p=0.3431).

It was marginally faster than the control, with a 0.77 ms (4.42 %) difference. The last molecule included in this screening was the nicotinic Acetylcholine Receptor α5 (nAChα5), an acetylcholine-gated receptor-channel complex. The measured difference in τ of 2.79 ms (16.02 %) was not significant ($\tau = 20.21\,\text{ms} \pm 3.66$, p=0.7573).

Strength of variance adaptation

The TRP channel mutation Wtrw also had no significant effect on the strength of adaptation, with a measured mean of 0.85 ± 0.03 (p=0.6925), which was 0.02 (2.3 %) weaker than the control (see Figure 4.6E). The Stops mutant also did not influence the strength of adaptation, we measured a mean strength of 0.81 ± 0.09 for this mutant (p=0.3451), which equals a reduction in strength of 0.06 (6.9 %) compared to the control. The last mutant of the screening nAChα5 also showed no significant change in the strength of adaptation, with a measured mean of 0.82 ± 0.05 (p=0.4277), so a strength 0.05 (5.75 %) weaker than the wild type.

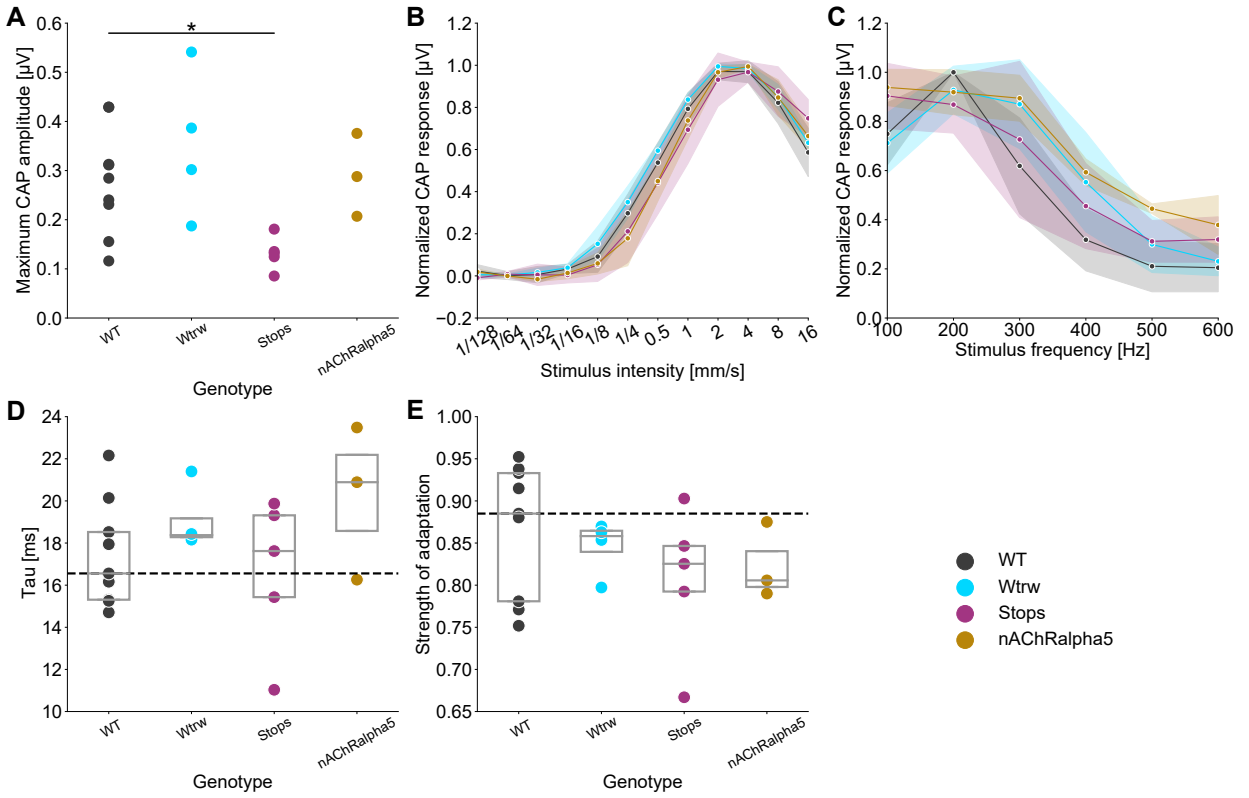

Figure 4.6: **Properties of screened miscellaneous mutants. A:** Maximal amplitude of the CAPs for the different genotypes. None of the mutant genotypes was distinctly different from the wild type, except for Stops, which showed a significant effect (p=0.0254). The wild type depicted in these plots is NM91. **B:** The average intensity tuning curve for the different genotypes is shown, with the shading representing the standard deviation. The tuning curves of the different genotypes were very similar. The data was normalized by maximum scaling approach. **C:** The average frequency tuning curve for the different genotypes is shown, with the shading representing the standard deviation. Also the frequency tuning curves of the genotypes were very similar, except for stops slightly peaking in response during the first stimulus. The data was normalized by maximum scaling approach. **D:** The median speed of adaptation of the individual flies is represented by the points, the box plot represents the individual genotypes. The dotted black line indicated the median tau of the control. None of the mutant genotypes had a significant effect on the speed of adaptation. **E:** The median strength of adaptation of the individual flies is represented by the points, the box plot represents the individual genotypes. The dotted black line indicated the median strength of the control. Also none of the mutant genotypes affected the strength of adaptation in a significant manner. n of flies: WT=9, Wtrw=4, Stops=5, nAChα5=3. *=p$<$0.05

4.2 Eag influenced both speed and strength in the screening making it the strongest candidate molecule

The results of the screening provided us with a good idea about how to proceed and what molecules to inspect closer in regards to their role in variance adaptation. We decided to not look closer into the K^+ channels of the Slowpoke and Shaker family, since we could not detect an effect of the mutation on the speed or the strength of adaptation. The same was the case for the TRP channel mutant Wtrw, the phototransduction related mutation Stops and the receptor-channel nAChα5. The Rgk1 (Minos) mutant also didn't show any effect, but the Rgk1 PBac mutation had an effect on the strength of adaptation. Since this effect could not also be observed affecting speed of adaptation it is questionable if Rgk1 is really a player in the mechanism of variance adaptation. The last mutation of a small GTPase, Rgk3, had an effect neither on speed of adaptation nor the strength of adaptation. While both mutations affecting the dynein heavy chain—Dnah3 and Dhc93AB—caused a reduction of speed of adaptation, no such effect could be observed on the strength of adaptation. The other two motor protein mutants—Dnai2 and prestin—did not affect variance adaptation at all during the screening. Furthermore, the mutations of Stops and nAChα5 also didn't influence variance adaptation at all. Finally, Eag was considered the most likely candidate from this screening. While the Eag (CRIMIC) mutant did not show a statistically significant reduction of the strength of adaptation, it showed a clear trend. The Eag^{sc29} on the other hand showed a weakly significant reduction of strength. Also both significantly reduced the speed of adaptation. While the third Eag mutation—Eag delta-full—also had in turn no statistically significant effect on speed of adaptation there was also a trend toward it slowing down, also the data had some variability to it. Furthermore, the Eag delta-full mutant had a strongly significant effect on the strength of adaptation.

In summary we found one mutation that influenced both the speed and strength of variance adaptation. This mutation was Eag^{sc29}. Eag (CRIMIC) only affected the speed of adaptation, while Eag delta-full only affected its strength. Aside from the Eag mutants we found the following other hits: The Rgk1 (PBac) mutant influenced only strength of adaptation. The motor protein mutants Dnah3 and Dhc93AB influenced only speed of adaptation. For an overview of the results of the screening refer to the Figures 4.7 and 4.8. Based on these observations we decided to take a closer look at variance adaptation using our most promising candidates—more precisely the Eag mutant strains. We also wanted to look into the mechanism of mean adaptation, so we conducted a screening probing for mean adaptation properties. We oriented ourselves at the results of the variance adaptation screening for

candidates for the mean adaptation screening.

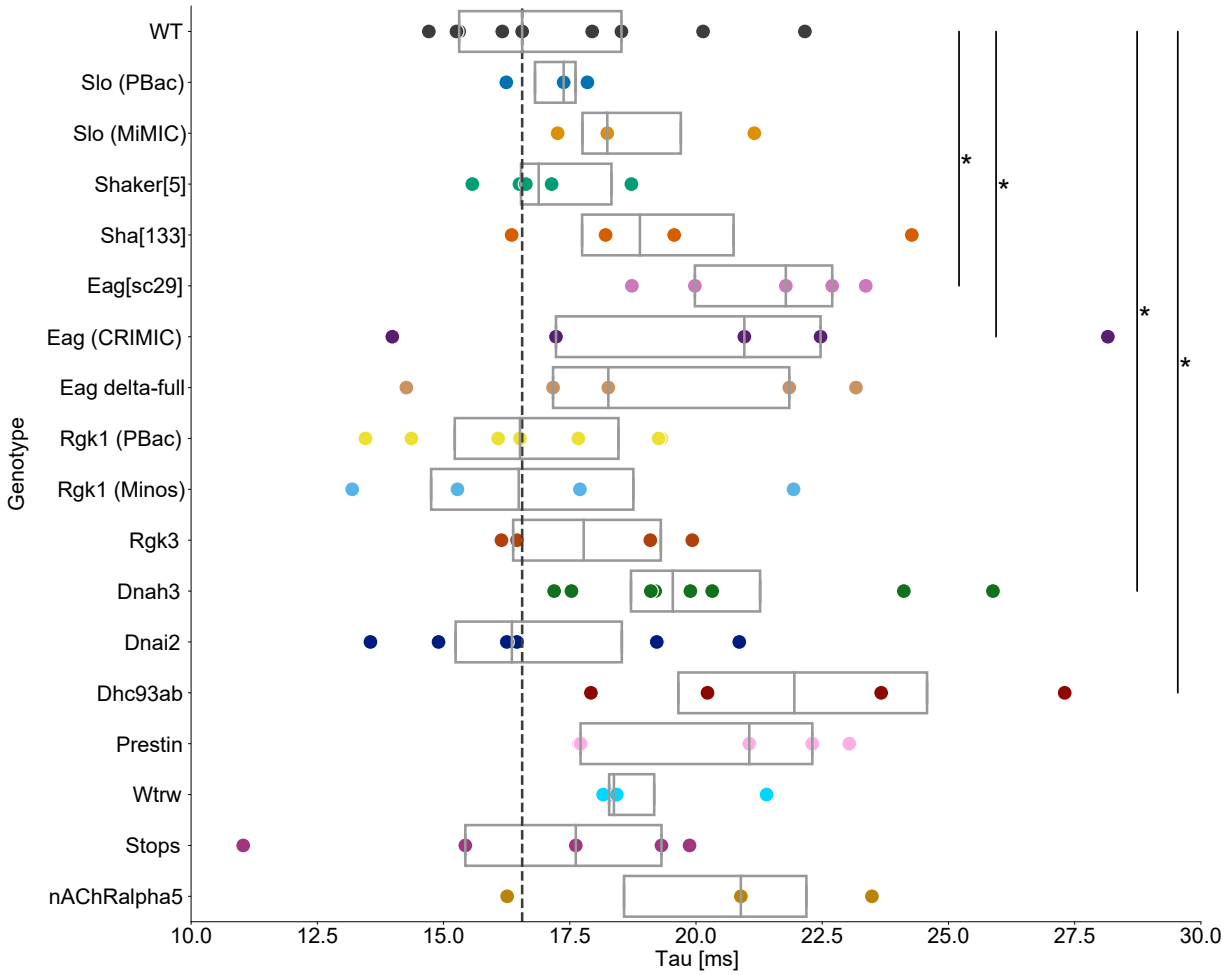

Figure 4.7: **Summary of speed of variance adaptation screening.** The median speed of adaptation of the individual flies is represented by the points, the box plot represents the individual genotypes. The dotted black line indicated the median tau of the NM91 wild type control. n of flies: WT=9, Slo=3, Slo (MiMIC)=3, Shaker^{5}=6, Shaker^{133}=4, Eag^{sc29}=5, Eag (CRIMIC)=5, Eag delta-full=5, Rgk1 (PBac)=7, Rgk1 (Minos)=4, Rgk3=4, Dnai3=8, Dhc93AB=4, Dnai2=6, Prestin=5, Wtrw=4, Stops=5, nAChα5=3. *=p$<$0.05.

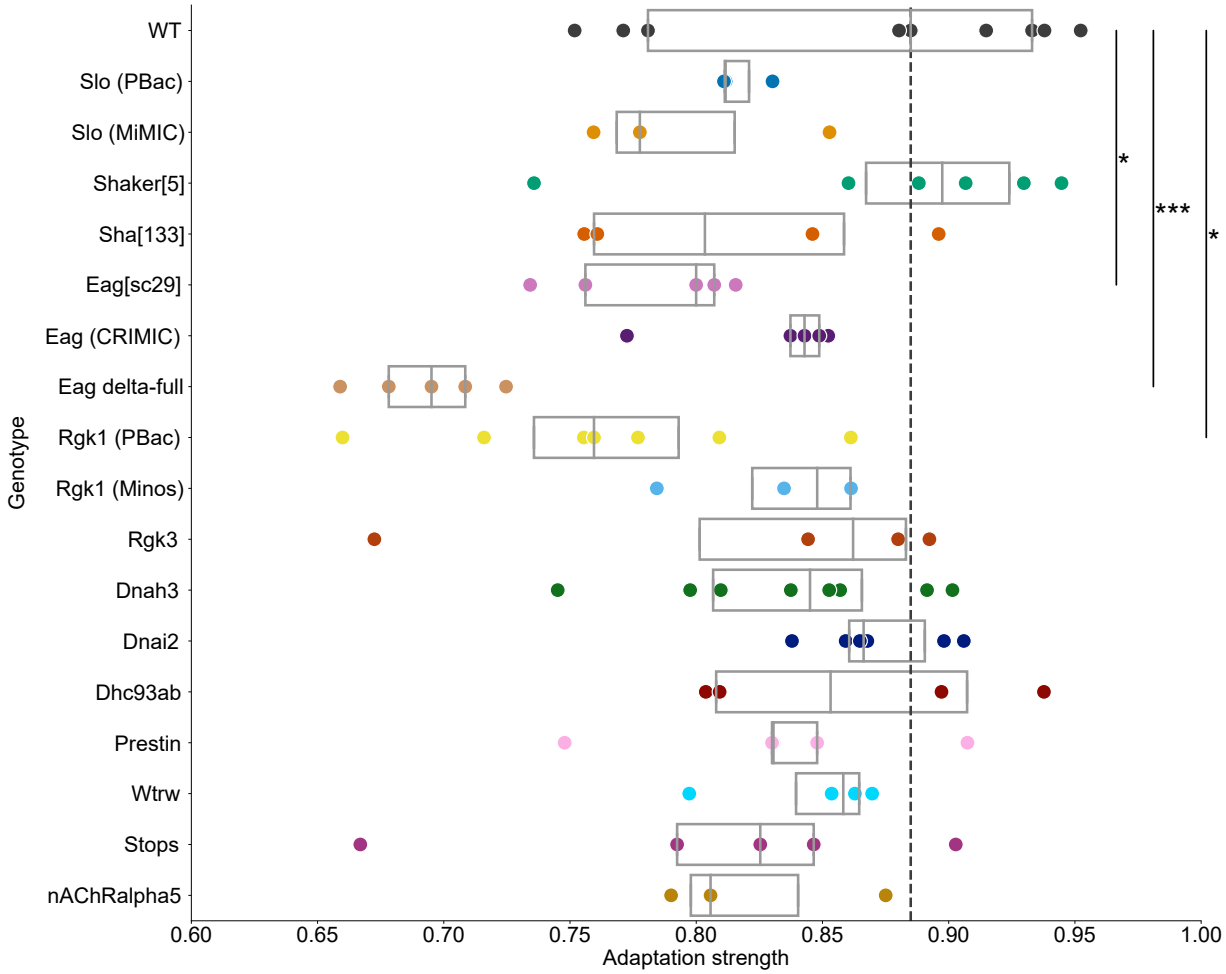

Figure 4.8: **Summary of strength of variance adaptation screening.** The median strength of adaptation of the individual flies is repented by the points, the box plot represents the individual genotypes. The dotted black line indicated the median strength of the NM91 wild type control. n of flies: WT=9, Slo=3, Slo (MiMIC)=3, Shaker^{5}=6, Shaker^{133}=4, Eag^{sc29}=5, Eag (CRIMIC)=5, Eag delta-full=5, Rgk1 (PBac)=7, Rgk1 (Minos)=4, Rgk3=4, Dnai3=8, Dhc93AB=4, Dnai2=6, Prestin=5, Wtrw=4, Stops=5, nAChα5=3. *=p<0.05, ***=p<0.001

4.3 Investigation of mean adaptation dynamics

For the second part of the project we investigated the mechanism of mean adaptation. There was evidence that mean and variance adaptation were two separate mechanisms. It was observed in prior studies that while variance adaptation could influence mean adaptation dynamics this is not the case the other way around (Clemens et al., 2018). On the basis of this a model about the computations happening during adaptation was formed. The first step of the model describes how an adaptation signal is constructed by low-pass filtering of the stimulus mean, which is then subtracted from the stimulus. This affects slower varying,

quasi static, stimuli components, but not the sound induced stimuli components, with fast and symmetrical fluctuations. Because their adaptation signal would be almost flat. It was concluded that this was the reason why mean adaptation did not affect sound sensitivity. In the next step of the model the output would then be rectified. This rectified signal was again low-pass filtered and that way encoded stimulus intensity. The model described that in the next step (the variance adaptation step) the stimulus was divided by the adaptation signal. Other than in the mean adaptation step, quasi static stimuli would also induce this divisive adaptation, which would lead to their responses being reduced. Thus the model explained the unidirectional interaction of these two adaptation processes, since the mean adaptation phase was basically blind to sound, but the variance adaptation phase reacted to deflections (Clemens et al., 2018). Furthermore, mean adaptation occurred already on the level of mechanotransduction and variance adaptation later down the auditory pathway (Jörg T. Albert et al., 2007; Nadrowski, Jörg T. Albert, et al., 2008).

What we expected due to this prior knowledge was that mean and variance adaptation probably have distinctly different underlying mechanisms, including other molecular players. We wanted to test this hypothesis and see if there was any similarity between the mechanisms involved in these two processes. Therefore, we conducted a second screening probing for mean adaptation, with many of the mutants used during the first screening. To access mean adaptation in the flies we compared their tuning curves. When the mean adaptation mechanism was working as intended the tuning curves, having different adaptation step magnitudes, should overlap when plotted for the relative magnitude of the antenna's displacement (displacement without the adaptation step) (see Figure 4.9A+B). If the mean adaptation was impaired by a mutation on the other hand, the tuning curves would become wider and flatter the bigger the adaptation step is (see Figure 4.9C+D). We quantified this curve shift and compared the mutant strains to the NM91 wild type. We also compared if there was a difference in the speed or strength of the mean adaptation. We had two main goals conducting this screen. First, we wanted to identify molecules involved in mean adaptation, by observing potential changes in the adaptation properties of mutant flies, like we did for the variance adaptation screen (see section 4.1). Additionally, we wanted to test the hypothesis if mean and variance adaptation are distinct mechanisms, involving separate ensembles of molecules. For this reason we tested many of the candidate molecules from the variance adaptation screen.

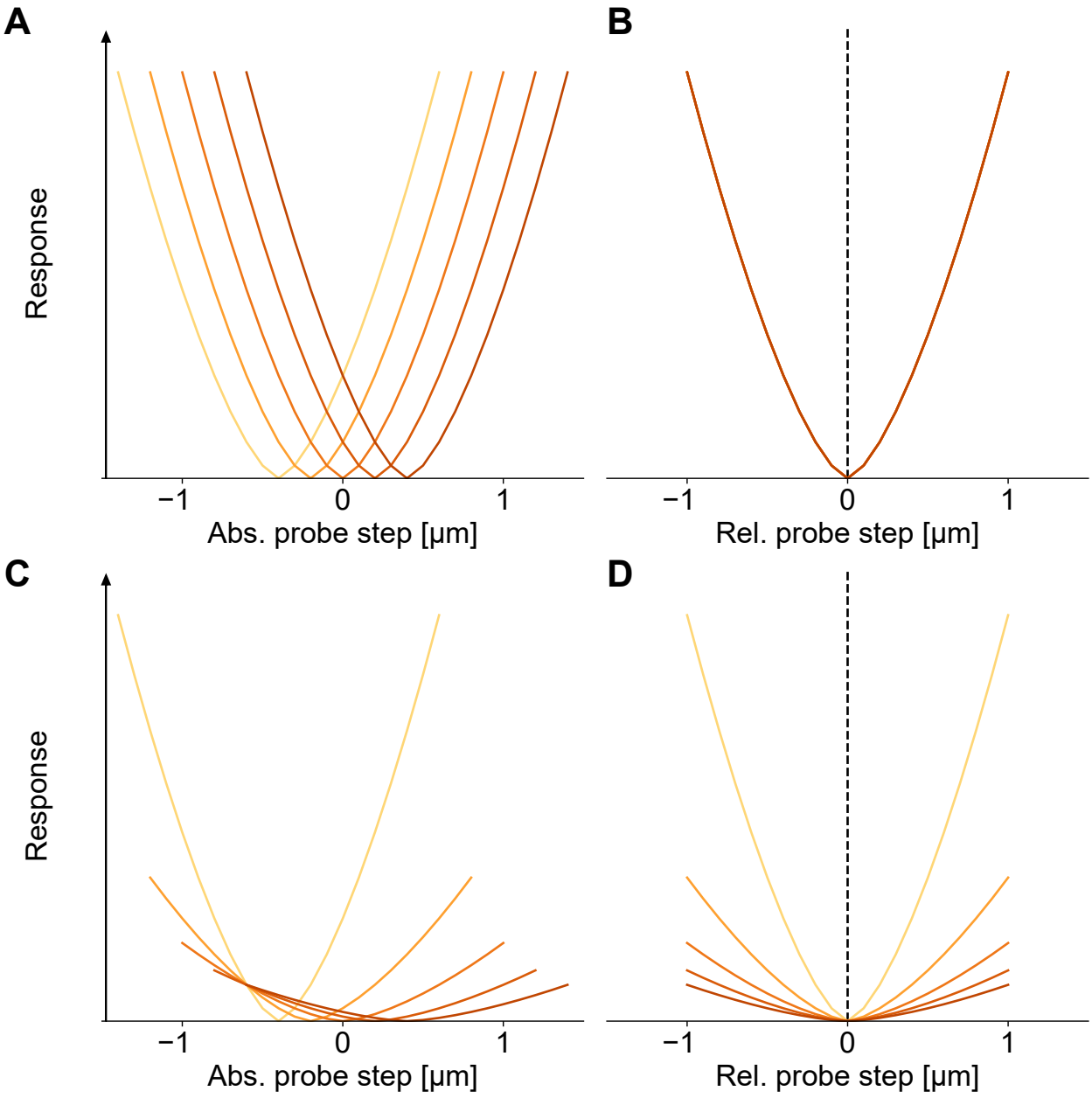

Figure 4.9: **Schematic of tuning curve shift in mean adaptation experiments.** This schematic is just for illustration purposes and does not contain real data. **A:** Intensity tuning curves plotted against the absolute size of the probe step (deflection of adaptation step + probe step). The shape of the curves should be very similar under normal conditions. **B:** The same tuning curves (from A) plotted against the relative size of the probe step (deflection of only the probe step). This should lead to the curves minimum converging at 0 µm and overlapping since their shape is so similar. **C:** Tuning curves plotted against the size of the absolute probe step if mean adaptation would be impaired. The shape of the tuning curves is distorted more and more depending on the size of the adaptation step. **D:** Because of their change in shape the tuning curves (from C) do not overlap anymore when plotted against the size of the relative probe step.

4.3.1 Mean adaptation did not show changes in screened mutant flies

The average slope of curve shift measured in NM91 was -0.09 ± 0.16 with an average speed of adaptation of $2.37\,\text{ms} \pm 0.47$ and an average strength of 1.04 ± 0.11, so these are the levels of shift we would expect during intact mean adaptation in this screen (see Figure 4.10A). While the over 1.0 value for the strength of adaptation seemed unlikely, this is well within the level of the standard deviation, so merely a result of the data's variability. The speed and strength of the wild type would also be used as a reference to judge possible changes in adaptation of the screened mutants (see Figure 4.10B+C). First we investigated the strongest candidate from the previous screen, the K^+ channel Eag. The first mutant strain, Eag^{sc29}, displayed an average slope of curve shift of -0.03 ± 0.05, a difference of 0.06 (66.67 %), the curve shift looks quite different from the wild type case, but was not statistically significant(p=0.74). The big proportional difference is due to the slope of the curve shift being very small under wild type conditions. The average speed of adaptation of the Eag^{sc29} was $2.17\,\text{ms} \pm 0.19$ (p=0.4324), the mutant was 0.2 ms (8.44 %) faster, but the difference was not significant. Also the average strength of adaptation, 0.94 ± 0.06, which was 0.1 (9.62 %) weaker than the wild type was also not significantly different (p=0.5325). We also tested the Eag (CRIMIC) mutant strain, which also exhibited no significant difference in slope of curve shift compared to the wild type, its average slope was -0.04 ± 0.04 (p=0.74), 0.05 (55.56 %) closer to 0. With an average speed of adaptation of $1.99\,\text{mm} \pm 0.13$ (p=0.1596), 0.38 ms (16.03 %) faster than the control, and an average strength of 0.89 ± 0.15 (p=0.5325), which was 0.15 (14.42 %) weaker than the control. Neither of the mutants affected mean adaptation in a statistically significant form. The last of the three Eag mutant strain screened was Eag delta-full. The slope of the curve shift from the Eag delta-full mutant also did not differ significantly from wild type levels, the average slope calculated was -0.05 ± 0.07 (p=0.74), which was 0.04 (44.44 %) flatter than the wild type, with an average speed of adaptation of $1.98\,\text{ms} \pm 0.23$ (p=0.1167), which was 0.39 ms (16.46 %) faster compared to the wild type. Finally, the mutant also had an average strength of adaptation of 0.95 ± 0.04 (p=0.5325), which was 0.09 (8.65 %) weaker than the wild type. None of these properties were statistically significantly different. This suggested that it would be not possible to derive the influence of a molecule on one type of adaptation by its influence on another type of adaptation. Despite the Eag mutants indicating a clear effect of variance adaptation before, they seemed to not affect mean adaptation in the slightest.

Next, we also tested the CaMBD mutants, where the binding site of CaM to the Eag channel was mutated (Bronk et al., 2018). The CaMBD 8.8.1 mutant had an average slope of curve shift -0.08 ± 0.1 (p=0.8165), which was 0.01 (11.11 %) flatter compared to the control (see

Figure 4.10A). An average speed of adaptation of 2.36 ms±0.3 (p=0.9792), which was almost identical to the wiltype, only 0.01 ms (0.42 %) faster (see Figure 4.10B). Finally, the average strength of adaptation of this mutant was 0.97 ± 0.12 (p=0.4107), which was a reduction of 0.07 (6.73 %) (see Figure 4.10C). Overall the mutant did not differ significantly from the control. The second CaMBD strain, CaMBD 17.4.1, also did not differ significantly, the average slope of its curve shift was -0.11 ± 0.14 (p=0.8165), signifying a 0.02 (22.22 %) increase of the slope. Its average speed was 2.42 ms ± 0.42 (p=0.8489), so its speed of adaptation slowed down by 0.05 ms (2.11 %). Finally, we calculated an average strength of adaptation of 0.83 ± 0.25 (p=0.4107) for the mutant, which was with a reduction by 0.21 (20.19 %) visibly weaker then the wild type, but not statistically significant. This further supports the assumption that Eag or its interaction with Ca^{2+} do not influence this mode of adaptation.

The small GTPase Rgk1 PBac was also screened again and showed no significant effect concerning the slope of the curve shift (p=0.74). The slope of the Rgk1 mutant had an average of -0.02 ± 0.008, so 0.07 (77.78 %) flatter than the wild type (see Figure 4.10A). Its speed of adaptation was also unremarkable with an average of $1.8\,\text{ms} \pm 0.08$ (p=0.0941), which was 0.57 ms (24.05 %) faster than the control (see Figure 4.10B). Its strength of adaptation with an average of 1.19 ± 0.65 (p=0.5325), so 0.15 (14.42 %) stronger than the wild type, but not statistically significant (see Figure 4.10C). The over 1.0 value of the mutant's average strength is due to the high variability of its data, which can be clearly seen in Figure 4.10C. This absence of an effect suggests that the mean adaptation is not influenced by any Rgk1 mediated Ca^{2+} channel activity.

Lastly, we also included mutant strains of the other K^+ channel families slowpoke and shaker. The Slowpoke mutant used in this screen was the PBac mutant, with an average slope of curve shift of -0.07 ± 0.13 (p=0.8165), so 0.02 (22.22 %) flatter than the wild type (see Figure 4.10A). We calculated an average speed of adaptation of $2.03\,\text{ms} \pm 0.04$, so 0.34 ms (14.35 %) faster than the control, which was not statistically significant (p=0.3532) (see Figure 4.10B).The average strength of adaptation of this mutant was 0.89 ± 0.04, so 0.15 (14.42 %) weaker, but this reduction was also not significant (see Figure 4.10C). The other K^+ channel mutant, $Shaker^{133}$, also showed no significant difference to the NM91 wild type regarding its slope of the curve shift (p=0.74). The average slope of the Shaker mutant was -0.16 ± 0.09, which was increased 0.07 (77.78 %) compared to the wild type (see Figure 4.10A). Aside from the effect not being statistically significant it indicates an increased downwards slope (decay). An effect on the adaptation would be visible through an increased positive slope. The increased decay we observed in this mutant was probably due to the spreading of its datapoints, with the most negative one shifting the mean in this direction (see Figure 4.10A). Its average speed of adaptation was $2.2\,\text{ms} \pm 0.54$ (p=0.5624), 0.17 ms

(7.17 %) faster then the control, but not significant (see Figure 4.10B). Finally, we observed an average strength of adaptation of 0.92 ± 0.07, so a reduction by 0.12 (11.54 %) compared to the wild type, which was also not statistically significant (p=0.5325) (see Figure 4.10C). Since we did not measure an significant effect of these K^+ channel mutants, like in Eag, they seemed to not play a role in mean adaptation. This could imply that K^+ channels in general do not play a role in mean adaptation of the fly. Many of the mutants show a slope change compared to the control which is big in comparison, but not statistically significant. This is probably an effect of the very small slope present in the wild type and also the mutants. So a small difference appears quite substantial when the effect size was expressed as percentages.

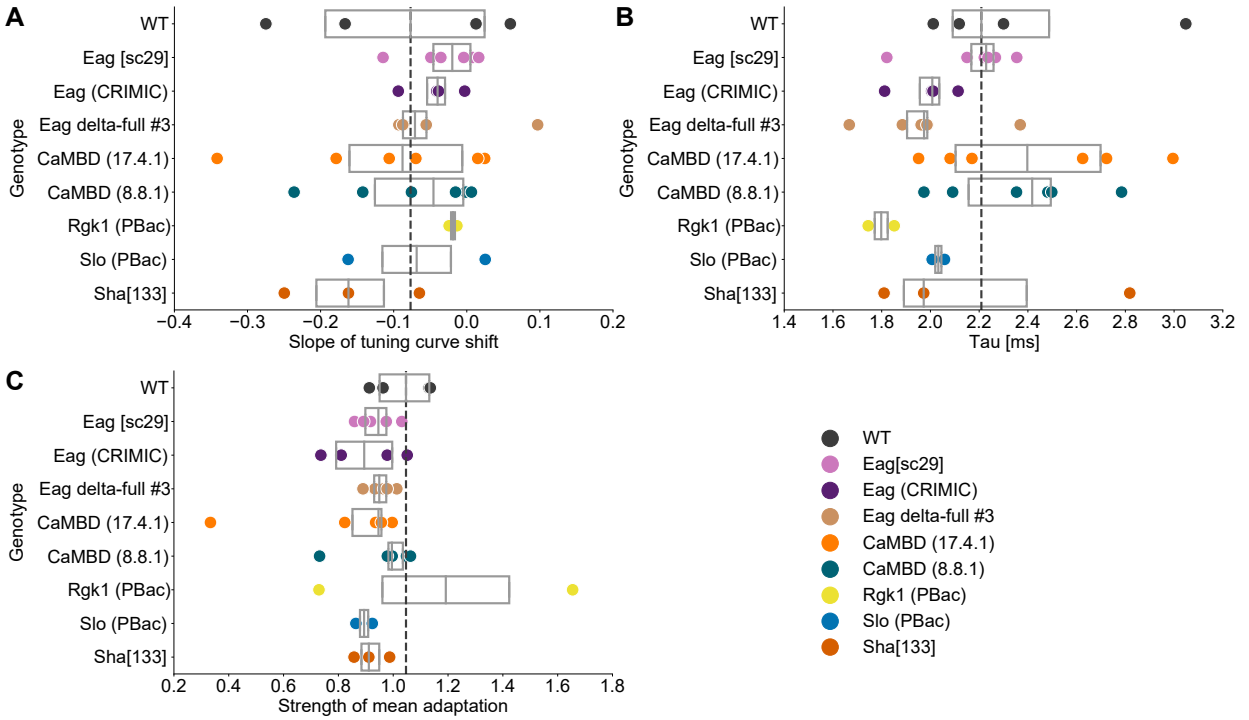

Figure 4.10: **Screening of mean adaptation dynamics. A:** Tuning curve shift of the different genotypes. Each point denoted the mean of the curve shift of one fly. The dotted black line denoted the overall median of the control. We could not observe a significant curve shift comparing the mutants and the wild type. The depicted control is the NM91 wild type. **B:** Speed of adaptation for the different genotypes. Each point denoted the mean of the curve shift of one fly. The dotted black line denoted the overall median of the control. The speed of adaptation was not significantly different between the mutants and the control. The depicted control is the NM91 wild type. **C:** Slope of the tuning curve shift. Each point denoted the mean slope of the curve shift of one fly. The dotted black line denoted the overall median of the control. The slope between the wild type control and mutant strains did not differ in a significant way. The depicted control is the NM91 wild type. n of flies: WT=4, Eag^{sc29}=6, Eag (CRIMIC)=4, Eag delta-full=6, CaMBD (17.4.1)=6, CaMBD (8.8.1)=6, Rgk1 (PBac)=2, Slo=2, $Shaker^{133}$=3.

4.3.2 The mean and variance adaptation mechanisms employ distinct molecules

While Eag clearly played a role in variance adaptation it seemed not to affect mean adaptation. This was further corroborated by the CaMBD results. This supports our hypothesis that the mechanisms involved in variance and mean adaptation are quite distinct. Eag seemed to not be part of the molecular mechanism of mean adaptation. It would be of course still possible that there is some overlapping in involved molecules, which could possibly be discovered by screening more candidates. With regards to mean adaptation, none of the mutants we screened had an effect on mean adaptation.

4.4 The effects of different Eag mutations confirm Eag as a part of the variance adaptation mechanisms

We decided to further investigate the putative effect of Eag mutations on variance adaptation. Eag had shown effects in all mutants during the screening and also was shown to be expressed in all JON non-selectively in immunostainings (see Figure 4.11), so it was a really strong candidate. For this we recorded a new set of data of the three Eag mutants and controls. We also added new controls to match the genotype of the control to the mutant if possible and else again used the NM91 control. We assumed that we also could produce a data set with less variability than in the screening since we were more adapt at the experimental procedure after the experiments conducted during the screening process.

First, we looked at the Eag^{sc29}, Eag (CRIMIC) and Eag delta-full again. We also compared the maximum amplitude of the response traces (see Figure 4.12A and Table 11.5) to rule out that the effects may be partly influenced by widely different amplitudes of the traces ultimately used for the analysis of speed and strength of adaptation. In the case of NM91, Eag^{sc29}, Eag (CRIMIC) and Eag delta-full, their response amplitude did not clearly differ by genotype. Eag^{sc29} and Eag delta-full showed less spread than the other two genotypes. When looking at the intensity tuning curves (see Figure 4.12B) the Eag^{sc29} and Eag delta-full mutants appeared to be shifted from the NM91 control (see Figure 4.12B). So the wild type response peaked at 2 mm/s, while the Eag mutants generally peaked at a stimulus intensity of 4 mm/s. The intensity tuning curve of the Eag (CRIMIC) mutant was almost identical to the wild type. Concerning the frequency tuning of the flies, the mutants also were slightly less sensitive then the wild type (see Figure 4.12C). This could be observed in the amplitude of the average CAP response, which was higher in the wild type, also the Eag

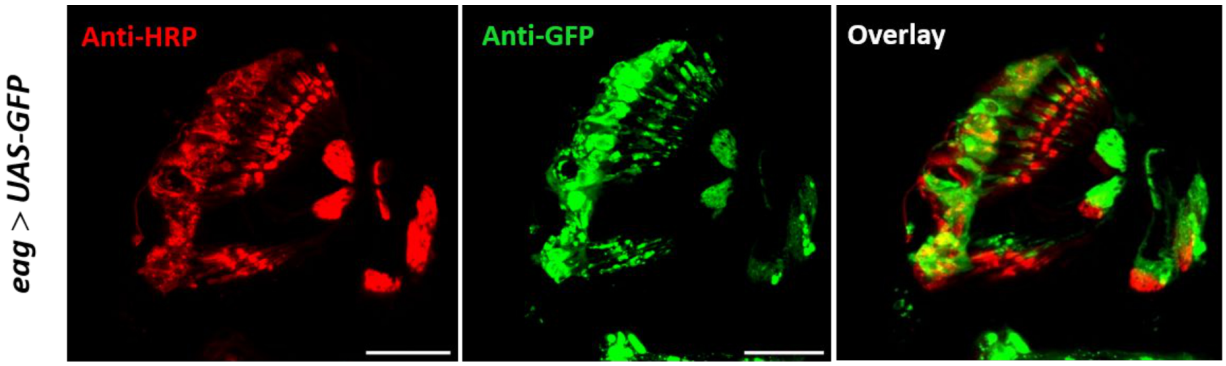

Figure 4.11: **Expression of Eag in the JO.** The expression of Eag in the JO visualized using the Gal4/UAS system. The immunostaining shows that Eag is non-selectively expressed in all JONs. The scale bar denotes a length of 20 µm. GFP=Green fluorescence protein, HRP=Horseradish peroxidase. The image was kindly provided by Xiaowei Zhan from the Göpfert lab (adapted from Zhang, 2022).

mutants peaked at a frequency of 300 Hz, while NM91 already peaked at 200 Hz. The Eag (CRIMIC) mutant was again almost identical to the wild type in terms of frequency tuning. The Eag^{sc29} showed a significant reduction of speed of adaptation (see Figure 4.12D) with a mean τ of 21.88 ms $\pm$ 2.43 compared to NM91 at 16.67 ms $\pm$ 1.54 (p=0.00649351), its τ was increased by 5.21 ms (31.25 %). When looking at the strength of adaptation of this Eag mutant (Figure 4.12E) we could now also observe a significant reduction (p=0.0065). While the NM91 wild type's mean strength was 0.88 $\pm$ 0.3 the strength of Eag^{sc29} was reduced to 0.73 $\pm$ 0.04, so the strength of adaptation was reduced by 0.15 (17.05 %). Also the Eag (CRIMIC) mutant affected variance adaptation greatly. Its speed of adaptation was 20.77 ms $\pm$ 1.64, so it was 4.1 ms (24.6 %) slower (p=0.013) (see Figure 4.12D). The mutation showed no significant effect on the strength of adaptation (p=0.3961). The Eag (CRIMIC) mutant showed an average strength of 0.81 $\pm$ 0.07, which means the strength of adaptation was weakened by 0.07 (8 %). The last mutant, Eag delta-full, also showed a significant effect on the speed of adaptation (p=0.0065), its mean τ was reduced to 17.62 ms $\pm$ 2.76. The mutant was 0.95 ms (5.7 %) slower compared to the wild type (see Figure 4.12D). We did not observe this effect during the screen, which suggests that it was masked in the screening data set due to the higher variability of the data and the rather small effect size. Additionally, the Eag delta-full mutant retained its significant reduction of strength of adaptation (p=0.0065), the mutants mean strength was reduced to 0.67 $\pm$ 0.04. The strength of adaptation was 0.21 (23.86 %) reduced in the mutant. Since the CAP amplitude of the mutants and the wild type are not significantly different (see Figure 4.12A), it is unlikely that the effects seen on adaptation are artifacts caused by low response levels.

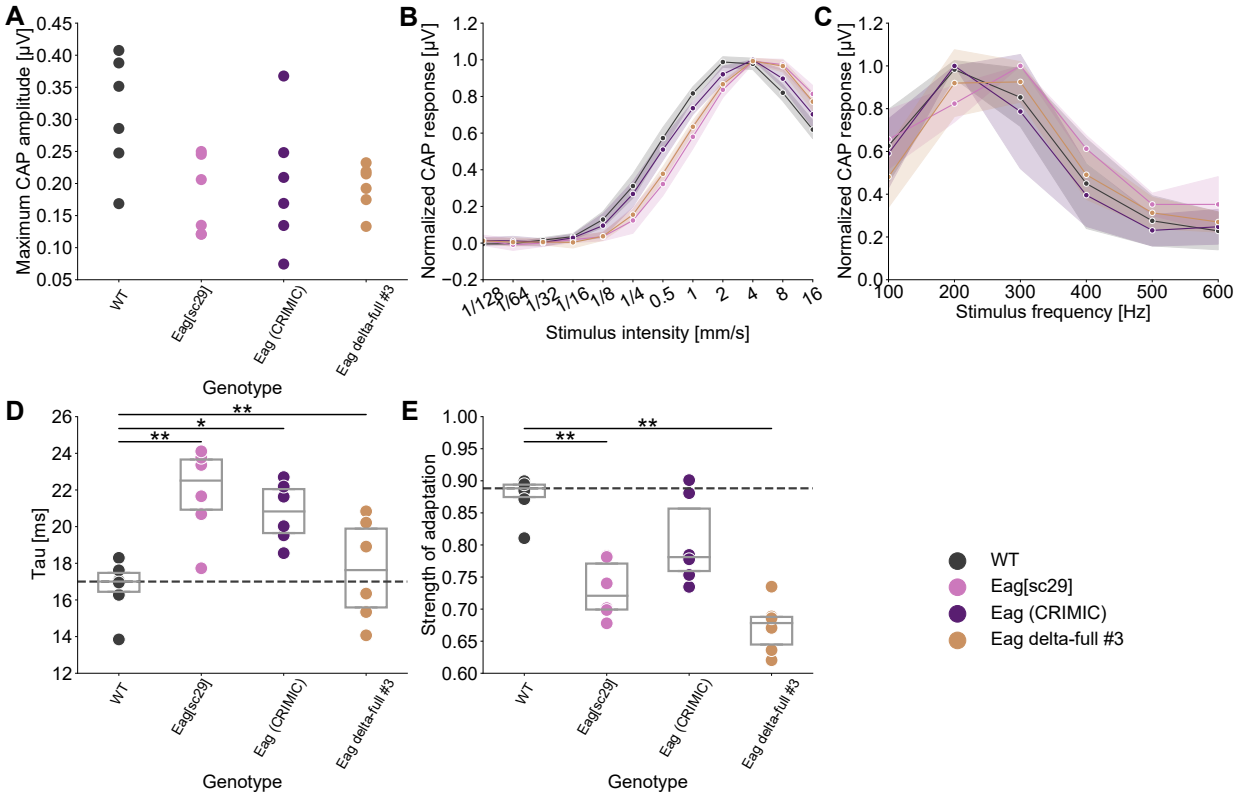

Figure 4.12: **Properties of the Eag mutants. A:** Maximum CAP response of the different genotypes. None of the mutants differed in a significant manner from the wiltype control. The wild type control depicted is NM91. **B:** The average intensity tuning curve for the different genotypes is shown, with the shading representing the standard deviation. Two of the mutants—Eag^{sc29} and Eag delta-full—shifted to the right, the overall shape of the curves were almost identical to one another. The tuning curve of the Eag (CRIMIC) mutant was almost identical to the wild type. The data was normalized by maximum scaling approach. **C:** The average frequency tuning curve for the different genotypes is shown, with the shading representing the standard deviation. There was no visual difference between the genotypes concerning their frequency training. The data was normalized by maximum scaling approach. **D:** The median speed of adaptation of the individual flies is represented by the points, the box plot represented the individual genotypes. The dotted black line indicated the median tau of the control. The speed of adaptation of all three mutants—Eag^{sc29} ($p=0.0065$), Eag (CRIMIC) ($p=0.01298701$) and Eag delta-full ($p=0.0065$)—was significantly reduced. **E:** The median strength of adaptation of the individual flies is represented by the points, the box plot represented the individual genotypes. Only the strength of the Eag delta-full mutant was significantly reduced ($p=0.0065$). The dotted black line indicated the median strength of the control. Flies for each genotype n=6.*=$p<0.05$, **=$p<0.01$.

4.5 Investigating the possible interaction of Eag and CaM during variance adaptation

After confirming the effect of Eag on variance adaptation we thought about how Eag fits into a putative mechanism/pathway of adaptation. Eag is known to be regulated by Ca^{2+}. More precisely Eag is inhibited by binding of the Ca^{2+}/CaM complex, in presence of elevated Ca^{2+} levels (Bronk et al., 2018; Lörinczi et al., 2016). Since calcium often plays a role in the adaptation of sensory systems (e.g. the visual system), we hypothesized that this could likely also be the case in the JONs (Krizaj, 2002). To investigate this hypothesis we measured the speed and strength of variance adaptation in flies bearing a mutation of the Eag CaM binding domain (CaMBD). What we expected by preventing the binding of the Ca^{2+}/CaM complex to the Eag channel, and therefore its inhibition, was an increased K^+-current from the channel. This should theoretically lead to increased speed and strength of adaptation or at least keeping up wild type-like levels.

We compared the CaMBD mutant data to controls with the same genetic background as the mutants instead to the NM91 wild type. We had two variants of this control—control 8.7.1 and control 12.8.1. Additionally, we created a transheterozygous cross from both, we used as additional control. The controls did not differ significantly in their variance adaptation (see Table 11.3).The maximum CAP amplitude of the depicted genotypes did not show any differences, only the the amplitude of CaMBD (8.8.1) seemed to be comparatively slightly lower, but this was only a trend (see Figure 4.13A and Table 11.5). The intensity tuning curves of the CaMBD mutants and the controls are identical (see Figure 4.13B). This is not surprising since they bear the same genetic background, but also reveals that the mutation does not affect intensity tuning. There was a difference in the frequency tuning of the CaMBD mutants (see Figure 4.13C). The CaMBD (8.8.1) showed the highest response at a frequency of 300 Hz, while all other genotypes peaked at 200 Hz. Also the both mutants show a steeper slope in the middle of the tuning curve, which is probably because of the difference of response to the 300 Hz stimulus, but all average responses become very similar for the 500 Hz stimulus. Again the differences observed are within the standard deviation observed. Looking at the speed of variance adaptation there seemed to be a visible difference between the two controls, control 8.7.1 with a mean tau of 17.08 ms ± 2.43 and control 12.6.1 with a mean tau of 21 ms ± 4.51, but the difference was not statistically significant (see Figure 4.13D) (p=1.0). The speed of the two CaMBD mutants was quite similar to each other. CaMBD 8.8.1 having a mean τ of 20.52 ms ± 1.72 and CaMBD 17.4.1 displaying a mean τ of 19.63 ms ± 2.06. The speed of the control 12.6.1 was very similar to what was recorded in the mutants, but the control 8.7.1 was 3.2 ms (15.24 %) faster. Nevertheless, the difference in speed was not statistically significant. It also was not significant for comparison

of control 8.7.1 to CaMBD 8.8.1 (p=0.18614719), which was 2.72 ms (15.28 %) slower, nor to CaMBD 17.4.1 (p=1.0), which was 1.83 ms (10.28 %) slower. Same when comparing control 12.6.1 to CaMBD 8.8.1 (τ = 20.52 ms ± 1.72, p=1.0), which was 0.48 ms (2.29 %) faster, or CaMBD 17.4.1 (τ = 19.63 ms ± 2.06, p=1.0), where the speed was increased by 1.37 ms (6.52 %) in comparison. Also compared to the TH control (average τ = 17.73 ms ± 0.86) we could not observe any effect. Compared to the TH control the CaMBD 8.8.1 mutant was 2.79 ms (15.73 %) slower, while the CaMBD 17.4.1 mutant was 1.9 ms (10.72 %) slower. Next, as we looked at the strength of variance adaptation, the two controls were more similar to one another (see Figure 4.13E). The mean strength of control 8.7.1 was 0.78 ± 0.03, while the strength of control 12.6.1 was slightly higher at 0.8 ± 0.06. Lastly, the average strength of the TH control was 0.81 ± 0.03. The mean strength recorded in the CaMBD 8.8.1 mutant was slightly reduced to 0.76±0.06. Similarly the mean strength of adaptation in the CaMBD 17.4.1 mutants was reduced to 0.74 ± 0.02. The difference in strength of adaptation was also not statistically significant. We did not observe a significant difference between control 8.7.1 and CaMBD 8.8.1 (p=1.0), the difference being 0.02 (2.56 %), or CaMBD 17.4.1 (p=0.1299), which showed a difference of 0.04 (5.13 %). This was also the case using control 12.6.1 and comparing to CaMBD 8.8.1 (p=0.3593), which was 0.04 (5 %) weaker, and CaMBD 17.4.1 (p=0.1299), where the strength of adaptation was reduced by 0.06 (7.5 %). Lastly, we also compared to the TH control (average strength of 0.81±0.03). The CaMBD 8.8.1 mutant was 0.05 (6.17 %) weaker compared to the TH control (p=0.12987013) and the CaMBD 17.4.1 mutant was 0.07 (8.64 %) weaker (p=0.0519). The CaMBD mutations showing no effect on variance adaptation aligns partially with our predictions. While we did expect an increased K^+ conductance of the Eag channels in these mutants and therefore faster/stronger variance adaptation it is not certain that this is how there properties interact. It might be the case that the increase of K^+ current, by obstructing the inhibition of Eag, does not suffice to increase variance adaptation or that variance adaptation can not become faster or stronger than what was observed in the controls.

We decided to look more closely into the interaction partners of Eag and CaM and found CaMKII. The kinase is known to modulate the function of Eag, since when it is inhibited the current of the channel was shown to be weakened (Zheng Wang et al., 2002). Also the CaMKII is activated by the Ca^{2+}/CaM complex, indicating a connection between these three molecules in a putative pathway of variance adaptation (Yamauchi and Fujisawa, 1980; Yamauchi, 2005). We compared the mutants to the NM91 wild type control. The kinase mutants showed no difference in amplitude to the wild type control (see Figure 4.14A and Table 11.5). The shape of the intensity tuning curves of the three genotypes was the same. The tuning curve of the CaMKII mutants was very slightly shifted towards the right compared to the wild type control (see Figure 4.14B). All genotypes started increasing their response from the 1/16 mm/s and also peaked during the same stimulus (4 mm/s). After

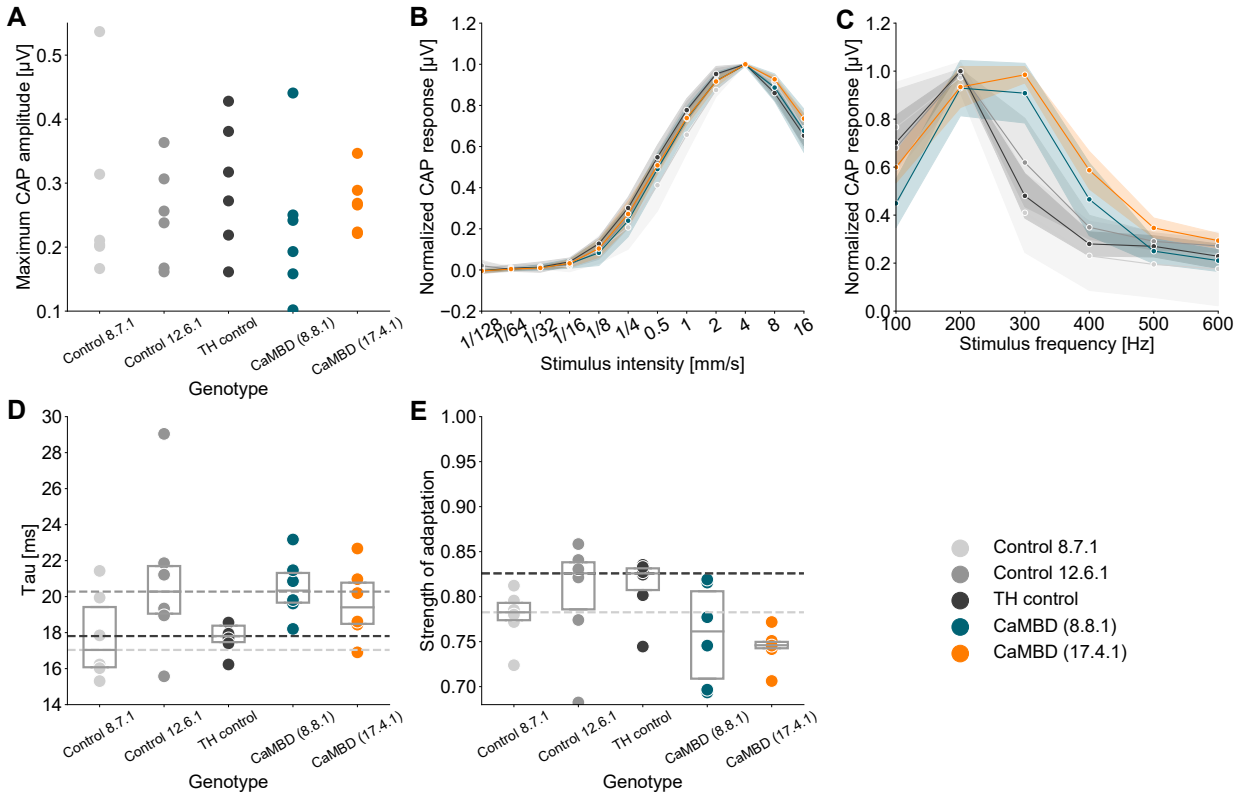

Figure 4.13: **Properties of the CaMBD mutant flies. A:** Maximum amplitude of the CAP response traces of the different genotypes. There was no significant difference between the three controls and the mutants. **B:** The tuning curves were constructed from the averaged tuning data of the different genotypes. The colored shading represents the respective standard deviation of the genotype's tuning. The intensity tuning curves of the genotypes were exactly the same. The intensity tuning curves were normalized using a maximum scaling approach. **C:** The average frequency tuning curve for the different genotypes is shown, with the shading representing the standard deviation. The slope in the middle of the tuning curve of the CaMBD mutants seemed steeper than the controls and the CaMBD (17.4.1) mutant's response peaked at 300 Hz. The data was normalized by maximum scaling approach. **D:** The median tau values of the individual flies are represented by the dots. The boxplot shows the collective data of the respective genotype. The dotted lines indicated the median tau for the controls of the same color (see legend). There was no difference in speed of adaptation between the mutants and the three controls. **E:** The median strength of adaptation of the individual flies are represented by the dots. The boxplot shows the collective data of the respective genotype. The dotted lines indicated the median strength of adaptation for the controls of the same color (see legend). The mutants showed also no difference to the controls regarding strength of adaptation. Flies for each genotype n=6.

they started to go into saturation the wild type and mutant tuning curves started diverging slightly. The frequency tuning curves were very similar within their standard deviation (see Figure 4.14C). The CaMKII (PE) mutant showed a higher response than the other two genotypes for the lowest frequency stimulus (100 Hz). The slope of the middle part of the frequency tuning curve was steeper in the CaMKII (PE) mutant. Next, we looked at the speed of adaptation of the kinase mutants. Neither the CaMKII (MiMIC) ($\tau = 17.05\,\text{ms} \pm 1.87$, p=0.619) nor the CaMKII (PE) mutant ($\tau = 19.48\,\text{ms} \pm 3.47$, p=0.3593) differed significantly from the speed of the NM91 wild type (see Figure 4.14D). In comparison to the wild type the speed of the CaMKII (PE) mutant was 2.81 ms (16.86 %) slower and 0.38 ms (2.28 % slower in the CaMKII (MiMIC) mutant. We could also observe no difference between the strength of adaptation of the wild type and the two mutant strains (see Figure 4.14E). The CaMKII (MiMIC) had an average strength of 0.84 ± 0.04 (p=0.3593), which was 0.04 (4.55 %) weaker than the wild type, and the CaMKII (PE) mutant showed an average strength of adaptation of 0.83 ± 0.02 (p=0.0823), so 0.05 (5.68 %) weaker than the wild type. The absence of an effect provided evidence against an influence of the CaMKII on variance adaptation, by for example interaction with the Eag channel.

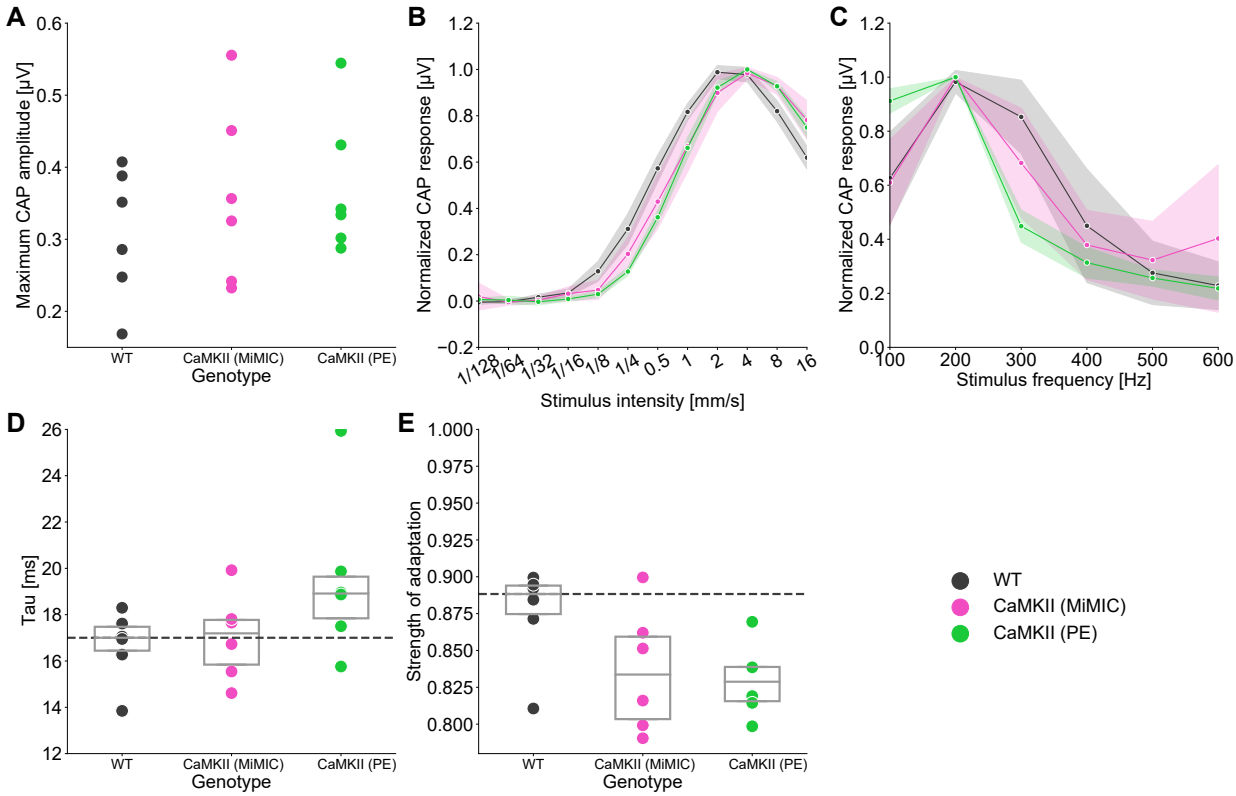

Figure 4.14: **Properties of CaMKII mutant flies. A:** Maximum amplitude of the CAP response traces of the different genotypes. There is no significant difference between the wild type control and the two CaMKII mutants. The wild type control depicted is NM91. **B:** The tuning curves were constructed from the averaged tuning data of the different genotypes. The intensity tuning curves of the different genotypes had the same shape. The colored shading represents the respective standard deviation of the genotype's tuning. The intensity tuning curves were normalized using a maximum scaling approach. **C:** The average frequency tuning curve for the different genotypes is shown, with the shading representing the standard deviation. The genotypes differed slightly in the steepness of their slope, but were not substantially different. The data was normalized by maximum scaling approach. **D:** The median tau values of the individual flies are represented by the dots. The boxplot shows the collective data of the respective genotype. The dotted black lines indicate the median tau for the controls used for comparison. The genotypes did not differ significantly in terms of speed of adaptation. **E:** The median strength of adaptation of the individual flies are represented by the dots. The boxplot shows the collective data of the respective genotype. The dotted black lines indicate the median strength of adaptation for the control for easier comparison. There was no significant difference between the wild type control and the CaMKII mutants. Flies for each genotype n=6.

5 Discussion

5.1 All three Eag mutants showed effects in both data sets

During the screening for candidate molecules influencing variance adaptation we tested 17 different candidates, four of these showed a significantly reduced speed of variance adaptation and three had significantly reduced strength of variance adaptation. Only one showed an significant reduction of both—the Eag^{sc29} mutants. All of the observed effects were generally weak, with the effects of the Eag mutants sometimes being more moderate in size (bigger than 20 %). The mutations of the dynein heavy chain—Dnah3 and Dhc93AB—lead to a slower adaptation, but did not affect the strength of adaptation. The mutation of the small GTPase Rgk1 on the other hand reduced only the strength of variance adaptation, but not its speed. This suggests that different molecules might affect different properties of the variance adaptation. The most prominent effects we observed were in the Eag mutants. All of the Eag mutant strains had reduced speed of adaptation in the hit data set. Also, the Eag^{sc29} and Eag delta-full mutants showed a significant reduction in strength of adaptation. There were significant effects on at least one aspect of variance adaptation in all Eag mutants in both the screening and the hit data set. This corroborated the Eag channel as part of the variance adaptation mechanism.

5.2 Smaller variation in the hit data set revealed smaller effects

Looking at the results hit data set we saw a new effects that did not during the screening. The Eag delta-full genotype showed a significant decrease in speed of adaptation. Why did this change in significance occur between data sets? A difference in variance of the data probably played a role. For example, we mostly used a NM91 wild type control, its τ ranged from 14.71 ms up to 22.16 ms during the screening (see Figure 4.7). This was a visibly

higher spread compared to the hit data set, where the τ of NM91 ranged from 13.85 ms up to 18.3 ms (see for example Figure 4.12D). This was also the case for the strength of adaptation data, where the data of NM91 ranged between 0.75–0.95 in the screening (see Figure 4.8). In the hit data set the strength of adaptation of NM91 was less variable, ranging between 0.81–0.9 (see for example Figure 4.12E). This greater spread of the data during the screening reduced the power to detect statistically weak effects. So the lesser variability in the hit data set contributed to revealing some smaller effects. For example, in the screening data set we could detect effects greater than ∼18 % for speed of variance adaptation. So we could detect the significant effects of Eag^{sc29}, Eag (CRIMIC) on the speed of adaptation. Concerning strength of adaptation we detected effects greater than ∼10 % during the screening. Meaning we could observe the significant effects in Eag^{sc29} and Eag delta-full. In the hit data set we could detected effects as small as 5.7 % of a change in τ. Therefore, Eag delta-full also had an significant effect on the speed in the hit data set. The smallest statistically significant effect on strength of adaptation we detected in the hit data set was 17.05 %. The effects of Eag^{sc29} and Eag delta-full were significant, like in the prior data set. Eag (CRIMIC) was not significant with an effect size of only 8 %.

5.3 Possible compensation within the mechanism of adaptation

These rather small to mediocre effect sizes of knocking down Eag possibly reveal some things about the mechanism of variance adaptation. Eag is probably not the only K^+ channel involved in variance adaptation hence the small effect. Maybe when we impaired the function of the Eag channel other channel did compensate the effects, at least partly. Something similar was reported happening when another K^+ channel, the Shaker cognate B (Shab) channel, was knocked down in *Drosophila* larva. After the Shab channel was mutated slowpoke was upregulated, to uphold the control of intrinsic excitability (E. Z. Kim et al., 2017). A way to test for this possible compensation could be to use an for example a temperature sensitive RNAi knockdown to induce an acute loss of Eag channel function. This should prevent compensation from influencing the recordings, but it was also shown that turnover of ion channels can happen within a short span of time (a few hours) (Marder et al., 2006; E. Z. Kim et al., 2017). So it might be of importance to time the recordings carefully to get conclusive results. Another way would be to induce an acute pharmaceutical inhibition of the Eag channel, which should be too fast for any compensatory mechanisms.

Furthermore, we saw several more small effects during the screening, for example the effect of both dynein heavy chain mutants—Dnah3 and Dhc93AB—on the speed of variance

adaptation. This suggests an involvement of dynein in variance adaptation, which should be investigated further like we did in this thesis with Eag. If this effect could be corroborated, it is likely that it will still be small, should the dynein heavy chain be just another part of the variance adaptation mechanism (like the Eag channel) and not essential for its function. On the other hand, if the dynein heavy chain was essential for variance adaptation we should have already seen a stronger effect during the screening. If dynein turns out to affect adaptation after further experiments, one could try to investigate how Eag and dynein are connected in this mechanism. Their relationship could be be tested by testing double mutants of the Eag channel and the dynein heavy chain. If both molecules work in parallel pathways the effect of the double mutant should be bigger than mutants of the respective genes alone, since a way of compensation was removed. If on the other hand Eag would be functionally downstream of dynein the effect should stay at the same size.

5.4 Tuning differences between fly strains

We also measured the intensity and frequency tuning of the different fly strains, to make sure they did not differ a great deal in their tuning properties. This was important since the response of a fly would be affected if the stimulus used was outside of its dynamic range. While generally the intensity tuning of the mutant strains did not really differ from the wild type, on one occurrence there was a slight shift. In the hit data set the intensity tuning curve of the Eag^{sc29} and Eag delta-full the intensity tuning curve was slightly shifted to the right (see Figure 4.12B). Implying that these mutants were slightly less sensitive to the noise stimuli than the wild type control and the Eag (CRIMIC) mutant. Also the Eag^{sc29} mutant and the Eag delta-full mutant showed an significant effect on strength of variance adaptation, while this was not the case for the Eag (CRIMIC) mutant (see Figure 4.12D). Could this correlation hint to an artifact caused by different sensitivity of the strains? It is unlikely that this small shift had a significant effect, since the dynamic range of the mutants was not influenced compared to the wild type (see Figure 4.12B). Furthermore, this shift would indicate a reduced response to a higher mean of a stimulus, not a difference in intensity. We could in general not observe a clear difference in frequency tuning between the wild type and the mutant strains, except for in the CaMBD mutants (see Figure 4.13C). The shape of the frequency tuning curve for both variants of the CaMBD mutantion— CaMBD (8.8.1) and CaMBD (17.4.1)—was distinctly different from all three of the controls. This could mean that the Eag/CaM interaction has an influence on frequency tuning in *Drosophila*.

5.5 The role of Eag in variance adaptation

The Eag mutants had the most prominent effect on variance adaptation we observed, suggesting this family of channels may be an important part of the mechanism inducing adaptation in the JONs in *Drosophila melanogaster*. As a K^+ channel the Eag channel probably would affect adaptation by lowering excitability of the neuron (after a stimulus) or shaping the decay of the response (adaptation) by inducing repolarization (Wu et al., 1983; Frolov et al., 2012; Nagel et al., 2011). Still not all mutants affected variance adaptations in the same way, while Eag^{sc29} affected both speed and strength of adaptation, the Eag (CRIMIC) strain only showed reduced speed. This difference could arise from the methods used in the mutation of eag. The three Eag mutants we used were created using three different methods. Eag^{sc29} was created using x-ray induced deletion (Drysdale et al., 1991). The Eag (CRIMIC) and Eag delta-full were created using more modern transposon insertion techniques. Eag (CRIMIC) was created using a CRIMIC insertion (Lee et al., 2018). The Eag delta-full mutant was created using a PBac insertion (Bronk et al., 2018). One would expect that a stronger effect would be induced by the two more modern techniques, but this was not the case in our experiments. Furthermore, while Eag delta-full did affect both speed and strength of adaptation this was not the case for the other transposon insertion mutant, Eag (CRIMIC) (see Figure 4.12D+E). This result was unexpected since one would expect the these insertions to affect Eag in a similar fashion. The different effects and effect sizes of the three eag mutants could not be explained simply through the different techniques used to induce them. The phenomenon of the different Eag mutants affecting variance adaptation in different forms, might be due to some form of compensation mechanism or other molecule interaction with the channel differing between the three mutants. Furthermore, Eag was also known to be regulated by Ca^{2+} concentration, we suspected an influence of Ca^{2+} concentration on adaptation through this pathway. This hypothesis was supported by many examples of Ca^{2+} playing an important role in the adaptation of other sensory systems. Like for example in the eye Ca^{2+} is involved in control of the gain of phototransduction during adaptation (Gray-Keller et al., 1996; Sokolov et al., 2002; Hardie, 2002). Another example for sensory adaptation through Ca^{2+} and CaM is in the mammalian vomeronasal organ (Spehr et al., 2009). Based on this common property of adaptation mechanisms of different sensory systems, we investigated possible interaction partners of the Eag channel involving Ca^{2+}. Eag has multiple binding sides of CaM, which inhibits the channel's conductance when it is activated by binding Ca^{2+} (see section 1.5) (Bronk et al., 2018). We expected that if we removed this inhibition by impairing the ability of Eag to bind CaM, we might be able to induce over-adaptation. To put this hypothesis to the test, we looked into the variance adaptation of the CaMBD mutants. These two mutant strains were, like the name suggests, altered at the CaM binding-domain of the Eag channel. We expected

possibly an increase in strength of adaptation compared to the controls, which might be possible since the controls do not adapt perfectly (strength of adaptation = 1) in our experiments so maybe the adaptation would be more complete in the mutants unaffected by inhibition. Additionally, we expected to possibly also see an increase of the speed of adaptation compared to the wild type controls, since now the channels would operate without regulation by Ca^{2+}/CaM. Our expectations were not met by the results (see Figure 4.13), neither the speed nor strength of variance adaptation was significantly different from the controls. This absence of an effect could have two reasons: First, it could be that despite the inhibition affecting the channel's conductance, this does not influence our measures of adaptation. This would be highly unlikely since mutating Eag was shown to be sufficient to negatively impact adaptation (see Figure 4.12), changing the conductance of the channel by removing the inhibition should also cause a visible change (Wu et al., 1983). Although, the Ca^{2+}/CaM of Eag could only be measured in presence of high Ca^{2+} concentrations in the millimolar level, which are normally only seen in a microdomain close to voltage-gated Ca^{2+} channels (Bronk et al., 2018). So an explanation might be that the concentration was too low for inhibition to function. An alternative interpretation of these results could be that the speed and strength we measure in the controls were already at maximum height for the respective genotype. Abolishing the inhibition therefore might result neither in increased speed nor strength of adaptation. Furthermore, we know little about the probably vast number of molecules involved in the mechanism of adaptation, most likely including additional ion channels, which also shape variance adaptation. So it might not be enough to solely interfere with the inhibition of Eag to produce a visible effect. What we can conclude from our screen regarding these potential ion channels is that they are not Slowpoke or Shaker channels, since these did not show any effect during our screening (see Figure 4.3). While the CaMBD mutant specifically impairs the interaction of Eag and CaM it was also shown in prior studies that adaptation was not affected in CaM mutant flies (Clemens et al., 2018). Since it was difficult to conclusively interpret these results, we investigated further into potential interaction partners. This lead us to CaMKII, Eag was known to be a substrate of this kinase, which enhances or at least is necessary to maintain the normal function of this channel (see section 1.5) (Griffith et al., 1994; Zheng Wang et al., 2002). In our results we could not observe a significant influence of the CaMKII mutation, reinforcing the assumption that variance adaptation in *Drosophila melanogaster* is not mediated by Ca^{2+} concentration affecting the Eag channel conductance.

5.6 Eag mutations did not influence mean adaptation

We conducted a second screening to investigate potential candidate molecules with influence on mean adaptation. We could not observe a statistical significant effect of any of the tested mutants on any properties of mean adaptation. This is especially interesting since it was hypothesized that variance and mean adaptation are two separated processes (Clemens et al., 2018; Benda, 2021; Jörg T. Albert et al., 2007; Nadrowski, Jörg T. Albert, et al., 2008). Our results showed that the Eag channel is likely a part of the mechanism inducing variance adaptation (see Figure 4.12), but does not influence mean adaptation (see Figure 4.10). This tells us that the molecular machinery inducing these two types of adaptation contains molecules unique to the respective mode of adaptation (variance or mean adaptation). It could also be two sets of completely different molecules with no common members. This should be further investigated by an expanded screening for molecules involved in mean adaptation. Since this mode of adaptation might already occur on the level of mechanotransduction, it might prove fruitful to investigate more molecules involved in this transduction, like motor proteins. After molecules affecting the mean adaptation have been identified, one could also take a further look into the interaction of mean and variance adaptation. This would probably require the connection of the fly's antenna to the piezo to be improved, since in the experiments, conducted as part of this project, the stimuli probing these interactions posed a problem. The resulting recording traces were very messy and shaky, most likely a result of the sinusoid part of the stimulus, since this problem did not occur using a static deflection alone. The root cause might be that the UV-glue was not sufficient securely attach the piezo tip to the antenna during these oscillations or maybe further movement within part of the rig caused by these.

5.7 The Eag channel as a candidate of adaptation

One thing to take into consideration about the channel as a player in the adaptation mechanism are its kinetics. For example the activation speeds and activation voltage should be fast and sensitive enough make sense for e.g. the timescale of adaptation. Eag is not just an ubiquitous, but also very multi-faceted channel. There have been many years of research about this K^+ channel in many different organisms and its kinetics are influenced by many factors like for example Ca^{2+} and Mg^{2+} concentration. Speeds of activation can range from around 10 ms to magnitudes slower, depending on the specific channel and context. The speed of adaptation we measured for the wild type (NM91) ranged around 15–20 ms in the hit data set. So the Eag channel should theoretically be fast enough to influence variance

adaptation. Also its activation threshold can be quite varied, for example in the rat channels with an activation threshold of −100 mV and −20 mV were reported (S. Wang et al., 1997; Meyer et al., 1998; Gutman et al., 2005). This activation threshold is low enough to theoreticaly open during subthreshold depolarizations and therefore reducting the amplitude of the spike generator currents (Clemens et al., 2018). Therefore, the Eag channel could have the necessary capabilities to act in adaptation mechanisms of the timescale we measured. Unfortunately, in the literature there seemed to be no measurements about the specific kinetics of the *Drosophila* Eag channel, which leaves the definitive answer to this question ambiguous. Further experiments could include measurements of the *Drosophila* Eag channel kinetics in the wild type and the mutants to answer the question whether or not these could physiologically explain the adaptation dynamics.

5.8 The methodological limitations of CAP recordings

By using extracellular recordings in our experiments to observe the activity of the JONs, we get the activity of all JONs as a population as our readout. Having these CAPs as readout creates certain limitations when interpreting the data. Since we can not distinguish the possible effect of certain JON subpopulations on the readout, but what we recorded was the bulk spiking activity of the JONs (Kamikouchi, Inagaki, et al., 2009; Clemens et al., 2018). The first question probably coming to mind is how we can be sure that what we recorded during the variance adaptation experiments was the adaptation of spiking activity of the JON subpobulations sensitive to sound (subpopulation A+B)? This concern was addressed in prior studies from flies with disrupted mechanotranduction and spiking in the JONs, caused by a mutation of iav. This was then rescued in all JONs, only the A and B subpopulations or only the B subpopulation. The adaptation dynamics recorded in these rescues proved to be indistinguishable from the wild type, showing that the activity of the A and B subpoplulations dominated the CAP response during these experiments (Clemens et al., 2018). Another concern was the issue of desynchronization, since extracellular signals were shown to be sensitive to synchrony among the neuron population (Einevoll et al., 2013). This meant that potentially, changes in the CAP amplitude we interpreted as changes in population firing rate might simply be due to effects of the mutations (in the candidate genes) on the synchrony between the JONs. Thus leading to false positive effects. To prevent this, the noise stimuli used were designed in a way to prevent desynchronization. A prior study tested this in a model of leaky integrate and fire neurons, showing that the noise stimuli prevented strong desynchronization. Furthermore, desynchronization was induced in the model to show that this could not sufficiently explain the CAP dynamics. Finally, the dynamics of the CAP were also confirmed using calcium imaging, which as a

readout should not be influenced by neural synchrony (Mainen et al., 1995; Clemens et al., 2018). Another risk for artifacts was possible response heterogeneity, which means differences in frequency or intensity tuning of the sound-sensitive JON subpopulations, causing the adaptation dynamics we observed. This concern was also addressed in the prior study by the Murthy lab with a proof of principle model, showing that heterogeneity is also not efficient to explain the adaptation dynamics. While this study supports that the observations made in the CAPs are based on adaptation and can not just be explained by desynchronization or heterogeneity, it is nevertheless impossible to verify whether or not these factors contribute to the observation in a different way (Clemens et al., 2018).

5.9 Alternative readouts

Additional alternative readouts would be helpful in verifying the reported observations. Recording in single JONs for example would rule out possible contributions of desynchronization and heterogeneity (as discussed in section 5.8). Unfortunately, it is not possible to record from single JONs by using intracellular patch-clamp since this was reported to interfere with the natural movement of the antenna and mechanotransduction (Clemens et al., 2018). An alternative could be provided by juxtacellular recordings from a single JON or a small subpopulation (Pinault, 2011; Tang et al., 2014). Other alternative strategies to visualize adaptation dynamics would be calcium or voltage imaging. Albeit calcium imaging is comparatively slow, it would be possible to measure JON spiking this way, without have to worry about the aforementioned neural synchrony (see section 5.8) (Kamikouchi, Inagaki, et al., 2009; Clemens et al., 2018). A method allowing for a higher temporal precision is voltage imaging. This would also allow for imaging specific JON subpopulations (Chamberland et al., 2017; Yang et al., 2016).

Another way to improve on the method we used, would be testing the mutants against a control more similar to their own genetic background instead of only a wild type control. Especially for mutations created using CRIMIC or MiMIC insertions there we have the possibility to revert the mutation using recombinase-mediated cassette exchange, which would yield us a wild type fly with exactly the same genetic background as the mutants (Venken et al., 2011; Li-Kroeger et al., 2018).

5.10 Outlook

In this thesis we showed that the Eag channel is part of the molecular mechanism underlying variance adaptation. Additionally, we could show that it is not part of the mechanism of mean adaptation. Also the contribution of the Eag channel to variance adaptation was not influenced by Ca^{2+} via the channels interactions with CaM or CaMKII.

In the future, this project would benefit from further experiments expanding on the findings described here. First, alternative readouts like described in section 5.9 (e.g. calcium or voltage imaging) should be employed to verify the effect of Eag. Since this would provide us with another mode of observation independent from electrophysiology. Furthermore, it would allow for imaging of spiking and threshold signals. Next, since the dynein mutants also showed an effect during the screening it might proof fruitful to perform further electrophysiological experiments on these mutants and record a second data set, like we did with the Eag mutants.

6 Bibliography

Aguinis, Herman, Ryan K. Gottfredson, and Harry Joo (Apr. 2013). "Best-Practice Recommendations for Defining, Identifying, and Handling Outliers". In: *Organizational Research Methods* 16.2, pp. 270–301. ISSN: 1094-4281. DOI: 10.1177/1094428112470848.

Albert, Jörg T and Martin C Göpfert (Oct. 2015). "Hearing in Drosophila". In: *Current Opinion in Neurobiology*. Molecular Biology of Sensation 34, pp. 79–85. ISSN: 0959-4388. DOI: 10.1016/j.conb.2015.02.001.

Albert, Jörg T., Björn Nadrowski, and Martin C. Göpfert (June 2007). "Mechanical Signatures of Transducer Gating in the Drosophila Ear". In: *Current Biology* 17.11, pp. 1000–1006. ISSN: 0960-9822. DOI: 10.1016/j.cub.2007.05.004.

Albuquerque, Edson X. et al. (Jan. 2009). "Mammalian Nicotinic Acetylcholine Receptors: From Structure to Function". In: *Physiological Reviews* 89.1, pp. 73–120. ISSN: 0031-9333, 1522-1210. DOI: 10.1152/physrev.00015.2008.

Atkinson, Nigel S., Gail A. Robertson, and Barry Ganetzky (Aug. 1991). "A Component of Calcium-activated Potassium Channels Encoded by the *Drosophila Slo* Locus". In: *Science* 253.5019, pp. 551–555. ISSN: 0036-8075, 1095-9203. DOI: 10.1126/science.1857984.

Becker, Mn, R Brenner, and Ns Atkinson (Sept. 1995). "Tissue-Specific Expression of a Drosophila Calcium-Activated Potassium Channel". In: *The Journal of Neuroscience* 15.9, pp. 6250–6259. ISSN: 0270-6474, 1529-2401. DOI: 10.1523/JNEUROSCI.15-09-06250.1995.

Béguin, Pascal et al. (June 2001). "Regulation of Ca 2+ Channel Expression at the Cell Surface by the Small G-protein Kir/Gem". In: *Nature* 411.6838, pp. 701–706. ISSN: 1476-4687. DOI: 10.1038/35079621.

Bellen, Hugo J et al. (July 2011). "The *Drosophila* Gene Disruption Project: Progress Using Transposons With Distinctive Site Specificities". In: *Genetics* 188.3, pp. 731–743. ISSN: 1943-2631. DOI: 10.1534/genetics.111.126995.

Benda, Jan (Feb. 2021). "Neural Adaptation". In: *Current Biology* 31.3, R110–R116. ISSN: 09609822. DOI: 10.1016/j.cub.2020.11.054.

Benda, Jan, Leonard Maler, and André Longtin (Nov. 2010). "Linear Versus Nonlinear Signal Transmission in Neuron Models With Adaptation Currents or Dynamic Thresholds". In: *Journal of Neurophysiology* 104.5, pp. 2806–2820. ISSN: 0022-3077, 1522-1598. DOI: 10.1152/jn.00240.2010.

Boekhoff-Falk, Grace and Daniel F. Eberl (Mar. 2014). "The *Drosophila* Auditory System: *Drosophila* Hearing". In: *Wiley Interdisciplinary Reviews: Developmental Biology* 3.2, pp. 179–191. ISSN: 17597684. DOI: 10.1002/wdev.128.

Bronk, Peter et al. (May 2018). "Regulation of Eag by Ca2+/Calmodulin Controls Presynaptic Excitability in Drosophila". In: *Journal of Neurophysiology* 119.5, pp. 1665–1680. ISSN: 1522-1598. DOI: 10.1152/jn.00820.2017.

Brüggemann, Andrea et al. (Sept. 1993). "Ether-à-Go-Go Encodes a Voltage-Gated Channel Permeable to K+ and Ca2+ and Modulated by cAMP". In: *Nature* 365.6445, pp. 445–448. ISSN: 0028-0836, 1476-4687. DOI: 10.1038/365445a0.

Carter, Andrew P. et al. (Mar. 2011). "Crystal Structure of the Dynein Motor Domain". In: *Science* 331.6021, pp. 1159–1165. ISSN: 0036-8075, 1095-9203. DOI: 10.1126/science.1202393.

Chamberland, Simon et al. (July 2017). "Fast Two-Photon Imaging of Subcellular Voltage Dynamics in Neuronal Tissue with Genetically Encoded Indicators". In: *eLife* 6, e25690. ISSN: 2050-084X. DOI: 10.7554/eLife.25690.

Clancy, Bason E et al. (Sept. 2011). "A Universal Pathway for Kinesin Stepping". In: *Nature Structural & Molecular Biology* 18.9, pp. 1020–1027. ISSN: 1545-9993, 1545-9985. DOI: 10.1038/nsmb.2104.

Clemens, Jan, Nofar Ozeri-Engelhard, and Mala Murthy (Jan. 2018). "Fast Intensity Adaptation Enhances the Encoding of Sound in Drosophila". In: *Nature Communications* 9.1, pp. 1–15. ISSN: 2041-1723. DOI: 10.1038/s41467-017-02453-9.

Colicelli, John (Sept. 2004). "Human RAS Superfamily Proteins and Related GTPases". In: *Science's STKE* 2004.250, re13–re13. ISSN: 1525-8882. DOI: 10.1126/stke.2502004re13.

Dallos, Peter and Burt N. Evans (Mar. 1995). "High-Frequency Motility of Outer Hair Cells and the Cochlear Amplifier". In: *Science* 267.5206, pp. 2006–2009. ISSN: 0036-8075, 1095-9203. DOI: 10.1126/science.7701325.

Dallos, Peter and Bernd Fakler (Feb. 2002). "Prestin, a New Type of Motor Protein". In: *Nature Reviews Molecular Cell Biology* 3.2, pp. 104–111. ISSN: 1471-0072, 1471-0080. DOI: 10.1038/nrm730.

de Bivort, Benjamin (Oct. 2022). *The de Bivort Lab, Organismic & Evolutionary Biology and Center for Brain Science, Harvard.* http://debivort.org/docs/flyclipart.pdf?

De La Cruz, Enrique M. et al. (Nov. 1999). "The Kinetic Mechanism of Myosin V". In: *Proceedings of the National Academy of Sciences* 96.24, pp. 13726–13731. ISSN: 0027-8424, 1091-6490. DOI: 10.1073/pnas.96.24.13726.

Drysdale, R et al. (Mar. 1991). "Molecular Characterization of Eag: A Gene Affecting Potassium Channels in Drosophila Melanogaster." In: *Genetics* 127.3, pp. 497–505. ISSN: 1943-2631. DOI: 10.1093/genetics/127.3.497.

Eatock, Ruth Anne (Mar. 2000). "Adaptation in Hair Cells". In: *Annual Review of Neuroscience* 23.1, pp. 285–314. ISSN: 0147-006X, 1545-4126. DOI: 10.1146/annurev.neuro.23.1.285.

Effertz, Thomas, Robert Wiek, and Martin C. Göpfert (Apr. 2011). "NompC TRP Channel Is Essential for Drosophila Sound Receptor Function". In: *Current Biology* 21.7, pp. 592–597. ISSN: 09609822. DOI: 10.1016/j.cub.2011.02.048.

Einevoll, Gaute T. et al. (Nov. 2013). "Modelling and Analysis of Local Field Potentials for Studying the Function of Cortical Circuits". In: *Nature Reviews Neuroscience* 14.11, pp. 770–785. ISSN: 1471-003X, 1471-0048. DOI: 10.1038/nrn3599.

Elkins, T, B Ganetzky, and C F Wu (Nov. 1986). "A Drosophila Mutation That Eliminates a Calcium-Dependent Potassium Current." In: *Proceedings of the National Academy of Sciences* 83.21, pp. 8415–8419. ISSN: 0027-8424, 1091-6490. DOI: 10.1073/pnas.83.21.8415.

Fairhall, Adrienne L. et al. (Aug. 2001). "Efficiency and Ambiguity in an Adaptive Neural Code". In: *Nature* 412.6849, pp. 787–792. ISSN: 0028-0836, 1476-4687. DOI: 10.1038/35090500.

Finlin, Brian S. et al. (Nov. 2003). "Regulation of Voltage-Gated Calcium Channel Activity by the Rem and Rad GTPases". In: *Proceedings of the National Academy of Sciences* 100.24, pp. 14469–14474. ISSN: 0027-8424, 1091-6490. DOI: 10.1073/pnas.2437756100.

Franchini, Lucía F. and A. Belén Elgoyhen (Dec. 2006). "Adaptive Evolution in Mammalian Proteins Involved in Cochlear Outer Hair Cell Electromotility". In: *Molecular Phylogenetics and Evolution* 41.3, pp. 622–635. ISSN: 10557903. DOI: 10.1016/j.ympev.2006.05.042.

Frolov, Roman V. et al. (Sept. 2012). "Potassium Channels in *Drosophila* : Historical Breakthroughs, Significance, and Perspectives". In: *Journal of Neurogenetics* 26.3-4, pp. 275–290. ISSN: 0167-7063, 1563-5260. DOI: 10.3109/01677063.2012.744990.

Gianulis, Elena C., Qiangni Liu, and Matthew C. Trudeau (Oct. 2013). "Direct Interaction of Eag Domains and Cyclic Nucleotide–Binding Homology Domains Regulate Deactivation Gating in hERG Channels". In: *Journal of General Physiology* 142.4, pp. 351–366. ISSN: 1540-7748, 0022-1295. DOI: 10.1085/jgp.201310995.

Gibbons, I. R. and A. J. Rowe (July 1965). "Dynein: A Protein with Adenosine Triphosphatase Activity from Cilia". In: *Science* 149.3682, pp. 424–426. ISSN: 0036-8075, 1095-9203. DOI: 10.1126/science.149.3682.424.

Gong, Z. (Oct. 2004). "Two Interdependent TRPV Channel Subunits, Inactive and Nanchung, Mediate Hearing in Drosophila". In: *Journal of Neuroscience* 24.41, pp. 9059–9066. ISSN: 0270-6474, 1529-2401. DOI: 10.1523/JNEUROSCI.1645-04.2004.

Göpfert, Martin C., Jörg T. Albert, et al. (Aug. 2006). "Specification of Auditory Sensitivity by Drosophila TRP Channels". In: *Nature Neuroscience* 9.8, pp. 999–1000. ISSN: 1546-1726. DOI: 10.1038/nn1735.

Göpfert, Martin C. and R. Matthias Hennig (2016). "Hearing in Insects". In: *Annual Review of Entomology* 61.1, pp. 257–276. DOI: 10.1146/annurev-ento-010715-023631.

Gray-Keller, Mark P and Peter B Detwiler (Aug. 1996). "Ca2+ Dependence of Dark- and Light-Adapted Flash Responses in Rod Photoreceptors". In: *Neuron* 17.2, pp. 323–331. ISSN: 08966273. DOI: 10.1016/S0896-6273(00)80163-4.

Griffith, L C et al. (Oct. 1994). "Calcium/Calmodulin-Dependent Protein Kinase II and Potassium Channel Subunit Eag Similarly Affect Plasticity in Drosophila." In: *Proceedings of the National Academy of Sciences* 91.21, pp. 10044–10048. ISSN: 0027-8424, 1091-6490. DOI: 10.1073/pnas.91.21.10044.

Gutman, George A. et al. (Dec. 2005). "International Union of Pharmacology. LIII. Nomenclature and Molecular Relationships of Voltage-Gated Potassium Channels". In: *Pharmacological Reviews* 57.4, pp. 473–508. ISSN: 0031-6997, 1521-0081. DOI: 10.1124/pr.57.4.10.

Hardie, Roger (Mar. 2002). "Adaptation through Translocation". In: *Neuron* 34.1, pp. 3–5. ISSN: 08966273. DOI: 10.1016/S0896-6273(02)00650-5.

He, David Z.Z. and Peter Dallos (Mar. 2000). "Properties of Voltage-Dependent Somatic Stiffness of Cochlear Outer Hair Cells". In: *Journal of the Association for Research in Otolaryngology* 1.1, pp. 64–81. ISSN: 1525-3961, 1438-7573. DOI: 10.1007/s101620010006.

He, David Z.Z., Sándor Lovas, et al. (May 2014). "Prestin at Year 14: Progress and Prospect". In: *Hearing Research* 311, pp. 25–35. ISSN: 03785955. DOI: 10.1016/j.heares.2013.12.002.

Hildebrandt, K. Jannis, Jan Benda, and R. Matthias Hennig (Feb. 2009). "The Origin of Adaptation in the Auditory Pathway of Locusts Is Specific to Cell Type and Function". In: *Journal of Neuroscience* 29.8, pp. 2626–2636. ISSN: 0270-6474, 1529-2401. DOI: 10.1523/JNEUROSCI.4800-08.2009.

Hoy, R. R. and D. Robert (Jan. 1996). "Tympanal Hearing in Insects". In: *Annual Review of Entomology* 41.1, pp. 433–450. ISSN: 0066-4170, 1545-4487. DOI: 10.1146/annurev.en.41.010196.002245.

Ishikawa, Yuki and Azusa Kamikouchi (Aug. 2016). "Auditory System of Fruit Flies". In: *Hearing Research* 338, pp. 1–8. ISSN: 03785955. DOI: 10.1016/j.heares.2015.10.017.

Jia, Shuping and David Z Z He (Aug. 2005). "Motility-Associated Hair-Bundle Motion in Mammalian Outer Hair Cells". In: *Nature Neuroscience* 8.8, pp. 1028–1034. ISSN: 1097-6256, 1546-1726. DOI: 10.1038/nn1509.

Jon Kull, F. et al. (Apr. 1996). "Crystal Structure of the Kinesin Motor Domain Reveals a Structural Similarity to Myosin". In: *Nature* 380.6574, pp. 550–555. ISSN: 0028-0836, 1476-4687. DOI: 10.1038/380550a0.

Jones, Andrew K., Laurence A. Brown, and David B. Sattelle (Feb. 2007). "Insect Nicotinic Acetylcholine Receptor Gene Families: From Genetic Model Organism to Vector, Pest and Beneficial Species". In: *Invertebrate Neuroscience* 7.1, pp. 67–73. ISSN: 1354-2516, 1439-1104. DOI: 10.1007/s10158-006-0039-6.

Kalloniatis, Michael and Charles Luu (1995). "Light and Dark Adaptation". In: *Webvision: The Organization of the Retina and Visual System*. Ed. by Helga Kolb, Eduardo Fernandez, and Ralph Nelson. Salt Lake City (UT): University of Utah Health Sciences Center.

Kamikouchi, Azusa, Hidehiko K. Inagaki, et al. (Mar. 2009). "The Neural Basis of Drosophila Gravity-Sensing and Hearing". In: *Nature* 458.7235, pp. 165–171. ISSN: 1476-4687. DOI: 10.1038/nature07810.

Kamikouchi, Azusa, Takashi Shimada, and Kei Ito (Nov. 2006). "Comprehensive Classification of the Auditory Sensory Projections in the Brain of the Fruit Fly *Drosophila Melanogaster*". In: *The Journal of Comparative Neurology* 499.3, pp. 317–356. ISSN: 00219967, 10969861. DOI: 10.1002/cne.21075.

Kanca, Oguz et al. (June 2022). "An Expanded Toolkit for Drosophila Gene Tagging Using Synthesized Homology Donor Constructs for CRISPR-mediated Homologous Recombination". In: *eLife* 11, e76077. ISSN: 2050-084X. DOI: 10.7554/eLife.76077.

Kaplan, William D and William E Trout (Feb. 1969). "The Behavior of Four Neurological Mutants of Drosophila". In: *Genetics* 61.2, pp. 399–409. ISSN: 1943-2631. DOI: 10.1093/genetics/61.2.399.

Kennedy, H. J., A. C. Crawford, and R. Fettiplace (Feb. 2005). "Force Generation by Mammalian Hair Bundles Supports a Role in Cochlear Amplification". In: *Nature* 433.7028, pp. 880–883. ISSN: 0028-0836, 1476-4687. DOI: 10.1038/nature03367.

Kile, Benjamin T et al. (May 2002). "The SOCS Box: A Tale of Destruction and Degradation". In: *Trends in Biochemical Sciences* 27.5, pp. 235–241. ISSN: 09680004. DOI: 10.1016/S0968-0004(02)02085-6.

Kim, Eugene Z. et al. (June 2017). "Nonreciprocal Homeostatic Compensation in *Drosophila* Potassium Channel Mutants". In: *Journal of Neurophysiology* 117.6, pp. 2125–2136. ISSN: 0022-3077, 1522-1598. DOI: 10.1152/jn.00002.2017.

Kim, Hyunsoo et al. (Feb. 2020). "Wiring Patterns from Auditory Sensory Neurons to the Escape and Song-Relay Pathways in Fruit Flies". In: *Journal of Comparative Neurology* 528.12, pp. 2068–2098. ISSN: 1096-9861. DOI: 10.1002/cne.24877.

King, S.M. (July 2000). "AAA Domains and Organization of the Dynein Motor Unit". In: *Journal of Cell Science* 113.14, pp. 2521–2526. ISSN: 1477-9137, 0021-9533. DOI: 10.1242/jcs.113.14.2521.

Krizaj, David (2002). "Calcium Regulation in Photoreceptors". In: *Frontiers in Bioscience* 7.4, pp. d2023–2044. ISSN: 10939946, 10934715. DOI: 10.2741/A896.

Li-Kroeger, David et al. (Aug. 2018). "An Expanded Toolkit for Gene Tagging Based on MiMIC and Scarless CRISPR Tagging in Drosophila". In: *eLife* 7, e38709. ISSN: 2050-084X. DOI: 10.7554/eLife.38709.

Kull, F. Jon and Sharyn A. Endow (Jan. 2012). "Force Generation by Kinesin and Myosin Cytoskeletal Motor Proteins". In: *Journal of Cell Science*, jcs.103911. ISSN: 1477-9137, 0021-9533. DOI: 10.1242/jcs.103911.

Lai, Jason Sih-Yu et al. (Feb. 2012). "Auditory Circuit in the Drosophila Brain". In: *Proceedings of the National Academy of Sciences of the United States of America* 109.7, pp. 2607–2612. ISSN: 0027-8424. DOI: 10.1073/pnas.1117307109.

Lansdell, Stuart J et al. (Dec. 2012). "The Drosophila Nicotinic Acetylcholine Receptor Subunits Dα5 and Dα7 Form Functional Homomeric and Heteromeric Ion Channels". In: *BMC Neuroscience* 13.1, p. 73. ISSN: 1471-2202. DOI: 10.1186/1471-2202-13-73.

Laughlin, Simon (Oct. 1981). "A Simple Coding Procedure Enhances a Neuron's Information Capacity". In: *Zeitschrift für Naturforschung C* 36.9-10, pp. 910–912. ISSN: 1865-7125, 0939-5075. DOI: 10.1515/znc-1981-9-1040.

Lee, Pei-Tseng et al. (Mar. 2018). "A Gene-Specific T2A-GAL4 Library for Drosophila". In: *eLife* 7, e35574. ISSN: 2050-084X. DOI: 10.7554/eLife.35574.

Lehnert, Brendan P. et al. (Jan. 2013). "Distinct Roles of TRP Channels in Auditory Transduction and Amplification in Drosophila". In: *Neuron* 77.1, pp. 115–128. ISSN: 08966273. DOI: 10.1016/j.neuron.2012.11.030.

Li, Xiaofan et al. (Feb. 2015). "Ether-à-Go-Go Family Voltage-Gated K+ Channels Evolved in an Ancestral Metazoan and Functionally Diversified in a Cnidarian–Bilaterian Ancestor". In: *Journal of Experimental Biology* 218.4, pp. 526–536. ISSN: 0022-0949, 1477-9145. DOI: 10.1242/jeb.110080.

Lichtinghagen, R. et al. (Dec. 1990). "Molecular Basis of Altered Excitability in Shaker Mutants of Drosophila Melanogaster." In: *The EMBO Journal* 9.13, pp. 4399–4407. ISSN: 02614189. DOI: 10.1002/j.1460-2075.1990.tb07890.x.

Liu, Lei et al. (Nov. 2007). "Drosophila Hygrosensation Requires the TRP Channels Water Witch and Nanchung". In: *Nature* 450.7167, pp. 294–298. ISSN: 0028-0836, 1476-4687. DOI: 10.1038/nature06223.

Lörinczi, Eva et al. (Aug. 2016). "Calmodulin Regulates Human Ether à Go-Go 1 (hEAG1) Potassium Channels through Interactions of the Eag Domain with the Cyclic Nucleotide

Binding Homology Domain". In: *Journal of Biological Chemistry* 291.34, pp. 17907–17918. ISSN: 00219258. DOI: 10.1074/jbc.M116.733576.

Mainen, Zachary F. and Terrence J. Sejnowski (June 1995). "Reliability of Spike Timing in Neocortical Neurons". In: *Science* 268.5216, pp. 1503–1506. ISSN: 0036-8075, 1095-9203. DOI: 10.1126/science.7770778.

Marder, Eve and Jean-Marc Goaillard (July 2006). "Variability, Compensation and Homeostasis in Neuron and Network Function". In: *Nature Reviews Neuroscience* 7.7, pp. 563–574. ISSN: 1471-003X, 1471-0048. DOI: 10.1038/nrn1949.

Matsuo, Eriko et al. (May 2014). "Identification of Novel Vibration- and Deflection-Sensitive Neuronal Subgroups in Johnston's Organ of the Fruit Fly". In: *Frontiers in Physiology* 5. ISSN: 1664-042X. DOI: 10.3389/fphys.2014.00179.

Metaxakis, Athanasios et al. (Oct. 2005). "*Minos* as a Genetic and Genomic Tool in *Drosophila Melanogaster*". In: *Genetics* 171.2, pp. 571–581. ISSN: 1943-2631. DOI: 10.1534/genetics.105.041848.

Meyer, Roman and Stefan H. Heinemann (Apr. 1998). "Characterization of an Eag-like Potassium Channel in Human Neuroblastoma Cells". In: *The Journal of Physiology* 508.1, pp. 49–56. ISSN: 00223751. DOI: 10.1111/j.1469-7793.1998.049br.x.

Murakami, Satoshi et al. (May 2017). "Two Components of Aversive Memory in Drosophila, Anesthesia-Sensitive and Anesthesia-Resistant Memory, Require Distinct Domains Within the Rgk1 Small GTPase". In: *Journal of Neuroscience* 37.22, pp. 5496–5510. ISSN: 0270-6474, 1529-2401. DOI: 10.1523/JNEUROSCI.3648-16.2017.

Nadrowski, Björn, Jörg T. Albert, and Martin C. Göpfert (Sept. 2008). "Transducer-Based Force Generation Explains Active Process in Drosophila Hearing". In: *Current Biology* 18.18, pp. 1365–1372. ISSN: 09609822. DOI: 10.1016/j.cub.2008.07.095.

Nadrowski, Björn, Thomas Effertz, et al. (Mar. 2011). "Antennal Hearing in Insects – New Findings, New Questions". In: *Hearing Research* 273.1-2, pp. 7–13. ISSN: 03785955. DOI: 10.1016/j.heares.2010.03.092.

Nagel, Katherine I and Rachel I Wilson (Feb. 2011). "Biophysical Mechanisms Underlying Olfactory Receptor Neuron Dynamics". In: *Nature Neuroscience* 14.2, pp. 208–216. ISSN: 1097-6256, 1546-1726. DOI: 10.1038/nn.2725.

Niven, Jeremy E. et al. (Feb. 2003). "The Contribution of Shaker K + Channels to the Information Capacity of Drosophila Photoreceptors". In: *Nature* 421.6923, pp. 630–634. ISSN: 1476-4687. DOI: 10.1038/nature01384.

Odronitz, Florian and Martin Kollmar (2007). "Drawing the Tree of Eukaryotic Life Based on the Analysis of 2,269 Manually Annotated Myosins from 328 Species". In: *Genome Biology* 8.9, R196. ISSN: 1465-6906. DOI: 10.1186/gb-2007-8-9-r196.

Ozuysal, Yusuf and Stephen A. Baccus (Mar. 2012). "Linking the Computational Structure of Variance Adaptation to Biophysical Mechanisms". In: *Neuron* 73.5, pp. 1002–1015. ISSN: 0896-6273. DOI: 10.1016/j.neuron.2011.12.029.

Pallanck, Leo and Barry Ganetzky (1994). "Cloning and Characterization of Human and Mouse Homologs of the Drosophila Calcium-Activated Potassium Channel Gene, Slowpoke". In: *Human Molecular Genetics* 3.8, pp. 1239–1243. ISSN: 0964-6906, 1460-2083. DOI: 10.1093/hmg/3.8.1239.

Patella, Paola and Rachel I. Wilson (Apr. 2018). "Functional Maps of Mechanosensory Features in the Drosophila Brain". In: *Current Biology* 28.8, 1189–1203.e5. ISSN: 09609822. DOI: 10.1016/j.cub.2018.02.074.

Pavlopoulos, Anastasios et al. (2007). "The DNA Transposon Minos as a Tool for Transgenesis and Functional Genomic Analysis in Vertebrates and Invertebrates". In: *Genome Biology* 8.Suppl 1, S2. ISSN: 14656906. DOI: 10.1186/gb-2007-8-s1-s2.

Pimentel, Diogo et al. (Aug. 2016). "Operation of a Homeostatic Sleep Switch". In: *Nature* 536.7616, pp. 333–337. ISSN: 1476-4687. DOI: 10.1038/nature19055.

Pinault, Didier (2011). "The Juxtacellular Recording-Labeling Technique". In: *Electrophysiological Recording Techniques*. Ed. by Robert P. Vertes and Robert W. Stackman. Vol. 54. Totowa, NJ: Humana Press, pp. 41–75. DOI: 10.1007/978-1-60327-202-5_3.

Puhl 3rd, Henry L. et al. (July 2014). "Ancient Origins of RGK Protein Function: Modulation of Voltage-Gated Calcium Channels Preceded the Protostome and Deuterostome Split". In: *PLOS ONE* 9.7, e100694. ISSN: 1932-6203. DOI: 10.1371/journal.pone.0100694.

Rayment, I et al. (July 1993). "Three-Dimensional Structure of Myosin Subfragment-1: A Molecular Motor". In: *Science* 261.5117, pp. 50–58. ISSN: 0036-8075, 1095-9203. DOI: 10.1126/science.8316857.

Rogero, Oscar, Barbara Hämmerle, and Francisco J. Tejedor (July 1997). "Diverse Expression and Distribution of *Shaker* Potassium Channels during the Development of the *Drosophila* Nervous System". In: *The Journal of Neuroscience* 17.13, pp. 5108–5118. ISSN: 0270-6474, 1529-2401. DOI: 10.1523/JNEUROSCI.17-13-05108.1997.

Salkoff, Lawrence, Alice Butler, et al. (Dec. 2006). "High-Conductance Potassium Channels of the SLO Family". In: *Nature Reviews Neuroscience* 7.12, pp. 921–931. ISSN: 1471-003X, 1471-0048. DOI: 10.1038/nrn1992.

Salkoff, Lawrence and Robert Wyman (Sept. 1981). "Genetic Modification of Potassium Channels in Drosophila Shaker Mutants". In: *Nature* 293.5829, pp. 228–230. ISSN: 0028-0836, 1476-4687. DOI: 10.1038/293228a0.

Sattelle, D.B. et al. (Apr. 2005). "Edit, Cut and Paste in the Nicotinic Acetylcholine Receptor Gene Family ofDrosophila Melanogaster". In: *BioEssays* 27.4, pp. 366–376. ISSN: 0265-9247, 1521-1878. DOI: 10.1002/bies.20207.

Schmidt, Helgo et al. (Feb. 2015). "Structure of Human Cytoplasmic Dynein-2 Primed for Its Power Stroke". In: *Nature* 518.7539, pp. 435–438. ISSN: 0028-0836, 1476-4687. DOI: 10.1038/nature14023.

Senthilan, Pingkalai R. et al. (Aug. 2012). "Drosophila Auditory Organ Genes and Genetic Hearing Defects". In: *Cell* 150.5, pp. 1042–1054. ISSN: 0092-8674. DOI: 10.1016/j.cell.2012.06.043.

Sokolov, Maxim et al. (Mar. 2002). "Massive Light-Driven Translocation of Transducin between the Two Major Compartments of Rod Cells". In: *Neuron* 34.1, pp. 95–106. ISSN: 08966273. DOI: 10.1016/S0896-6273(02)00636-0.

Spehr, J. et al. (Feb. 2009). "Ca2+-Calmodulin Feedback Mediates Sensory Adaptation and Inhibits Pheromone-Sensitive Ion Channels in the Vomeronasal Organ". In: *Journal of Neuroscience* 29.7, pp. 2125–2135. ISSN: 0270-6474, 1529-2401. DOI: 10.1523/JNEUROSCI.5416-08.2009.

Sun, Xiu Xia et al. (Mar. 2004). "The Eag Potassium Channel Binds and Locally Activates Calcium/Calmodulin-dependent Protein Kinase II". In: *Journal of Biological Chemistry* 279.11, pp. 10206–10214. ISSN: 00219258. DOI: 10.1074/jbc.M310728200.

Sweeney, H. Lee and David W. Hammers (Feb. 2018). "Muscle Contraction". In: *Cold Spring Harbor Perspectives in Biology* 10.2, a023200. ISSN: 1943-0264. DOI: 10.1101/cshperspect.a023200.

Sweeney, H. Lee and Erika L.F. Holzbaur (May 2018). "Motor Proteins". In: *Cold Spring Harbor Perspectives in Biology* 10.5, a021931. ISSN: 1943-0264. DOI: 10.1101/cshperspect.a021931.

Tamsett, T. J., K. E. Picchione, and A. Bhattacharjee (Apr. 2009). "NAD+ Activates KNa Channels in Dorsal Root Ganglion Neurons". In: *Journal of Neuroscience* 29.16, pp. 5127–5134. ISSN: 0270-6474, 1529-2401. DOI: 10.1523/JNEUROSCI.0859-09.2009.

Tang, Qiusong, Michael Brecht, and Andrea Burgalossi (Oct. 2014). "Juxtacellular Recording and Morphological Identification of Single Neurons in Freely Moving Rats". In: *Nature Protocols* 9.10, pp. 2369–2381. ISSN: 1754-2189, 1750-2799. DOI: 10.1038/nprot.2014.161.

Tanouye, Mark A. and Alberto Ferrus (Jan. 1985). "Action Potentials in Normal and Shaker Mutant Drosophila". In: *Journal of Neurogenetics* 2.4, pp. 253–271. ISSN: 0167-7063, 1563-5260. DOI: 10.3109/01677068509102322.

Todi, Sokol V., Yashoda Sharma, and Daniel F. Eberl (Apr. 2004). "Anatomical and Molecular Design of theDrosophila Antenna as a Flagellar Auditory Organ". In: *Microscopy Research and Technique* 63.6, pp. 388–399. ISSN: 1059-910X, 1097-0029. DOI: 10.1002/jemt.20053.

Vale, R, T Reese, and M Sheetz (Aug. 1985). "Identification of a Novel Force-Generating Protein, Kinesin, Involved in Microtubule-Based Motility". In: *Cell* 42.1, pp. 39–50. ISSN: 00928674. DOI: 10.1016/S0092-8674(85)80099-4.

Venken, Koen J T et al. (Sept. 2011). "MiMIC: A Highly Versatile Transposon Insertion Resource for Engineering Drosophila Melanogaster Genes". In: *Nature Methods* 8.9, pp. 737–743. ISSN: 1548-7091, 1548-7105. DOI: 10.1038/nmeth.1662.

Wang, S. et al. (July 1997). "A Quantitative Analysis of the Activation and Inactivation Kinetics of HERG Expressed in Xenopus Oocytes". In: *The Journal of Physiology* 502 (Pt 1), pp. 45–60. ISSN: 0022-3751. DOI: 10.1111/j.1469-7793.1997.045bl.x.

Wang, Tao et al. (Jan. 2008). "The SOCS Box Protein STOPS Is Required for Phototransduction through Its Effects on Phospholipase C". In: *Neuron* 57.1, pp. 56–68. ISSN: 08966273. DOI: 10.1016/j.neuron.2007.11.020.

Wang, Z., S. Khan, and M.P. Sheetz (Nov. 1995). "Single Cytoplasmic Dynein Molecule Movements: Characterization and Comparison with Kinesin". In: *Biophysical Journal* 69.5, pp. 2011–2023. ISSN: 00063495. DOI: 10.1016/S0006-3495(95)80071-8.

Wang, Zheng, Gisela F. Wilson, and Leslie C. Griffith (July 2002). "Calcium/Calmodulin-dependent Protein Kinase II Phosphorylates and Regulates the Drosophila Eag Potassium Channel". In: *Journal of Biological Chemistry* 277.27, pp. 24022–24029. ISSN: 00219258. DOI: 10.1074/jbc.M201949200.

Wark, Barry, Brian Nils Lundstrom, and Adrienne Fairhall (Aug. 2007). "Sensory Adaptation". In: *Current Opinion in Neurobiology*. Sensory Systems 17.4, pp. 423–429. ISSN: 0959-4388. DOI: 10.1016/j.conb.2007.07.001.

Warmke, J W and B Ganetzky (Apr. 1994). "A Family of Potassium Channel Genes Related to Eag in Drosophila and Mammals." In: *Proceedings of the National Academy of Sciences* 91.8, pp. 3438–3442. ISSN: 0027-8424, 1091-6490. DOI: 10.1073/pnas.91.8.3438.

Warmke, Jeffrey, Rachel Drysdale, and Barry Ganetzky (June 1991). "A Distinct Potassium Channel Polypeptide Encoded by the *Drosophila Eag* Locus". In: *Science* 252.5012, pp. 1560–1562. ISSN: 0036-8075, 1095-9203. DOI: 10.1126/science.1840699.

Whicher, Jonathan R. and Roderick MacKinnon (Aug. 2016). "Structure of the Voltage-Gated K^+ Channel Eag1 Reveals an Alternative Voltage Sensing Mechanism". In: *Science* 353.6300, pp. 664–669. ISSN: 0036-8075, 1095-9203. DOI: 10.1126/science.aaf8070.

Whitmire, Clarissa J. and Garrett B. Stanley (Oct. 2016). "Rapid Sensory Adaptation Redux: A Circuit Perspective". In: *Neuron* 92.2, pp. 298–315. ISSN: 08966273. DOI: 10.1016/j.neuron.2016.09.046.

Witsell, Alice et al. (Nov. 2009). "Removal of the Bloom Syndrome DNA Helicase Extends the Utility of Imprecise Transposon Excision for Making Null Mutations in Drosophila". In: *Genetics* 183.3, pp. 1187–1193. ISSN: 1943-2631. DOI: 10.1534/genetics.109.108472.

Wu, Chun-Fang et al. (June 1983). "Potassium Currents in *Drosophila* : Different Components Affected by Mutations of Two Genes". In: *Science* 220.4601, pp. 1076–1078. ISSN: 0036-8075, 1095-9203. DOI: 10.1126/science.6302847.

Yamauchi, Takashi (2005). "Neuronal Ca2+/Calmodulin-Dependent Protein Kinase II-Discovery, Progress in a Quarter of a Century, and Perspective: Implication for Learning and Memory". In: *Biological and Pharmaceutical Bulletin* 28.8, pp. 1342–1354. ISSN: 0918-6158, 1347-5215. DOI: 10.1248/bpb.28.1342.

Yamauchi, Takashi and Hitoshi Fujisawa (July 1980). "Evidence for Three Distinct Forms of Calmodulin-Dependent Protein Kinases from Rat Brain". In: *FEBS Letters* 116.2, pp. 141–144. ISSN: 00145793. DOI: 10.1016/0014-5793(80)80628-4.

Yang, Helen H. et al. (June 2016). "Subcellular Imaging of Voltage and Calcium Signals Reveals Neural Processing In Vivo". In: *Cell* 166.1, pp. 245–257. ISSN: 00928674. DOI: 10.1016/j.cell.2016.05.031.

Yorozu, Suzuko et al. (Mar. 2009). "Distinct Sensory Representations of Wind and Near-Field Sound in the Drosophila Brain". In: *Nature* 458.7235, pp. 201–205. ISSN: 1476-4687. DOI: 10.1038/nature07843.

Zhang, Xiaowei (2022). "Molecular Mechanism of Sound Frequency Discrimination in Drosophila Ear". PhD thesis. Georg-August University School of Science.

Zheng, Jing et al. (May 2000). "Prestin Is the Motor Protein of Cochlear Outer Hair Cells". In: *Nature* 405.6783, pp. 149–155. ISSN: 0028-0836, 1476-4687. DOI: 10.1038/35012009.

7 Acknowledgments

I want to take this opportunity to thank everybody who supported me during my PhD project and made this thesis possible. First and foremost I want to thank Jan Clemens for being an excellent supervisor, always offering great advice and unlimited patience during this project. Furthermore, I want to thank Martin Göpfert and Tim Gollisch for being part of my Thesis Advisory Committee, providing helpful insights, ideas and feedback to me. I want to give a special thanks to the Göpfert lab and Xiaowei Zhang for so readily sharing their knowledge on *Drosophila* and their stocks with me.

I want to thank all of my excellent lab mates (both past and current), which made these almost 4 years not just very instructive for me, but also a really fun experience. So thank you Elsa, Deniz, Adrian, Afshin, Kimia, Sarath, Daesung and Winston! A special thanks to the three wonderful coworkers, that shared an office with me: Melanie, Dawn and Sudeshna. You were always trying to keep my spirits high and graciously tolerating my sounds of frustration while I was working on my thesis.

Furthermore, I also want to thank the staff of the ENI for their great support, making working at the institute such a great experience.

I would also like to thank my partner Vitana Bill for always supporting me, especially during the last months of writing. No matter if offering support from a distance or taking care of me here in Göttingen. Thank you for always having my back!

Finally, I want to thank my friends and family, who were always there for me and were infinitely understanding for me falling off the face of the earth during the last months of writing.

I feel that no matter how long I stretch this part, I could never satisfactory convey how grateful I am to have these outstanding people in my life. A final thanks to all of you!

8 Abbreviations

AAA	ATPases associated with cellular activity
AMMC	Antennal mechanosensory motor center
ATP	Adenosine triphosphate
BDSC	Bloomington Drosophila Stock Center
CaM	Calmodulin
CaMBD	Calmodulin binding domain
CaMKII	Ca^{2+}/calmodulin dependent kinase II
CAP	Compound action potential
CNBHD	cyclic nucleotide-binding homology domain
CRIMIC	CRISPR-mediated integration cassett
Dhc	Dynein heavy chain
Dnah	Dynein, axonemal, heavy chain
Dnai	Dynein, axonemal, intermediate chain
Eag	Ether a go-go
Eag D	Ether a go-go domain
IVLP	Inferior ventrolateral protocerebrum
GFN	Giant fiber neuron
G-protein	GTPase
GFP	Green fluorescence protein
GTP	Guanosine triphosphate
HRP	Horseradish peroxidase
JO	Johnston's organ
JON	Johnston's organ neuron
nAChα5	Nicotinic Acetylcholine Receptor α5
MET	Mechano-electrical transduction
MiMIC	*Minos*-mediated integration cassette
Nan	Nanchung
NMJ	Neuromuscular junction
NompC	No mechanoreceptor channel potential C
PBac	*piggyBac*

PE	*P*element
Rgk	Rad, Gem/Kir family member
Sha	Shaker
Shab	Shaker cognate B
Slo	Slowpoke
SNR	Signal-to-noise ratio
Stops	Slow termination of phototransduction
SOCS	Suppressor of cytokine signaling
TH	Transheterozygous
TRP	Transient receptor potential
WED	Wedge
WT	Wildtype
Wtrw	Water witch

9 List of Figures

1.1 Adaptation of a hypothetical neuron over time 3
1.2 Antenna of *Drosophila melanogaster* and its JO 5
1.3 Structure of EAG subunit 10
1.4 The Eag channel's Ca^{2+} mediated interaction with CaM and CaMKII 12

3.1 Fly holder we used in the experiments 21
3.2 Schematic of fly fixation inside the fly holder 21
3.3 Photo of the electrophysiology setu 22
3.4 Schematic of the electrode and stimulus source placement during the experiments 23
3.5 Example of the noise stimuli used to determine intensity tuning 25
3.6 Example of pure tone stimuli used to determine intensity tuning 26
3.7 Example of pure tone stimuli used to determine frequency tuning 26
3.8 Example of the stimuli used for probing variance adaptation 27
3.9 Example of stimuli used to probe mean adaptation dynamics 28
3.10 Example of stimuli used to determine influence of variance adaptation on mean adaptation dynamics 29
3.11 Example of stimuli used to determine influence of mean adaptation on variance adaptation dynamics 30
3.12 Extracting the speed of variance adaptation from the envelope of the CAP response 35
3.13 Calculating the strength variance of adaptation from the CAP envelopes . . 36
3.14 Example of different variance adaptation dynamics 36
3.15 Extraction of the measures of mean adaptation from the data 39

4.1 Example of wild type CAP responses and tuning curves 43
4.2 Example for effect of impaired variance adaptation on CAP envelope traces . 44
4.3 Properties of the screened potassium channel mutants 47
4.4 Properties of the screened Rgk mutants 50
4.5 Properties of the screened motor protein mutants 52
4.6 Properties of screened miscellaneous mutants 56

4.7 Summary of speed of variance adaptation screening 58
4.8 Summary of strength of variance adaptation screening 59
4.9 Schematic of tuning curve shift in mean adaptation experiments 61
4.10 Screening of mean adaptation dynamics 64
4.11 Expression of Eag in the JO. 66
4.12 Properties of the Eag mutants 67
4.13 Properties of the CaMBD mutant flies 70
4.14 Properties of CaMKII mutant flies 72

10 List of Tables

2.1 General laboratory materials and equipment 14
2.2 Solutions 15
2.3 Fly food (for 5 liters) 15
2.4 Components of the electrophysiology rig 16

3.1 Genotypes of the fly stocks used 18
3.2 Settings of the extracellular amplifier 23
3.3 Sutter horizontal puller settings 24

11.1 P-values of variance adaptation screening experiments 99
11.2 P-values of mean adaptation screening experiments 100
11.3 P-values of variance adaptation hit dataset experiments 100
11.4 P-values of the response amplitude of the screening experiments 101
11.5 P-values of the response amplitude of the hit dataset experiments 102

11 Appendix

Table 11.1: P-values of variance adaptation screening experiments

		P-values	
Control	**Mutant**	**Speed of adaptation**	**Strength of adaptation**
NM91	Slo (PBac)	0.7669	0.3819
NM91	Slo (MiMIC)	0.3565	0.2493
NM91	$Shaker^{5}$	0.8814	0.6925
NM91	Sha^{133}	0.0913	0.3654
NM91	Eag^{sc29}	0.0216	0.0368
NM91	Eag (CRIMIC)	0.0311	0.4277
NM91	Eag delta-full	0.074	0.0004
NM91	Rgk1	0.9776	0.0104
NM91	Rgk1 (Minos)	0.5541	0.525
NM91	Rgk3	0.5541	0.525
NM91	Dnah3	0.0354	0.43
NM91	Dhc93AB	0.0311	0.8159
NM91	Dnai2	0.5541	0.6925
NM91	Prestin	0.0565	0.43
NM91	Wtrw	0.5726	0.6925
NM91	Stops	0.3565	0.3451
NM91	nAChα5	0.7349	0.4277

Table 11.2: P-values of mean adaptation screening experiments

			P-values	
Control	**Mutant**	**Slope**	**Speed of adaptation**	**Strength of adaptation**
NM91	Eag^{sc29}	0.74	0.4324	0.5325
NM91	Eag (CRIMIC)	0.74	0.1596	0.5325
NM91	Eag delta-full	0.74	0.1167	0.5325
NM91	CaMBD 8.8.1	0.8165	0.9792	0.5679
NM91	CaMBD 17.4.1	0.8165	0.8489	0.4107
NM91	Rgk1	0.74	0.0941	0.5325
NM91	Slo (PBac)	0.8165	0.3532	0.5325
NM91	Sha^{133}	0.74	0.5624	0.5325

Table 11.3: P-values of variance adaptation hit dataset experiments

		P-values	
Control	**Mutant**	**Speed of adaptation**	**Strength of adaptation**
NM91	Eag^{sc29}	0.00649351	0.00649351
NM91	Eag (CRIMIC)	0.01298701	0.3961039
NM91	Eag delta-full	0.00649351	0.00649351
TH control	CaMBD 8.8.1	0.61904762	0.12987013
TH control	CaMBD 17.4.1	1.0	0.05194805
Control 8.7.1	CaMBD 8.8.1	0.18614719	1.0
Control 8.7.1	CaMBD 17.4.1	1.0	0.12987013
Control 12.6.1	CaMBD 8.8.1	1.0	0.35930736
Control 12.6.1	CaMBD 17.4.1	1.0	0.12987013
NM91	CaMKII	0.35930739	0.08225108
NM91	CaMKII (MiMIC)	0.61904762	0.35930736
TH control	Control 8.7.1	1.0	0.12987013
TH control	Control 12.6.1	1.0	1.0
Control 8.7.1	Control 12.6.1	1.0	0.48051948
Control 8.7.1	TH control	1.0	0.12987013

Table 11.4: P-values of the response amplitude of the screening experiments

Control	**Mutant**	**P-values**
NM91	Slo (PBac)	0.0647
NM91	Slo (MiMIC)	0.1247
NM91	$Shaker^{5}$	0.4735
NM91	Sha^{133}	0.8274
NM91	Eag^{sc29}	0.9387
NM91	Eag (CRIMIC)	0.6309
NM91	Eag delta-full	0.0554
NM91	Rgk1	0.3968
NM91	Rgk1 (Minos)	0.4083
NM91	Rgk3	0.0647
NM91	Dnah3	0.4083
NM91	Dhc93AB	0.3968
NM91	Dnai2	0.0718
NM91	Prestin	0.2150
NM91	Wtrw	0.2924
NM91	Stops	0.0254
NM91	nAChα5	0.8933

Table 11.5: P-values of the response amplitude of the hit dataset experiments

Control	**Mutant**	**P-values**
NM91	Eag^{sc29}	0.077
NM91	Eag (CRIMIC)	0.3961
NM91	Eag delta-full	0.1234
TH control	CaMBD 8.8.1	0.619
TH control	CaMBD 17.4.1	1.0
Control 8.7.1	CaMBD 8.8.1	1.0
Control 8.7.1	CaMBD 17.4.1	0.619
Control 12.6.1	CaMBD 8.8.1	1.0
Control 12.6.1	CaMBD 17.4.1	1.0
NM91	CaMKII	0.7879
NM91	CaMKII (MiMIC)	1.0
TH control	Control 8.7.1	0.9697
TH control	Control 12.6.1	0.9697
Control 8.7.1	Control 12.6.1	1.0
Control 8.7.1	TH control	0.9697